Development of an Integrated Tracking Control Algorithm and a Test Platform for Autonomous Excavation

by

Niraj N. Reginald

A thesis submitted to the
School of Graduate and Postdoctoral Studies in partial
fulfillment of the requirements for the degree of

Master of Applied Science in Mechanical Engineering

Faculty of Engineering and Applied Sciences

University of Ontario Institute of Technology (Ontario Tech University)

Oshawa, Ontario, Canada

March 2020

THESIS EXAMINATION INFORMATION

Submitted by: **Niraj Reginald**

Master of Applied Science in **Mechanical Engineering**

Thesis title: Development of an Integrated Tracking Control Algorithm and a Test Platform for Autonomous Excavation

An oral defense of this thesis took place on April 7, 2020 in front of the following examining committee:

Examining Committee:

Chair of Examining Committee	Dr. Xianke Lin
Research Supervisor	Dr. Jaho Seo
Examining Committee Member	Dr. Carlos Rossa
Thesis Examiner	Dr. Yuping He

The above committee determined that the thesis is acceptable in form and content and that a satisfactory knowledge of the field covered by the thesis was demonstrated by the candidate during an oral examination. A signed copy of the Certificate of Approval is available from the School of Graduate and Postdoctoral Studies.

ABSTRACT

Since construction is part of the industrial sector where a large amount of labor is required and workers operate under harsh environmental conditions, the transformation from manual to autonomous operation in modern construction sites can be a solution to improve productivity, accuracy, and efficiency. Excavator is one of the key equipment in the construction field for earthmoving operations. In this study, an effective control strategy for excavation is introduced considering the position, contour, and force which are mutually associated factors for successful autonomous excavation. For position tracking of the bucket tip, a non-linear PI controller was devised to control the hydraulic actuators of the boom, arm, and bucket links of the excavator. To compensate for the ground resistive forces, an impedance controller was designed. Finally, contour compensation was considered to generate an optimal path of the bucket tip by reducing the contour profile error that is vital for skilled tasks such as ground levelling. Furthermore, the time-delayed control strategy was adopted to mitigate dynamic uncertainties.
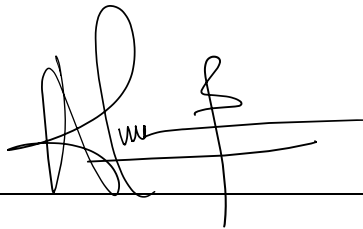
The performance of the developed algorithm was evaluated through co-simulation in multi-physics domains. Simulation results showed the designed control algorithm provided good tracking results in terms of the desired position and force of the bucket tip. In addition, the controller could reduce the contour error between the desired trajectory of the bucket tip and its actual trajectory. The simulation results were tested experimentally using the test platform that was developed by modifying an existing mini-hydraulic excavator. Experimental data was gathered to conduct an analysis of the bucket tip's tracking error and, the error between the desired ground terrain profile and the excavated ground terrain profile. Experimental results showed the developed effective control strategy provided good tracking results of the bucket tip and reduced the standard deviation between the desired ground terrain profile and actual excavated ground terrain profile.

Keywords: excavator; position control; contour control; force control; simulation

AUTHOR'S DECLARATION

I hereby declare that this thesis consists of original work of which I have authored. This is a true copy of the thesis, including any required final revisions, as accepted by my examiners.

I authorize the University of Ontario Institute of Technology to lend this thesis to other institutions or individuals for the purpose of scholarly research. I further authorize University of Ontario Institute of Technology to reproduce this thesis by photocopying or by other means, in total or in part, at the request of other institutions or individuals for the purpose of scholarly research. I understand that my thesis will be made electronically available to the public.

Niraj Reginald

STATEMENT OF CONTRIBUTIONS

Part of the work described in Chapter 5 and Chapter 6 has been published as:

N. Reginald, J. Seo, "Force/Position Control for an Excavator with Contour Control Compensation", in *2019 Symposium on Mechanisms, Machines, and Mechatronics (CCToMM), pp. 176 – 187.*

Part of the work described in Chapter 4 and Chapter 6 has been accepted for publication as:

N. Reginald, J. Seo, A. Rasul, "Tracking Control of Force/Position and Contour for an Excavator with Co-simulation", in *2020 IEEE Conference on Electrical and computer engineering* (CCECE).

Part of the work described in Chapter 1, Chapter 3 and Chapter 7 has been contributed for the submitted potential publication as below:

A. Rasul, J. Seo, K. Oh, A. Kahjpour, N. Reginald, "Predicted Safety Algorithms for Autonomous Excavators using a 3D LiDAR Sensor", in *2020 IEEE Conference on Control Technology and Applications* (CCTA).

Finally, at the time of writing components of Chapter 7 are to be submitted to *Journal of Dynamic Systems, Measurement, and Control* (ASME) *as*:

N. Reginald, J. Seo, "Integrated Tracking Control Methodology for Autonomous Excavators"

ACKNOWLEDGEMENTS

First and foremost, I would like to acknowledge my thesis supervisor Dr. Jaho Seo for providing me with the research insight along with the technical guidance to explore an interesting field of study. In addition, I would like to thank Dr. Seo for consistently having weekly meetings and dedicating his time to discuss limitations and improvements of the ongoing work.

I would also like to thank my parents Surahi and Ranjith, for their consistent support provided during the period of my studies. Furthermore, I am very thankful for them who also provided me with financial support when needed during the course of my studies.

Finally, I would like to thank Zeenath, my girlfriend, for her continuous encouragement which boosted my motivation along the journey of my thesis studies.

TABLE OF CONTENTS

LIST OF TABLES

LIST OF FIGURES

xiii

LIST OF ABBREVIATIONS AND SYMBOLS

3D	Three Dimensional
ANN	Artificial Neural Networks
BFGS	Broyden, Fletcher, Goldfarb and Shanno
CAD	Computer Aided Design
CAE	Computer Aided Engineering
CAM	Computer Aided Manufacturing
CAN	Controller Area Network
CBV	Counter-Balance Valve
CCP	Cross Coupled Pre-Compensation
CNC	Computer Numerical Control
DAQ	Data Acquisition
DC	Direct Current
DCV	Directional Control Valves
D-H	Denavit Hartenberg
DOF	Degree of Freedom
ECU	Electronic Control Unit
EHD	Electro-Hydraulic Driver
EHPV	Electro-Hydraulic Proportional Valve
FC	Force Control
GND	Ground
HW	Hardware

I/O	Input/output
ISO	International Standards Organization
LQR	Linear Quadratic Regulator
LVDT	Linear Variable Differential Transformer
MPC	Model Predictive Control
NPI	Non-Linear Proportional Integral
ODE	Ordinary Differential Equation
OSHA	Occupational Safety and Health Administration
PID	Proportional Integral Derivative
PWM	Pulse Width Modulation
RMS	Root Mean Squared
RPM	Revolutions per minute
RTI	Real time interface
SAE	Society of Automotive Engineers
STD	Standard Deviation
TDC	Time Delayed Control
VG	Viscosity Grade

Chapter 1. Introduction

The key function of construction equipment is to mechanize construction activities to improve productivity, efficiency, and accuracy. However, construction equipment relies on a human operator and hence, the aforementioned advantages of construction equipment heavily depend on the human operator itself. Due to this reason, the automation of construction equipment is desired.

Out of the existing construction equipment, the excavator is one of the key construction equipment which is used to conduct earthmoving tasks such as digging, trenching, leveling, demolition, etc. Automated excavation has been a research topic for the past few decades due to the following reasons;

- The operation of the excavator is dependent on the operator, and therefore the precision of the work can be improved. Further, the high dependency on skilled labor can be eliminated [1].
- Excavation tasks such as trenching, and ground levelling are repetitive in nature and therefore they can be automated for better efficiency. Consequently, the excavator can be dynamically controlled to achieve optimum energy efficiency [2].
- To achieve economic feasibility by improving quality, increasing productivity, and reducing labor cost.
- To take advantage of the technological advancements in hardware, sensing techniques, DAQ systems, and processing, novel adaptive and intelligent control methodologies, etc. to achieve high efficiency and productivity of construction equipment [3].
- To improve safety in construction sites and eliminate existing potential hazards linked to construction machinery such as excavators. There are many instances that construction equipment such as excavators may operate at dangerous proximity to workers at a construction site, which may lead to collision-related accidents, injuring workers as well as damaging other equipment and property [4].
- To reduce costs and time associated with adhering to occupational safety and health administration (OSHA) regulations [5].

1

Considering the aforementioned reasons, automation of the excavation process is a very broad research area. The automation process can be implemented at different functional levels of the machine. In fact, some might not even be directly associated with the physical process of removal of soil. Some examples are safety control of excavators, energy conservation, path planning for a mobile excavator to reach excavation site location, scheduling of trucks for loading excavated soil, etc. Considering these facts, automation of the excavation process has gained the attention of researchers and there have been technical advancements in research and development in this area which will be further discussed in chapter 2.

Automation of the excavation process is challenging due to the resistive forces acting against the bucket of the excavator. The resistive forces are hard to model due to the non-homogenous dynamics of soil (excavation media). Apart from this, the nonlinear dynamics of the mechanical system and the hydraulic system makes kinematic tracking control of the excavator manipulator difficult. Due to these reasons, the motivation of this thesis work targets to compile the required control aspects going forward for autonomous excavation by providing an effective control strategy utilizing these components. The main scope, objectives and working methodologies used in this thesis are described in this chapter.

1.1 Project scope and objectives

The primary scope of this work is to provide an effective control strategy for autonomous excavation. In addition, completion of this work includes the development of a test platform by modifying an existing mini wheeled excavator for autonomous excavation.

The detailed objectives of this research include:

- Development of an effective algorithm to control position, contour, and force of the bucket tip position.
- Modification of a mini hydraulic excavator to create a prototype test platform for autonomous excavation research work.
- Development of a multi-domain simulation model to develop control algorithms.
- Electronic system architecture design, sensor instrumentation, and embedded controller integration to the test platform.

- Development of low-level software to control the actuators of the excavator. In addition to this, high-level software was developed for functions such as driving, steering, emergency stop, etc.

- Integrate dSPACE environment utilizing MicroAutobox II embedded PC controller.

- Integrate the developed software to the experimental platform to perform physical experiments and validation.

- Development of a sensing methodology to estimate the error between the desired excavation ground terrain and actual excavated ground terrain.

- Provide conclusions and possible future improvements considering the outcomes of this research work.

1.2 Thesis outline

Chapter 1 introduces the scope, objectives, and deliverables of this project by discussing the research area and motivation. In addition, the working foundations used for this work are explained.

Chapter 2 provides a literature review for autonomous excavation. The components and methodologies required for successful excavation are discussed. Current work that has been carried out in robotic excavation is also presented.

Chapter 3 discusses the development of a prototype test platform for experimental research by modifying a mini wheeled excavator. Electronic hardware architecture design and integration along with mechanical modification are discussed. The integration of various types of sensors for data acquisition is explained.

Chapter 4 explains the development of a multi-domain simulation model for control algorithm design. The modelling of dynamics, hydraulics, and kinematics are discussed as the main components of system modelling. The developed simulation model is compared with an experimental setup in chapter 6.

Chapter 5 explains the developed control structure in terms of position, contour, and force control. The developed control algorithms are then tested in the simulation model

in Chapter 6. This includes the time-delayed control framework to compensate for the unknown dynamics.

Chapter 6 includes the verification of the simulation model by comparing the simulation model outputs to the test platform output results. Furthermore, the simulation results of the developed control structure are followed by a discussion.

 Chapter 7 presents results, and a discussion of the experimental results obtained using the developed test platform. As a test scenario, digging and ground leveling tasks were considered. The Digging task was carried out using two different types of media; sand and soil to validate the controller's performance. For each scenario, the controller performance is compared as given below:

1. Position control only
2. Position control along with contour compensation control
3. Position control, contour compensation with force control

Using a stereo vision camera, the error and standard deviation between the current excavated profile and target profile are calculated to validate tracking accuracy with each of these controller types.

Chapter 8 provides the concluding remarks of this thesis and suggests future improvements for the way forward of autonomous excavation as well as the discussion of benefits and limitations of the proposed research.

1.3 Project foundations

The main working foundations and technologies utilized in this thesis work are described in this section. The framework of software developed is presented as well as a summary on modelling foundation and co-simulation.

1.3.1 dSPACE

The main controller used was MicroAutobox II embedded PC by dSPACE. It is a prototyping system that is compact as well as robust for in-vehicle applications. A PC or a laptop is connected for application download, model parameterization, and data analysis via Ethernet. It also consists of major automotive bus systems such as controller area

network (CAN) which is used to transmit and receive data from controller to other components of interest. The following steps describe how the dSPACE system can be integrated with MATLAB Simulink to work in real-time.

- Model design

    The control logic is first developed in MATLAB Simulink.

- Graphical I/O configuration

    Once the developed control logic is simulated and tested, it has to be implemented on the real-time hardware. This is accomplished by replacing the simulation model with an interface between the controller and actual test platform by configuring I/O blocks such as AIO (analog input-output) and DIO (digital input-output) as given in Fig. 1-1 which form the interfaces to the real controlled system.
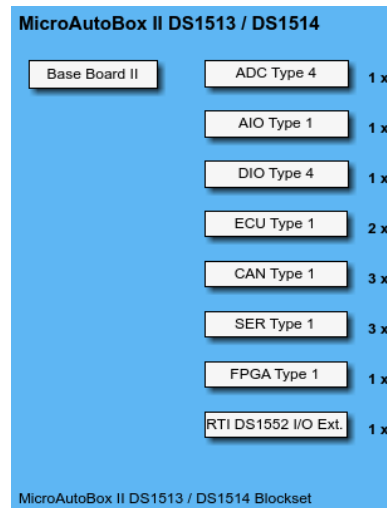
Figure 1-1: dSPACE interface block-set

- Parameter specification

    I/O parameters are specified according to the pin layout of the physical hardware. Other interfaces such as CAN and Ethernet are specified in the same way.

- Implementation of control algorithms on dSPACE platform

    Once the interfacing between the Simulink model and the physical hardware is done, the developed Simulink model is converted to C code through Simulink code generation and compiled. This compiled software is then downloaded into the controller which then can be run in real-time.

- Interaction with experiment software

After the application is implemented, it is run on the real-time hardware. The software control desk by dSPACE provides an instrument panel that accommodates changing of parameters and monitoring of signals without the need for regenerating the code. Also, data of various signals can be recorded for future processing and analysis.

1.3.2 Co-simulation

Simulation is fundamental in mechanical engineering discipline as it gives vital information to the design engineer such as controllability, reliability, and stability. Real-world systems to be modelled generally comprises of multi-domain integrated system components. Available simulation packages for system modelling and integration of components generally cover only one domain while simplifying the others [6]. Hence, the multibody dynamic effects cannot be assessed properly during the simulation stage. Co-simulation overcomes this by merging various software environments and solvers together. Each simulator has its solvers and these simulators are dynamically connected using their input and output variables. Figure 1-1 shows the working methodology of co-simulation. The steps taken to develop the co-simulation model will be discussed in detail in Chapter 3.
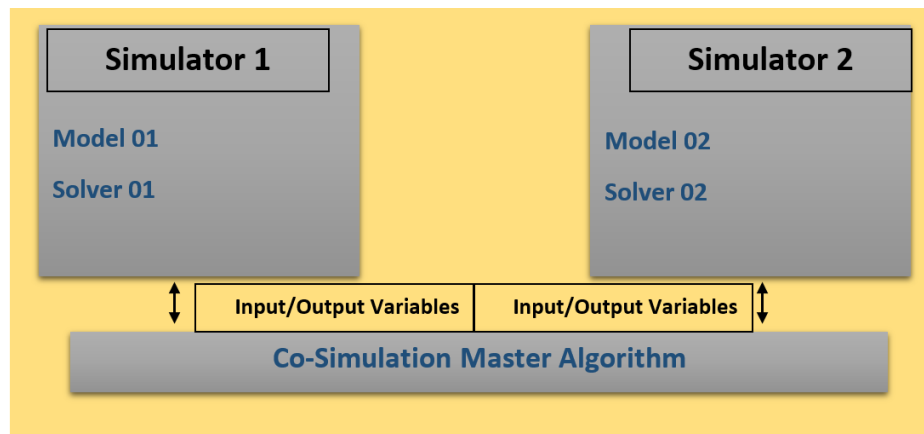
Figure 1-2: Co-simulation environment

To model the multi-domain system for co-simulation the hydraulic system of the excavator was modeled in Amesim. This software offers multi-physics libraries with a focus on modelling and simulation of hydraulic components/systems and mechanical planar models. It is a commercial simulation software for the modelling and analysis of

multi-domain systems. It can be easily integrated with computer-aided design (CAD) software and numerical computing software for analysis and co-simulation.

The control algorithms were developed in the MATLAB/Simulink environment where the analysis of the control performance and its suitability for embedding with the test platform control hardware was carried out.

1.3.3 Software framework

Mutually associated factors for successful excavation were surveyed and studied. To manage these factors, control algorithms comprising of position, contour, and force control were developed as a unified approach for autonomous excavation. The devised controllers were tested for digging and ground leveling, which are the two most common tasks carried out by an excavator.

1.3.4 Stereo vision

A stereo camera can create a three dimensional (3D) map of the area by comparing the distance between the left and right images using its two separate cameras [7]. Using this property of stereo vision, the depth information of the excavation area can be gathered and used for the autonomous properties of the excavator. As a type of stereo camera, the ZED was used to monitor and calculate the deviation between the excavated ground profile and the desired one.

1.3.5 Communication protocols and sensing instrumentation

The communication between the main controller and the host computer is done through Ethernet communication. The developed control algorithms in the Host PC is compiled and deployed into the main controller through Ethernet. Also, control signals are transmitted through the CAN bus interface to actuators. CAN communication is an attractive communication solution for prototype embedded system development due to its low cost, error detection and retransmission, easy light protocol management [8]. The protocol used was SAE J1939 with a baud rate of 250 Kbit/s, which is a standard framework for different electronic systems. In addition, this also allows different ECUs for communication between each other.

In addition to communication protocols, the integration of sensors with the test platform was important to extract vital sensing information required for functioning of the controllers. Linear Variable Differential Transformer (LVDT) sensors were attached to each hydraulic actuator of the excavator which is required for kinematic analysis. Pressure sensors were installed at the inlet and outlet of each hydraulic actuator to calculate the force exerted by each actuator. This information is required as an input to the force tracking algorithm.

Chapter 2. Literature Review

2.1 Introduction

Earthmoving machines such as an excavator are considered to be one of the most important equipment in the construction industry. As shown in Fig. 2-1, the excavator generally consists of the main body that is movable by wheels or steel tracks and a manipulator system in which earthmoving tasks are carried out. Its manipulator system is divided into the boom, arm, and bucket links that are connected by joints for motion. The joint motion is limited to the length of the respective hydraulic actuator stroke.
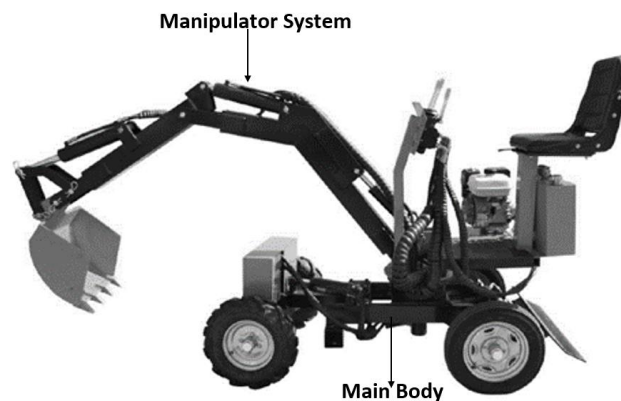
Figure 2-1: A typical mini wheeled excavator

2.2 Autonomous excavation and its challenges

This section describes the challenges of tracking control for autonomous excavation. Unlike the indoor manufacturing robots that perform repetitive tasks interacting with similar material in a confined workspace, construction robots are required to work in random and unstructured environments with many uncertainties and physical obstructions. The detailed explanations on the challenges are provided as follows;

2.2.1 Non-linarites

The excavator has several components that make the system behave in a nonlinear manner. One such nonlinearity existing in the electro-hydraulic proportional valves (EHPV) is the valve dead-band. EHPVs are popular in hydraulic actuator control due to its simple structure and low cost. Dead-band is the range of the control input signal where the valve remains closed. Physically it is the range of valve spool positions where hydraulic

fluid flow is blocked from the pump source to its outputs [9]. This leads to delays and errors in the hydraulic actuation process [10]. The following Fig. 2-2 represents the hysteresis of the EHPV used for this study that is one of the representatives of nonlinear characteristics for the excavator system.
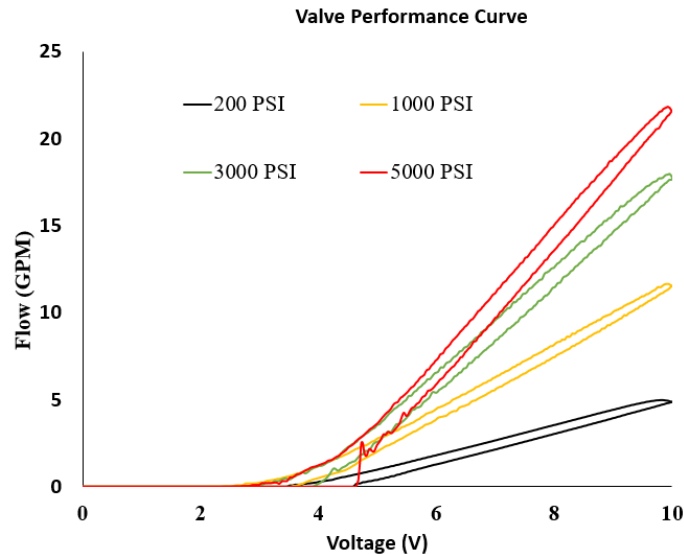
Figure 2-2: Hydraulic valve non-linear hysteresis

Furthermore to this, other inherent nonlinearity's such as friction, fluid leakages, mechanical wear, and other uncertainties exist in the hydraulic system including the hydraulic cylinder actuator. Due to these reasons, adaptive control techniques are required for the motion control of hydraulic actuators to compensate for the uncertainty.

2.2.2 External ground force

It is evident that strict position or trajectory control can only be achieved in low-density media such as air while the resistive ground forces prevent an accurate tracking of trajectory in the ground contact space. Excavators typically must interact with different media such as sand, mud, soil, gravel, fragmented rock, etc. The most crucial problem towards autonomous excavation arises from the fact that it is impossible to accurately model the exact bucket tip and environment interaction. To overcome this issue a form of compliance control is required where the controller tries to modify the end-effector trajectory in compliance of resistive forces acting on the end effector tool [11].

Alternatively, researchers have also try to model the interaction between the bucket and the ground environment [12,13]. The drawbacks of these models are that they can be computationally very expensive due to the nature of its complexity and cannot be used in real-time. Furthermore, a reliable model for the bucket and environment interaction has not yet been achieved.

2.2.3 Unknown dynamics

Motion control of a hydraulic robotic excavator can be difficult due to the highly complex nonlinearities of the manipulator. Apart from this, mechanical structure vibration and other un-modelled mechanical disturbances make the task challenging. Therefore to achieve sufficient earthmoving tolerances a thorough system identification process was required or else extensive tuning of the parameters was required [14].

2.3 Position control

Researchers have studied trajectory tracking as a critical component for autonomous excavation. Although trajectory tracking of the bucket tip is one of the crucial components, it alone is not sufficient for the successful excavation. This is due to, tracking of the bucket tip is more challenging in a higher density media due to high resistive forces. The target of the excavation process is to remove soil rather than follow a predefined path of the bucket tip [15, 16]. As an example, while following a predefined path of the bucket tip during an excavation task, if the bucket is filled to its fullest capacity this accumulated soil needs to be removed first before following the predefined path of the bucket tip. This is another argument to establish that trajectory tracking alone itself is not sufficient for autonomous excavation and hence, should not have the priority. For automated excavation tasks, previous studies have implemented and proposed methodologies to track a desired reference trajectory of the bucket tip as given in Table 2-1.

Table 2-1: Position tracking literature review

Approach	OBJECTIVE	REF.
Fuzzy based controllers	▪ To introduce fuzzy self-tuning in order for better adaptability and compensate for high nonlinearities.	[17]
		[18]

	▪ A hybrid control method which is a fuzzy and PI controller-based method which is termed as fuzzy-proportional-integral soft-switch controller. Results were only based on simulation.	
Artificial Neural Network (ANN) based controllers	▪ To couple RBF Neural Networks with conventional PID controllers to obtain tracking results better than that of a conventional PID controller and to compensate for the highly coupled, multivariable, and non-linear system.	[19]
PI	▪ Used PI controllers for actuator control of an excavator	[20]
	▪ PI control with anti-windup was suggested in simulation	[21]
Optimization	▪ Used the LQR controller combined with the PD controller to compare the performance with the PD controller.	[22]
	▪ To use Genetic Algorithms to obtain the optimal PID gains for better control. However, the authors suggested experimental tracking results are yet sufficiently large due to vibration and other uncertainties.	[23]
	▪ Utilized the PSO algorithm to obtain the optimal PID gains for better control in the simulation model.	[24]
Model Predictive control (MPC)	▪ Presented MPC control techniques for trajectory tracking of hydraulic excavators. MPC was used to take advantage of its optimizing capability to avoid a rapid change in velocity utilizing constraints. However, it is difficult to react to unknown forces exerted by ground conditions.	[25], [26]

Although researchers have proposed various methods for trajectory control of an excavator, the majority of existed methods did not focus on compensating for the resistive ground forces when the excavator performs earthmoving tasks. Hence, force control is one of the crucial components to be encapsulated in the control strategy for tracking control.

2.4 Contour control

Contour control is popular among machining tasks such as CNC machining to achieve the desired machining contour [27]. From this motivation, the same knowledge could be transformed for excavation in a suitable manner. Gound levelling is a skilled earthmoving task where coordinated control of boom, arm, and bucket combined with the operator's perception is required to achieve the levelled surface of the ground. In the ground grading/levelling task, the final finished surface is more important than tracking the desired reference trajectory since other construction tasks such as concreting depends on the accuracy of the achieved final surface. Due to this reason, the reduction of contour error is as important as the tracking error. Hence, contour control can be implied as one of the crucial components for the automation and autonomation of excavators. Figure 2-3 describes and compares contour error with tracking error. Contour error denoted by ε can be described as the shortest distance between the desired trajectory and the current trajectory at any given time [28]. The tracking error (either e_x in x-axis or e_y in y-axis) is the direct vector difference between the desired reference position and the current position of the bucket tip.
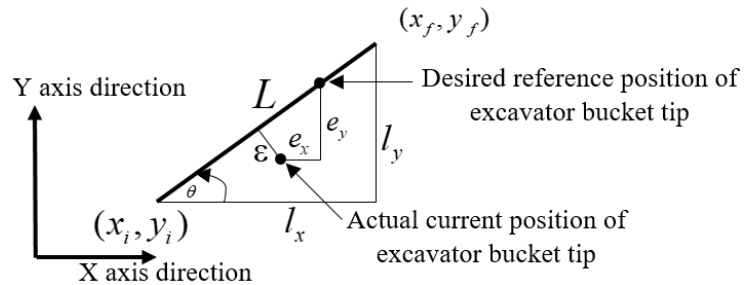
Figure 2-3: Contour error and tracking error

In robotic excavators, the motion of each individual actuator boom, arm and bucket is controlled by separate individual closed loop controllers. However, an individual actuator control does not guarantee the desired output trajectory of the coordinated position tracking of the bucket tip using the boom, arm and bucket actuators combined [29]. Structural differences and load/inertia uncertainties increase the bucket tip tracking error. Hence additional measures for coordinated multi-actuator control should be carried out to reduce the contour error simultaneously. Previous authors [20, 29] have used contour

compensation techniques in the field of autonomous excavation but is very limited compared to position control.

2.5 Force control

Force control can be deemed as the most important factor for hydraulic robots such as robotic excavators. Typically, hydraulic manipulators exert large forces against a physical environment or operate against heavy objects. Although the motive of hydraulic manipulators is to generate force only a few studies exist regarding constrained motion control of hydraulic manipulators [30]. In constrained motion control of manipulators, it is evident that modulation and control to the dynamic behavior of the manipulator are required alongside commanding its position or velocity. Hence, for excavation, it is required to create the counterforce in the direction of resistive ground forces to follow a desired ground cutting profile. This is extremely difficult due to the uncertainties of reactive force occurring from the targeted ground to be excavated, as a result of variation in density, humidity, granularity, and many other properties along with possible obstacles such as roots and stones [31].

Therefore, a compliant control scheme that accommodates both position and force is required. One such method is hybrid position/force control, where the control module comprises of two subspaces, namely the force-controlled subspace and the position-controlled subspace [32]. Accordingly, the controller is required to switch between force control and position control depending on the requirement. Due to this reason, force impedance control can be looked like an option to overcome this obstacle as a unified approach for the bucket tip control in both non-contact and contact space. Impedance control targets to establish a desired dynamic relationship between the end-effector position and contact force [33]. Impedance $I(s)$ in the Laplace domain can be described as given in Eq. (2-1), where $E_F(s)$ is the deviation in force and $E_X(s)$ is the deviation in position. In other words, impedance can be defined as an analogy to convert flow input into an effort output [34].

$$I(s) = \frac{E_F(s)}{E_X(s)} \qquad\qquad (2\text{-}1)$$

Several researchers have proposed the force impedance control [35–37] for earthmoving tasks of excavators but limited attention has been given compared to position control. Impedance control is suited for excavator applications as it can deal with both free and constraint motion.

2.6 Summary

Based on the literature included in this chapter it is clear that improvements can be made to autonomous excavation in-terms of providing an integrative control strategy. The control strategy should take into account force, position, and contour control as they are mutually associated factors for successful autonomous excavation.

1. Position control is a necessity to keep track of the desired bucket tip position. The position controller should be able to react against the inherent nonlinearities of the hydraulic system.
2. Highly non-linear dynamics should be estimated for proper control of the manipulator.
3. Contour control is required for coordinated control of the boom, arm, and bucket links as the final desired ground surface (contour profile) is important than merely keeping a track of the position of the bucket tip.
4. Force control is utilized to act against the resistive forces arising from the ground.

Chapter 3. Prototype Experimental Setup

3.1 Introduction

This chapter describes the development of an experimental setup for research work in the area of autonomous excavation. The integration of hardware, electronics, and software architecture is discussed. The physical prototype consists of 3 main subsystems; namely the hydraulic system, mechanical system, and the electronic system. Each of these subsystems is illustrated to explain its design details. The mechanical system comprises of the main body and the main mechanical links which are fixed on the body. The main mechanical links are the boom, arm, and bucket link. The main components of the hydraulic sub-system are the hydraulic pump, EHPV's, directional control valves (DCV) and the hydraulic actuators. The electronic subsystem includes the main controller, power supply system, electro-hydraulic drivers (EHD) to control the EHPV's and various sensors which also will be discussed. An overview of the full system hardware architecture is represented in Fig. 3-1. Figure 3-2 shows the experimental prototype platform developed for this thesis work as well as improved future experiments. Table 3-1 describes the type, make and model of each main component integrated to the excavator for modification. Furthermore, the importance of each added component required is described in detail in the following section.
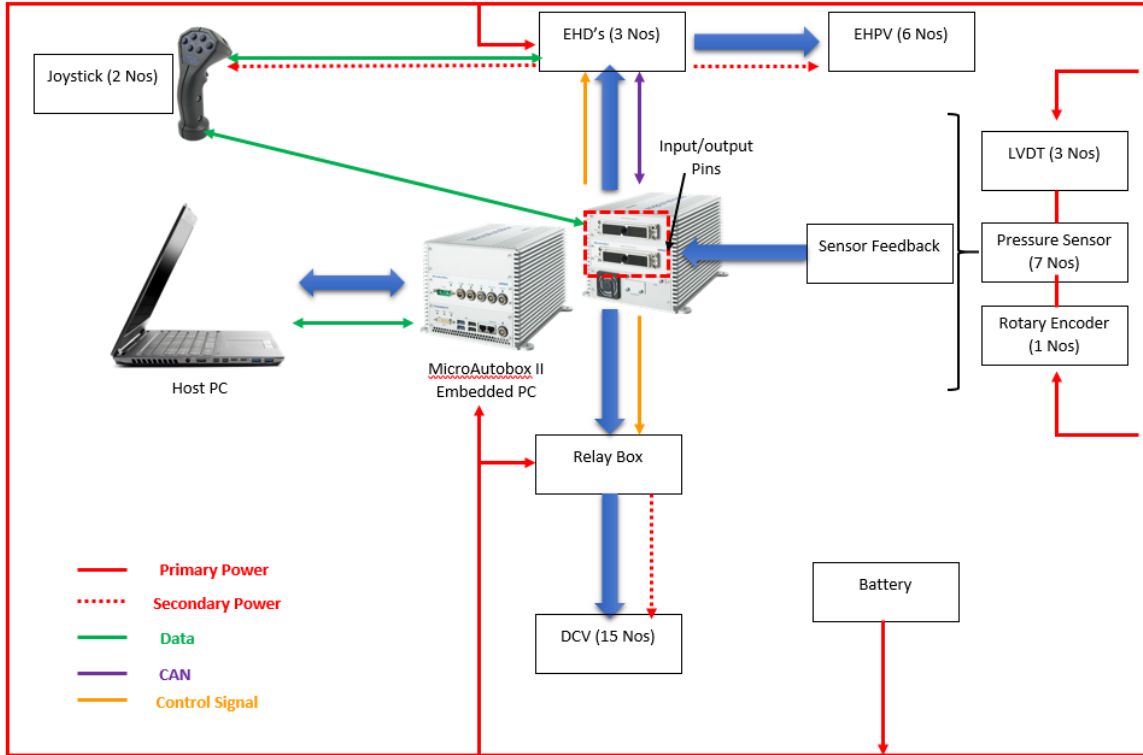
Figure 3-1: Full system hardware architecture

Figure 3-2: Test platform (modified excavator)

Table 3-1: Major components of the test platform

Component	Specification
Host PC	Lambda Tensor-Book, Intel Core i7-8750, 32 GB RAM

Battery	12 V DC	
Controller	Type	Microautobox II Embedded PC
	Processor	Intel® Core™ i7-6822EQ quad-core processor, 4 x 2.0/2.8 GHz, 8 MB cache
	Interfaces	3 × Gigabit Ethernet, 4 × USB 3.0, 1 × DisplayPort, 3 × Mini Card slots for optional WLAN, CAN/CAN FD
	RAM	16 GB DDR4
EHPV	Sun Hydraulics FPBF-XD*	
DCV	Atos solenoid directional valve type DHE-071*-DC	
CBV	Sun Hydraulics 3:1 pilot ratio, ultra-restrictive counter-balance valve	
EHD	Sun Hydraulics XMD	
Hydraulic motor	Type	Marazocchipompe fixed hydraulic pump
	flow	4.8 l/min at 1500 RPM
	Pressure	210 – 250 bars
LVDT	Type	Baluff micropulse linear position transducer BTL2UMJ
Pressure Sensor	Type	Baluff Pressure transmitter BSP00H6
Rotary Encoder	Type	Novotechnik RFC non-contact series RFC-4800

3.2 Mechanical system

As shown in Fig. 3-1, a wheeled-type mini excavator was chosen for modification as it is easily maneuverable to excavation locations for experiments. The mechanical system has the following specifications as shown in the table below.

Table 3-2: Physical specifications of the mechanical system

Description	Specification
Rotation	360°
Steering	Angle: right 30° / left 30° – Radius 3m
Min overall dimensions	$193 \times 95 \times 210$cm or $270 \times 95 \times 150$cm
Weight	550kg (without added components)

3.3 Hydraulic system

The hydraulic system of the developed test vehicle consists of hydraulic actuators, EHPV's, DCV's, hydraulic pump and a hydraulic reservoir. The hydraulic fluid used for the operation is AW 46 hydraulic Oil Fluid (ISO VG 46, SAE 15). Figure 3-1 gives an overview of the hydraulic circuit of the actuator system. The load valve was used to supply pressure from the pump to the other valves. Hydraulic fluid pressure of about 200 bar, using the fixed speed hydraulic motor was supplied for the functions of steering, stabilizer, translation (move forward/back) and the prismatic motions of bucket link actuator, arm link actuator, boom link actuator and rotational motion of the main body. Rotation and translation are done by hydraulic motors and the rest of the functions are driven through hydraulic cylinder actuators.
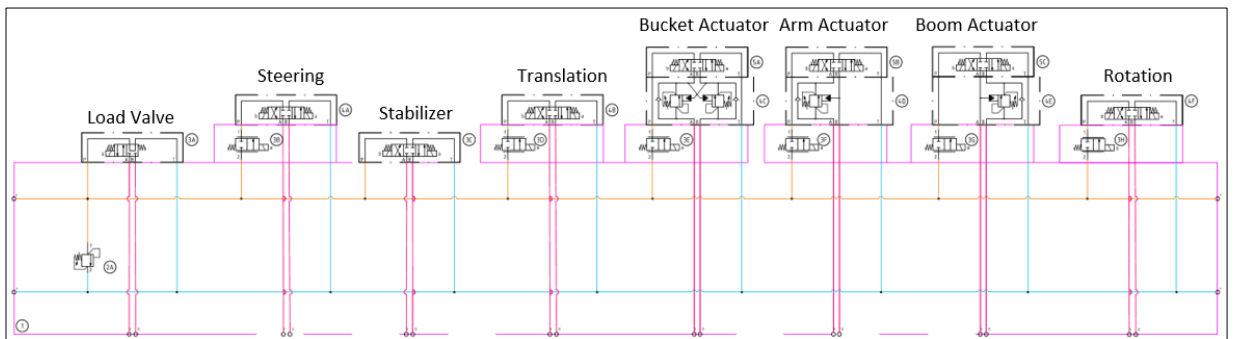
Figure 3-3: Hydraulic circuit of actuator system
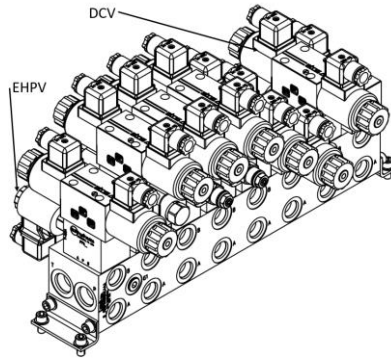
Figure 3-4: Valve module assembly

3.3.1 Hydraulic cylinders

Hydraulic cylinders can generate the largest amount of force compared to other available active actuation methods. Due to this reason excavators are equipped with hydraulic actuators which can mitigate the force exerted from the ground in earthmoving tasks. Figure 3-5 gives the location information of the main links and actuators of the experimental setup. Table 3-3 below shows the main physical specifications of the hydraulic cylinders.
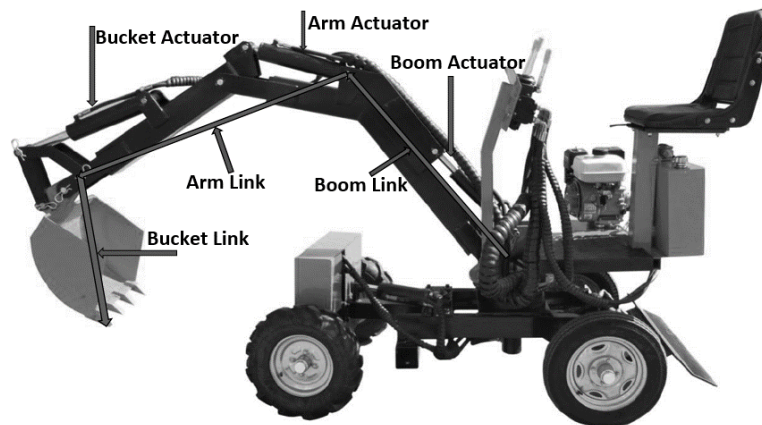
Figure 3-5: Excavator main links and actuators

Table 3-3: Hydraulic actuator specifications

Actuator	Stroke Length (mm)	Head Diameter (mm)	Rod Diameter (mm)	Mass of piston (kg)	Mass of Piston Rod (kg)
Boom	0.263	70	40	3	0.5

20

Arm	0.263	70	40	3	0.5
Bucket	0.263	70	40	3	0.5
Steering	0.263	70	40	3	0.5

3.3.2 Electro-hydraulic proportional valves and directional control valves

EHPV's are widely used in various industrial and mobile hydraulics applications for pressure/flow control applications [38]. The term 'proportional' describes that these valves are operated using proportional solenoids where the output flowrate is modulated according to the input signal [39]. In this work, the EHPV's were used for flow regulation in which a reference position of the hydraulic actuator can be obtained by controlling the spool opening of the proportional valve, which is driven by a solenoid and a position sensor. The DCV's are used for direction control of actuation (extension and retraction) of the hydraulic actuator. The type of DCV's used was 3 position/4 port. Apart from these, counter-balance valves were utilized to ensure stability as well as safety for the vehicle. For heavy hydraulic industrial equipment if the direction of motion and the load direction are the same there is a risk of losing control over the desired motion [40]. This also ensures that the excavator's arm link does not fall due to gravity during a major fluid leakage. To eliminate this hazard a counter-balance valve in a loop can be added as shown in the following Fig. 3-6. In addition, Table 3-4 provides important parameters of the proportional valve obtained for simulation model development.
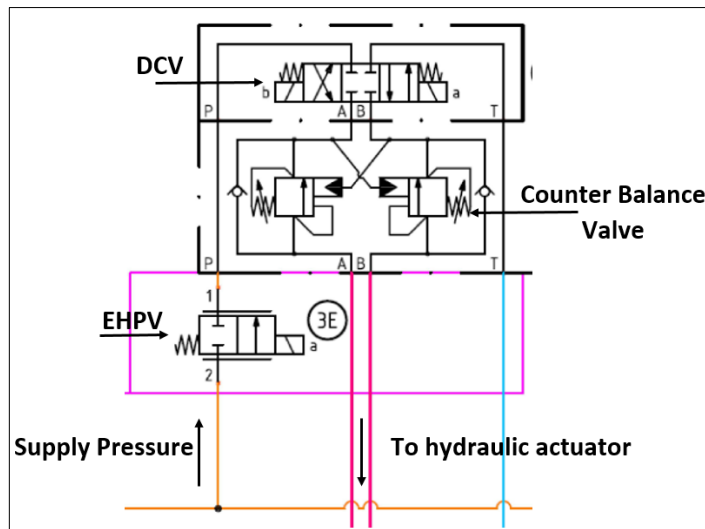
Figure 3-6: Hydraulic valve circuit for bucket link actuator

Table 3-4: Proportional valve parameters

Parameter	Value
Nominal flow rate/capacity	18.9 L/min
Typical cracking pressure	6.9 bar
Max Internal Leakage at 350 bars	0.07 cm^3/min
Dead band as % of current input	48%
Valve Rated Current	590 mA

3.4 Electronic system

Figure 3-7 shows the block diagram of the designed electronic/electrical system. The full schematic diagram of the electronic/electrical system can be found in section Appendix A.
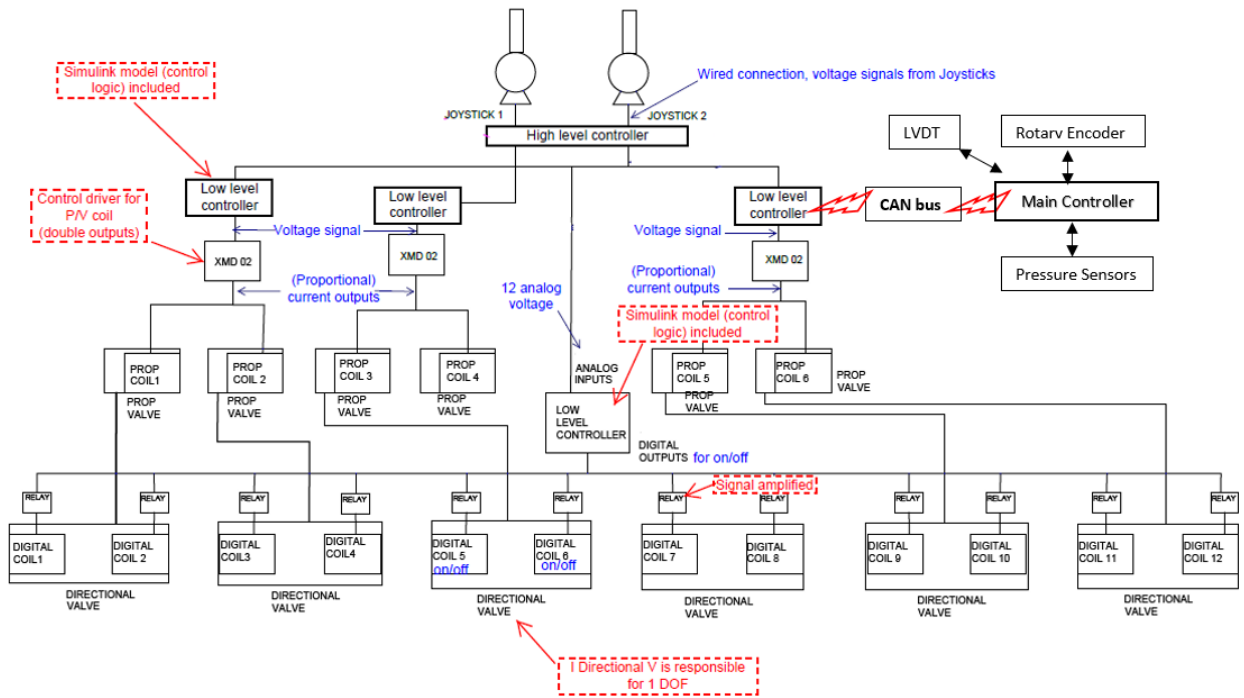
Figure 3-7: Electronic system with sensor integration and actuator interface

3.4.1 Main controller

As the main controller, the Microautobox II embedded PC (dSPACE) was used. The role of the main controller is to perform the actions specified by the control logic in real-time on the physical prototype excavator test platform by processing the sensing information.

3.4.2 Power supply system

A 12V DC battery was used as the main power supply for the system. The battery supplies power to the main controller, EHD's (proportional current amplifiers), relay box sensors, and other instrumentation. Additionally, it can also be used to remotely start the engine as needed.

3.4.2.1 Electro-Hydraulic Drivers

The electro-hydraulic driver supplies current to the EHPV's according to the control signal provided. This controls the hydraulic fluid flowrate to the actuator and thereby directly controls its velocity. The EHD's current amplifiers use CAN protocol to communicate with the controller as well as the EHPV's. Figure 3-9 shows the integration of the EHD with the rest of the electronic system. There is a total of 3 EHD's in the system. Each EHD controls two hydraulic actuators functions as given in Fig. 3-8.
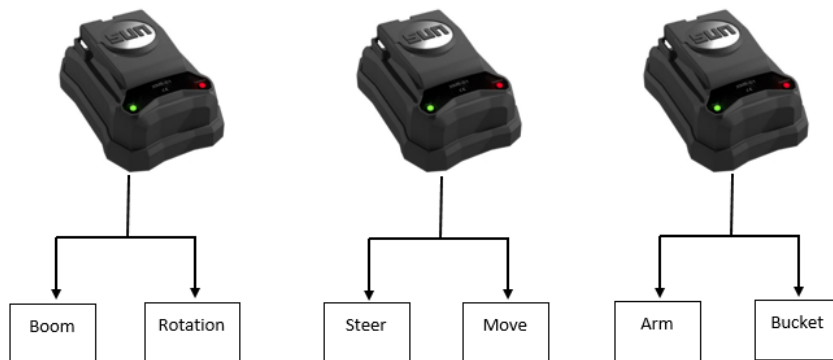
Figure 3-8: EHD to actuator interface
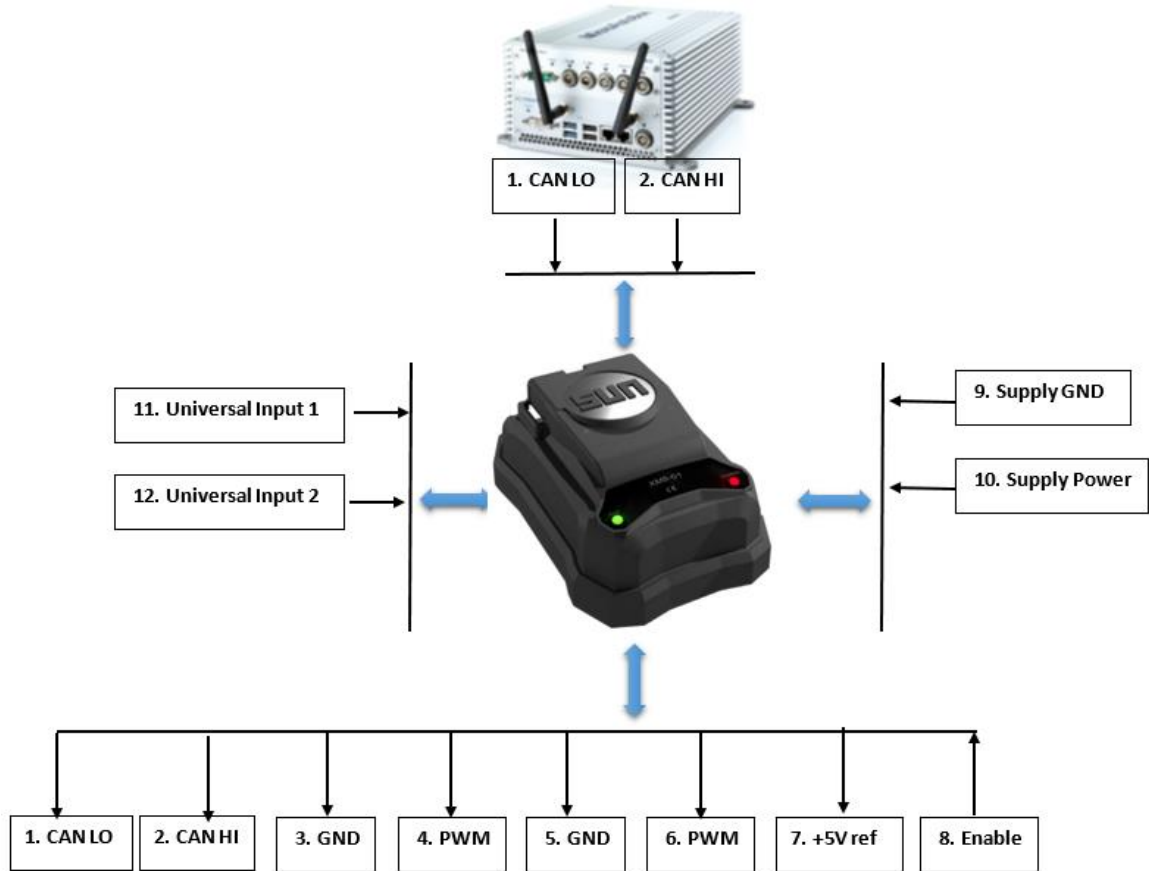
Figure 3-9: Electro-hydraulic driver integration

Table 3-5: EHD functions

Port	**Function**
1. CAN LO	Provide CAN LO Signal
2. CAN HI	Provide CAN HI Signal
3. GND	Provide Ground to EHPV 1
4. PWM	Provide Current to EHPV 1 (0 – 3 A)
5. GND	Provide Ground to EHPV 2
6. PWM	Provide Current to EHPV 2 (0 – 3 A)
7. +5V ref	Provide power to Joystick as 5V source
8. Enable	Logical input from joystick as a safety feature. If this input is not received the current is not supplied to EHPV's and thereby eliminating the motion of the excavator manipulators.
9. Supply GND	Supply ground from battery

10. Supply Power	Supply power from the battery
11. Universal Input 1	Joystick input 1
12. Universal Input 2	Joystick input 2

As explained in Fig. 3-9 and Table 3-5 CAN communication uses two dedicated wires for communication namely CAN high and CAN Low. When the CAN bus does not transmit any signal, both lines output 2.5 V. But when the CAN bus starts to transmit signals the CAN high line reads 3.75 V whereas the CAN low line reads 1.25 V. As shown in Fig. 3-10 this generates a 2.5 V difference between the lines. Since the communication rely on the potential voltage difference of the two lines the CAN bus is not sensitive to electrical fields, inductive noise and other forms of noise making it a suitable and reliable candidate for the application of mobile equipment such as excavators.
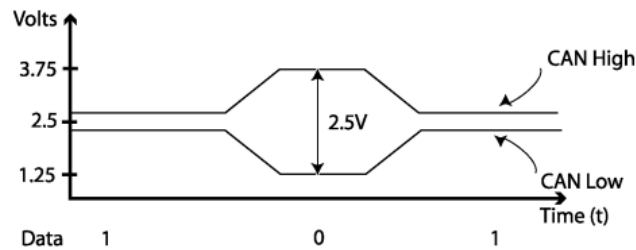
Figure 3-10: CAN data signal

3.4.2.2 Relay box

The purpose of the relay box is to transmit the current to the DCV's according to the logical input provided by the controller. This controls the actuator movement direction and bridges low voltage side to high voltage side. Figure 3-11 shows the integration of the relay box with other system components.
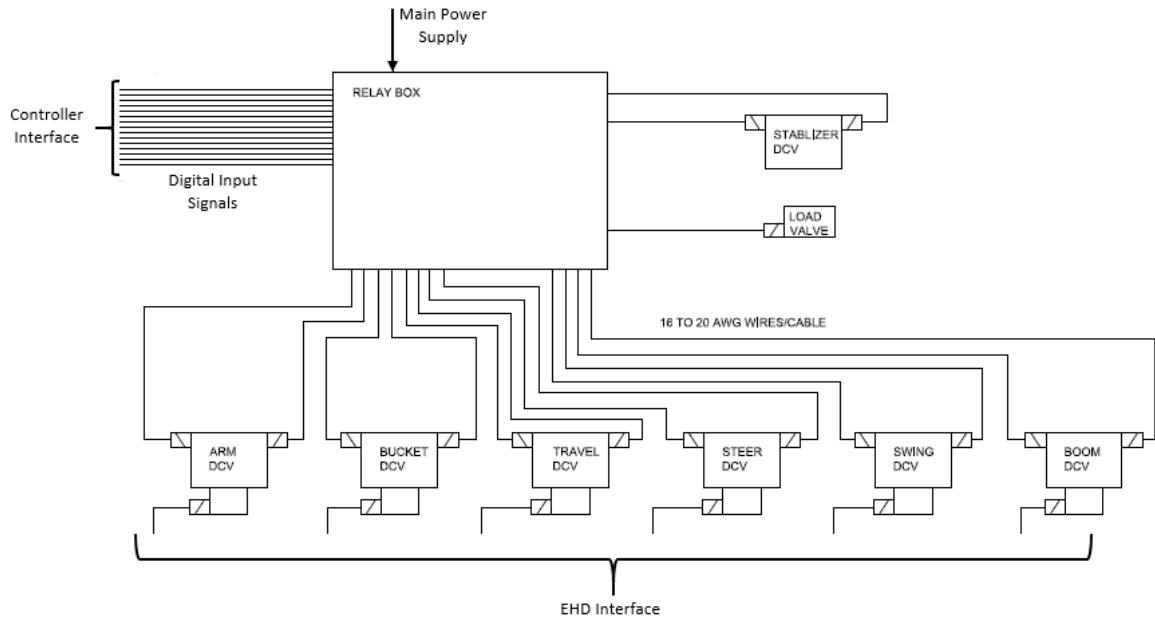
Figure 3-11: Relay box integration

3.4.3 Sensors and instrumentation

3.4.3.1 Pressure sensors

Pressure sensors were used to calculate the force exerted by the boom, arm and bucket actuators as shown in Eq. (3-1) where F_{cyl} is the force exerted by the hydraulic actuator, P_H is the pressure at the piston head side of the actuator, A_H is the area of the piston head side, P_R is the pressure at the piston rod side of the actuator and A_R is the area of the piston rod side. The specifications of the installed pressure sensors are given in Table 3-6. The cylinder force information of each actuator can be converted into joint torques. The control algorithm utilizes this joint torque information to calculate the force required to compensate for the external ground force during excavation and leveling. This force information of each actuator can be used to calculate the torques needed for each joint as given in Appendix B-B2.

Table 3-6: Pressure sensor specifications

Description	Specification
Type	Pressure transmitter
Measurement units	Bar

Measurement range	0 – 600 bar
Input voltage range	8 – 32 V DC
Output voltage signal	0 – 10 V DC

$$F_{cyl} = P_H A_H - P_R A_R \qquad\qquad (3\text{-}1)$$

Figure 3-12: Pressure sensor location

3.4.3.2 LVDT sensors

LVDT sensors were mounted alongside the boom, arm, and bucket actuators to measure the position of each actuator as shown in Fig. 3-8. The strokes calculated by the LVDT sensor can be mapped into joint angles. These joint angles were used for kinematic analysis. Hence, the LVDT sensor is the most important hardware component for kinematic analysis. The current cylinder stroke can be calculated as given in Eq. (3-2). The main specifications of the installed LVDT sensors are given in Table 3-7.

Table 3-7: LVDT sensor specification

Description	Specification
Type	Magneto-strictive linear position sensor
Interface	Analog, voltage
Measuring length	500 mm
Operative voltage	10 – 30 V DC
Output signal	0 – 5 V

$$Stroke_C = \frac{Stroke_{max}}{V_2 - V_1} \times V_C \qquad (3\text{-}2)$$

Where $Stroke_C$ is the current stroke, $Stroke_{max}$ is the maximum possible cylinder stroke, $V_2 - V_1$ is the voltage difference between the maximum position and minimum position of the cylinder, and V_C is the current-voltage reading from the LVDT.
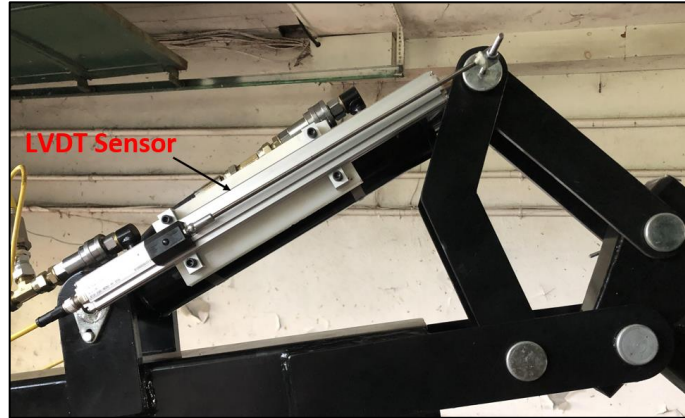
Figure 3-13: LVDT sensor location

3.4.3.3 Rotary encoder

A Rotary encoder was used to measure the yaw angle of the main body. As shown in Fig. 3-14 a contactless rotary encoder was used, where if the position marker is pointing towards the cable the sensor output is near its electrical center position. This was mounted in the center of the body. The earthmoving tasks of an excavator generally occur in 2D space where rotation is not involved. However, when the excavator is required to transfer material from one location to another, it requires rotational movement and hence the rotational position needs to be measured for robotic excavation using a rotary encoder. The main specifications of the installed rotary encoder are given in table 3-8.
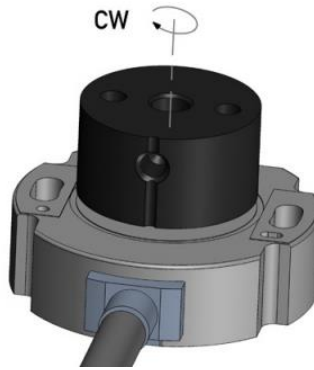
Figure 3-14: Rotary encoder

Table 3-8: Rotary encoder specification

Description	Specification
Type	Non-contact
Output signal	0.5 – 4.5 V
Range	360°
Supply voltage	12 V

3.4.3.4 Stereo vision sensor

As an external stereo vision sensor, the ZED camera was used. This was equipped for the function of determining the deviation of the excavated ground terrain and the desired ground terrain to be excavated. The depth information of the ground terrain was obtained in a point cloud format and mathematical functions were created to obtain this deviation error.

Table 3-9: ZED camera specification

Description	Specification
Type	Stereo vision camera
Depth Range	0.3 – 25 m
Field of view	90° (H) $\times$ 60° (V) $\times$ 100° (D) max
Power	5V / 380 mA

3.5 Summary

In summary, this chapter described the development of a test bench for the research purpose of autonomous excavation. As part of the work carried out in this thesis, the hardware design of a complete electronic system and integration of the test bench were carried out by the author. Electronic hardware integration of the sensors, EHPV's, DCV's, and EHD's was described in detail. EHPV's were added to convert the conventional excavator into an electro-hydraulic controlled system for robotic excavation. EHD's were added to control the EHPV's according to the controller's signal. Pressure sensors, LVDT, and rotary encoder were added to sense force, position and rotational position respectively, which are required as sensing information for the control logic. A host PC was connected with the dSPACE controller to create, compile, and download control algorithms. CAN communication modules were added for communication with the selected sensors and actuators as needed. Also, high-level software functions were developed for utility functions such as driving, steering, emergency stop, and stabilizer control.

Chapter 4. Simulation Model Development

This chapter provides detailed information on the simulation model development including the co-simulation environment. The main sub-topics discussed in this section include kinematic modelling, hydraulic modelling, dynamic modelling, and co-simulation. The mathematical model of each subtopic will be explained with the final simulation model integration.

4.1 Kinematic modelling

The kinematics of an excavator manipulator system can be modelled using the well-known Denavit–Hartenberg procedure as given in [41]. The coordinates $O_0 \rightarrow [X_0, Y_0, Z_0]$, $O_1 \rightarrow [X_1, Y_1, Z_1]$, $O_2 \rightarrow [X_2, Y_2, Z_2]$, $O_3 \rightarrow [X_3, Y_3, Z_3]$ can be represented as given in Fig. 4-1, where $O_4 \rightarrow [X_4, Y_4, Z_4]$ is the tip of the bucket. In addition to this, Fig. 4-2 provides the effective working space of the excavator which illustrates the reachability and kinematic constraints of the experimental setup. Table 4-1 illustrates the kinematic parameters of the experimental setup. Consequently, Table 4-2, provides the D-H kinematic parameters.

Table 4-1: Structural kinematic parameters

Actuator	Link Length (mm)	Joint Constraints (deg°)
Boom	1460.5	-29° to 70°
Arm	869.95	-59° to -155°
Bucket	615.95	-11° to -157°

Table 4-2: D-H kinematic parameters

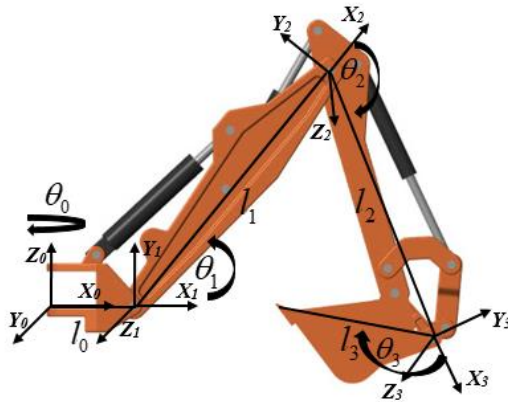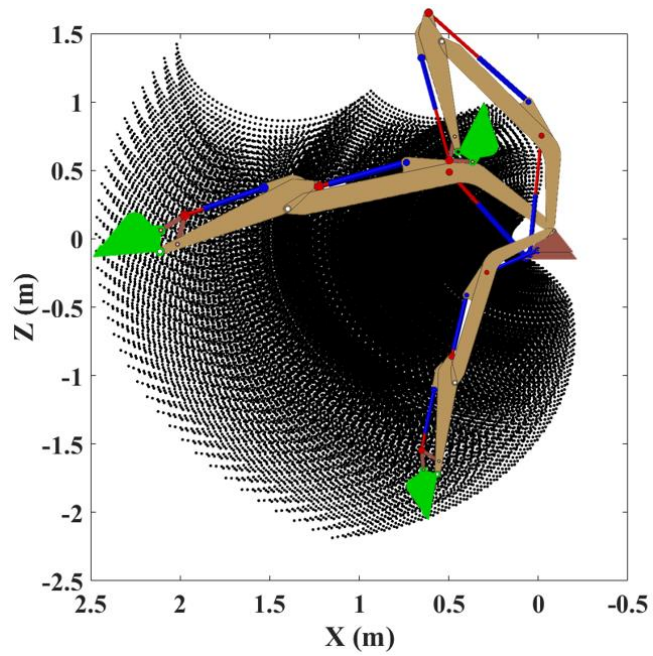| Link i	d_i	a_i	α_i	θ_i
Base	0	0	90°	θ_0
Boom	0	1460.5	0	θ_1
Arm	0	869.95	0	θ_2
Bucket	0	615.95	0	θ_3

Figure 4-1: D-H coordinate system [42]

Figure 4-2: Simulated excavator workspace

As shown in Fig. 4-2, the motion in x-z plane is expressed as Eq. (4-1) using the D-H convention.

$$
{}^1O_4 = {}^1O_2\,{}^2O_3\,{}^3O_4 =
\begin{bmatrix}
C_{123} & -S_{123} & 0 & L_1C_1 + L_2C_{12} + L_3C_{123} \\
S_{123} & C_{123} & 0 & L_1S_1 + L_2S_{12} + L_3S_{123} \\
0 & 0 & 1 & 0 \\
0 & 0 & 0 & 1
\end{bmatrix}
\tag{4-1}
$$

where ${}^1O_2, {}^2O_3, {}^3O_4$ is given as

$$
{}^1O_2 =
\begin{bmatrix}
C_1 & -S_1 & 0 & L_1C_1 \\
S_1 & C_1 & 0 & L_1S_1 \\
0 & 0 & 1 & 0 \\
0 & 0 & 0 & 1
\end{bmatrix},\;
{}^2O_3 =
\begin{bmatrix}
C_2 & -S_2 & 0 & L_2C_2 \\
S_2 & C_2 & 0 & L_2S_2 \\
0 & 0 & 1 & 0 \\
0 & 0 & 0 & 1
\end{bmatrix},\;
{}^3O_4 =
\begin{bmatrix}
C_3 & -S_3 & 0 & L_3C_3 \\
S_3 & C_3 & 0 & L_3S_3 \\
0 & 0 & 1 & 0 \\
0 & 0 & 0 & 1
\end{bmatrix}
$$

Here C_i (i=1,2,3) and S_i (i=1,2,3) represent $cos(\theta_i)$ and $sin(\theta_i)$ respectively. Also C_{123} and S_{123} represent $cos(\theta_1+\theta_2+\theta_3)$ and $sin(\theta_1+\theta_2+\theta_3)$.

The forward kinematics of the excavator bucket tip can be expressed as in Eq. (4-2).

$$
\begin{cases}
x = \cos(\theta_0)[l_3\cos(\theta_1+\theta_2+\theta_3)+l_2\cos(\theta_1+\theta_2)+l_1\cos(\theta_1)] \\
y = \sin(\theta_0)[l_3\sin(\theta_1+\theta_2+\theta_3)+l_2\sin(\theta_1+\theta_2)+l_1\sin(\theta_1)] \\
z = l_3\sin(\theta_1+\theta_2+\theta_3)+l_2\sin(\theta_1+\theta_2)+l_1\sin(\theta_1) \\
\gamma = \theta_1+\theta_2+\theta_3
\end{cases}
\tag{4-2}
$$

where *x, y, z* represents the desired position coordinates of the bucket tip and γ represents the desired orientation of the bucket. Considering the excavator only works in the *x-z* plane when performing earthmoving tasks Eq. (4-2) can be further simplified as Eq. (4-3) using Eq. (4-1).

$$
\begin{cases}
x = l_3\cos(\theta_1+\theta_2+\theta_3)+l_2\cos(\theta_1+\theta_2)+l_1\cos(\theta_1) \\
z = l_3\sin(\theta_1+\theta_2+\theta_3)+l_2\sin(\theta_1+\theta_2)+l_1\sin(\theta_1) \\
\gamma = \theta_1+\theta_2+\theta_3
\end{cases}
\tag{4-3}
$$

Similarly, for a given bucket tip position and orientation the desired manipulator link angles can be calculated using inverse kinematics. Although the excavator system has four degrees of freedom (DOF) that allow the swing and rotational motions with three revolute joints for the boom, arm, and bucket, we considered only 3 DOFs (i.e., revolute

joints) without the swing motion that the representative earth-moving operations such as leveling and digging without dumping require.

The inverse kinematics problem can be challenging due to reachability constraints arising from the joint limitations of the excavator manipulator as a result of the hydraulic actuator's stroke limitation. To avoid this, mostly trajectory planning is done in joint space [43]. However, for autonomous excavation, task space trajectory planning is required to achieve the desired excavation profile without a pre-calculating joint space profile each time. As a solution to this, a MATLAB library (Robotic System Toolbox) was utilized for inverse kinematics consisting of a quasi-Newton algorithm based on Broyden, Fletcher, Goldfarb, and Shanno (BFGS) method.

For the conversion between joint space to Cartesian space, it is required to transform the hydraulic actuator strokes to joint angles. Fig. 4-3 shows the mapped relationship between the hydraulic actuator stroke and the joint angle for each link of the excavator. Appendix B1 provides the full kinematic equations used to map between the joint space and the Cartesian space of the excavator. Furthermore, the kinematics of the four-bar mechanism attached to the bucket which is responsible for driving the bucket link is also provided.
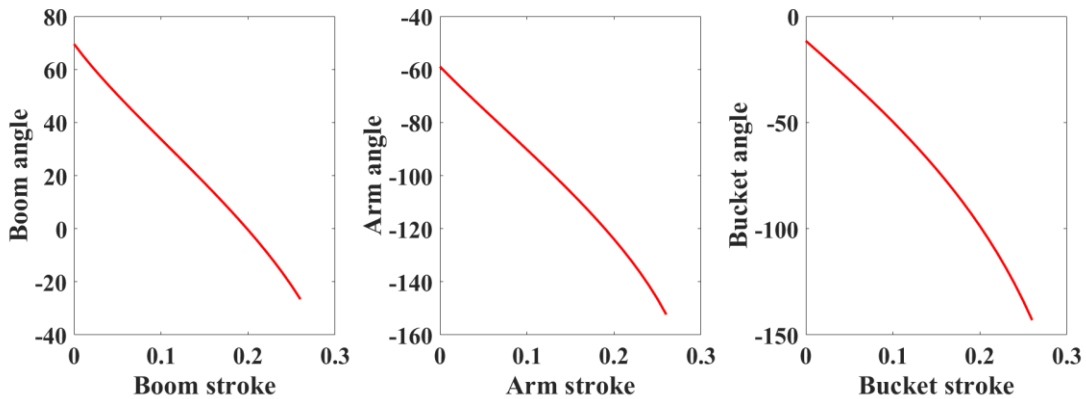
Figure 4-3: Hydraulic actuator stroke to angle mapping

4.2 Hydraulic system model

4.2.1 Mathematical model

The main two components of the hydraulic system are the EHPV and cylinder model. As shown in Fig. 4-3 the close loop integrated EHPV and cylinder model works in a way such that a desired control signal voltage for a target reference position of the cylinder is generated which is converted to current using a proportional current amplifier. This amplification stage can be modelled as a proportional stage as shown in Eq. (4-4). This current controls the valve spool displacement by opening and closing which controls the hydraulic fluid through the valve.

$$i_v = K_a u \tag{4-4}$$

where i_v is the amplified output current to the valve, K_a is the proportional current amplifier coefficient, and u is the input control voltage generated by the controller.
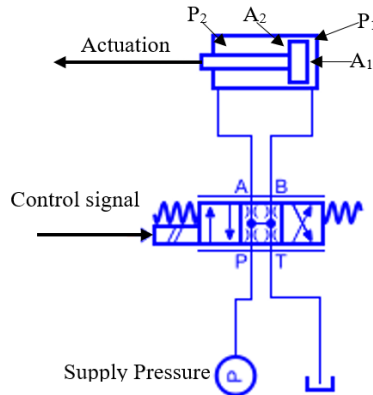
Figure 4-4 Hydraulic valve and cylinder model

A linearized load flow equation for the EHPV can be obtained as expressed below in Eq. (4-5) using a Taylor Series Linearization [44]. It is assumed that the valve is assembled with ideal zero lapping and zero opening, and is matched symmetrically [24].

$$Q_{Lv} = K_q x_v - K_c P_L \tag{4-5}$$

where Q_{Lv} is the flow across the servo valve, K_q is the valve flow coefficient, K_c is the valve flow-pressure gain, x_v is the spool servo valve displacement and P_L is the load pressure

given as $P_L = P_1 - P_2$ where P_1 is cylinder head side pressure, and P_2 is cylinder rod side pressure. The flow continuity equation for cylinders can be expressed as

$$Q_{LP} = C_{tp}P_L + A_p\dot{x}_p + \frac{V_e}{4\beta_e}\dot{P}_L + Q_{tad} \tag{4-6}$$

where Q_{LP} is the flow continuity of cylinder, A_P is the equivalent piston area, and x_P is the piston position of the cylinder. C_{tp} is the total leakage coefficient, V_t is total cylinder volume, V_e is the equivalent cylinder volume, Q_{tad} is any other additional leakage flow, and β_e is the effective bulk modulus of the hydraulic oil.

Using the load force of inertia, external forces, viscous friction, and elastic force, the dynamic model of the cylinder can be expressed as given in [45]. Hence the force equation for the cylinder has the form of Eq. (4-7).

$$A_P P_L = M_t \frac{d^2 x_p}{dt^2} + B_p \frac{dx_p}{dt} + F_L + K_S x_p \tag{4-7}$$

where M_t is the gross mass of piston and load, B_P is the viscous damping coefficient, F_L is the external disturbance, and K_s is the spring constant.

Similarly, the dynamics of the proportional valve can also be expressed as given in Eq. (4-8)

$$\frac{d^2 x_v}{dt^2} + 2\delta_v \omega_v \frac{dx_v}{dt} + \omega_v^2 x_v = K_a K_v \omega_v^2 u \tag{4-8}$$

where δ_v is the valve damping ratio, ω_v is the valve natural frequency, K_a is the proportional amplification coefficient, Kv is the gain of spool displacement-current (m/A), u is the valve control signal, and x_v is valve spool position. Using the Eq. (4-5) and (4-6) we can take the Laplace transformations and express the load pressure PL as given in Eq. (4-8).

$$P_L = \frac{K_q X_v - A_p S X_P - Q_{tad}}{K_c + C_{tp} + \frac{V_e}{4\beta_e}s} \tag{4-9}$$

By taking the Laplace transform of Eq. (4-8) and substituting the load pressure P_L into Eq. (4-8), we can obtain a relationship between the cylinder piston position and the valve spool position can be obtained as a transfer function $Z_1(S)$ given below

$$Z_1(s) = \frac{X_P}{X_v} = \frac{\dfrac{K_q}{A_P}}{s\left(\dfrac{s^2}{\omega_h^2} + \dfrac{2\xi_h s}{\omega_h} + 1\right)} \tag{4-10}$$

where $\omega_h = A_p \sqrt{\dfrac{4\beta_e}{V_e M_t}}$ and $\zeta_h = \dfrac{K_{ce}}{A_P} \sqrt{\dfrac{\beta_e M_t}{V_e}}$

Similarly, by taking the Laplace transform of Eq. (4-8) the relationship between the valve spool position and the input control signal could be obtained as given below in Eq. (4-8).

$$Z_2(S) = \frac{X_v}{U} = \frac{K_a K_v}{\dfrac{s^2}{\omega_v^2} + \dfrac{2\delta_v s}{\omega_v} + 1} \tag{4-11}$$

By using these two transfer functions $Z_1(s)$ and $Z_2(s)$, we can obtain the final desired relationship between the desired cylinder position and the input control signal to the EHPV $G(s)$ as

$$G(s) = \frac{X_p}{U} = Z_1(s).Z_2(s) \tag{4-12}$$

4.2.2 Amesim model

The developed mathematical model was converted into an Amesim model to represent the hydraulic dynamics. In comparison to a pure mathematical model, an Amesim model can provide a more realistic simulation model for hydraulic applications. This is achieved by incorporating details that are not easy to incorporate into the mathematical model. As an example, the EHPV's characteristics such as pressure drop across each input/output port, hysteresis information, and leakage can be defined. Furthermore, each component in the Amesim model as a 1D model can be simulated independently with its

input and parameters. As a result, the model can give an accurate simulation of the system by taking interactions of the various components with each other into account [46].

This section describes the development of the hydraulic model in Amesim for co-simulation. A detailed procedure of the hydraulic system modelling is described as follows.

The physical components of the developed CAD model in Siemens NX environment are imported into the Amesim environment as shown in Fig. 4-5, which is then integrated with the hydraulic system.
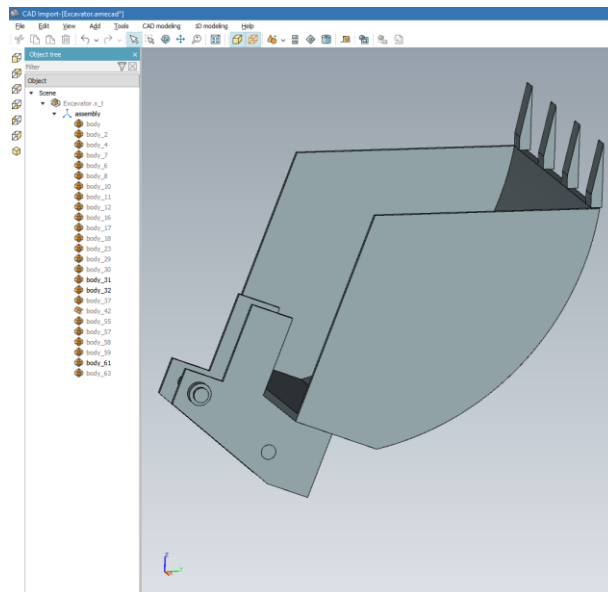
Figure 4-5: Import of physical component into Amesim environment

Figure 4-6 depicts the modelling of the arm actuator system. The same strategy was applied when modelling the boom and bucket actuators. Since the EHPV's, CBV's, DCV's, and actuators are the same the hydraulic system has the same modelling framework. The hydraulic loop consists of the EHPV where at port P the pump pressure is applied, and the return line is connected to a hydraulic reservoir through port T. The cylinder head side and rod side are connected to ports A and B using hydraulic hoses. Apart from this a CBV is added in between the cylinder and the EHPV to follow the dynamics of the prototype test platform. The main parameters used for modelling each hydraulic component is described in Table 4-2.
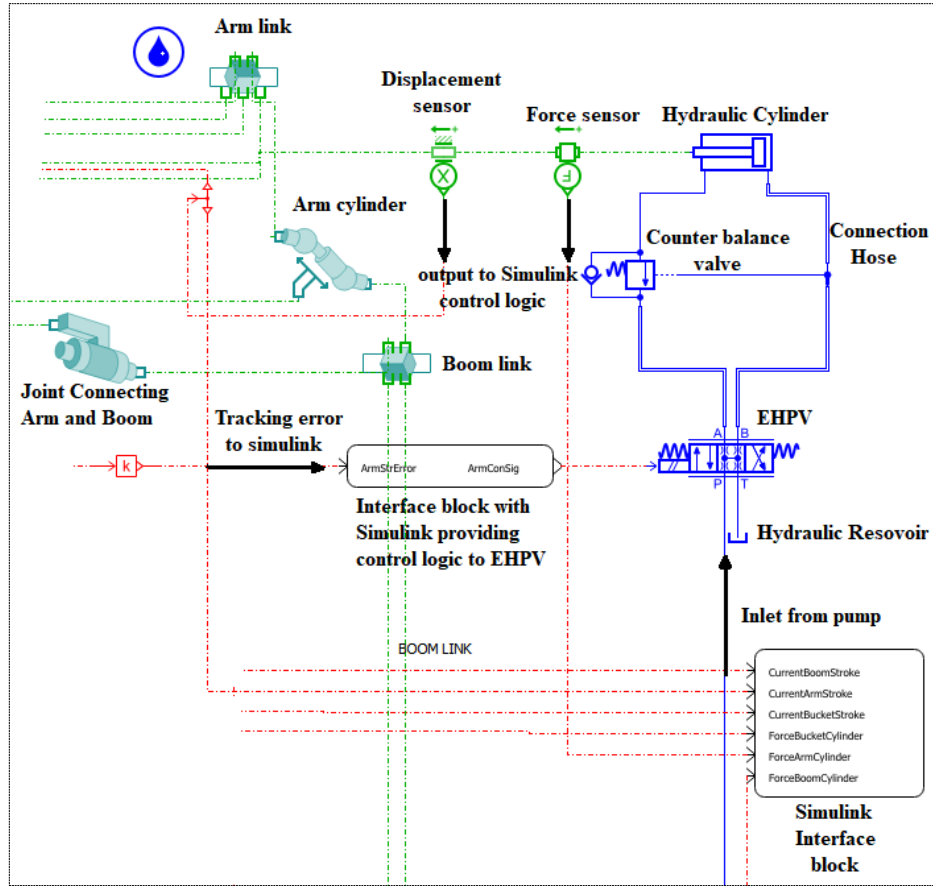
Figure 4-6: Arm actuator system Amesim model

Each actuator system is developed as explained in Fig. 4-5 and combined to form the complete hydraulic system. This system is then merged with the physical dynamic model as shown in Fig. 4-7. Finally, the complete integrated Amesim model is represented in Fig. 4-8.
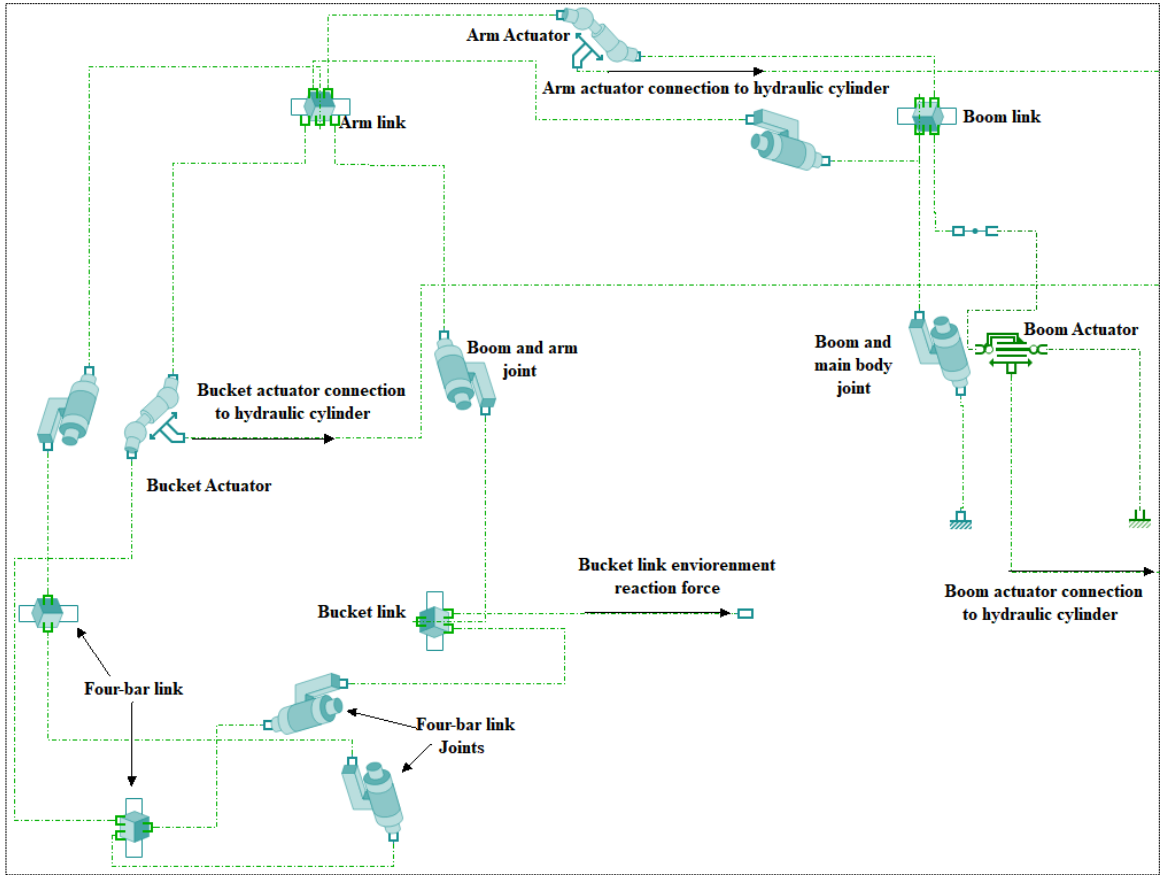
Figure 4-7: Excavator physical model in Amesim

Table 4-3: Main hydraulic component parameters

Component	Description	Specification
EHPV	Valve rated current	590 mA
	Dead band as a fraction of spool travel	0.48
	Dynamics	
	Valve natural frequency	80 Hz
	Valve damping ratio	0.8
	Pressure drop characteristics	
	characteristic flow rate at maximum opening	18.9 L/min
	corresponding pressure drop (cracking pressure)	14 bar
	critical flow number (laminar/turbulent)	1000
Hydraulic reservoir	Tank pressure	1 bar
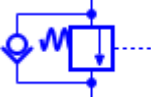
Hydraulic actuator	Piston diameter	70 mm
	Rod diameter	40 mm
	Length of stroke	0.263 mm
	Dead volume at piston side	50 cm^3
	Dead volume at rod side	50 cm^3
	Viscous friction coefficient	100000 Nm^{-1}s^{-1}
	Leakage coefficient	0.05 Lmin^{-1}bar^{-1}
	Spring rate at end stops	100000 Nmm^{-1}
	damping coefficient on end-stops	100000 Nm^{-1}s^{-1}
	deformation on end-stops at which damping rate is fully effective	0.001 mm
CBV	setting pressure	115 bar
	pilot differential pressure for maximum opening	14 bar
	characteristic flow rate at maximum opening	9.46 L/min
	corresponding pressure drop	5 bar
	critical flow number (laminar/turbulent)	1000
	cracking pressure	1 bar
	flow rate pressure gradient	10 Lmin^{-1}bar^{-1}
	characteristic flow rate at maximum opening (check valve)	9.46 L/min
	corresponding pressure drop (check valve)	5 bars
Connection hose	section type	Circular
	diameter	25 mm
	length	1m average

Table 4-3 provides the main parameters of the dynamic model integrated with the hydraulic system.

Table 4-4: Main dynamic component parameters

Component	Description	Specification (kg/mm^2)
Boom link	moment of inertia around Gx axis	18.5043

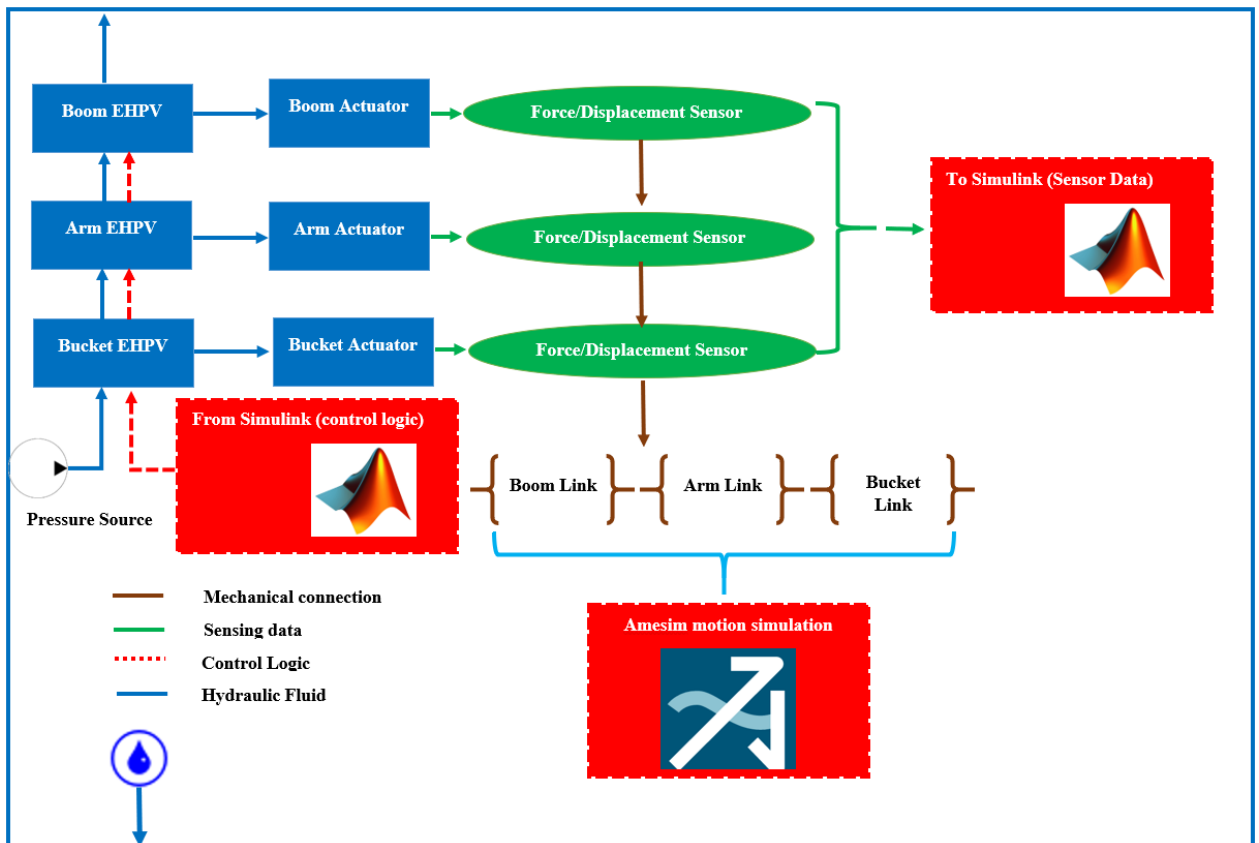|		
	moment of inertia around Gy axis	9.2385
	moment of inertia around Gz axis	9.4694
Arm link	moment of inertia around Gx axis	1.0256
	moment of inertia around Gy axis	1.0190
	moment of inertia around Gz axis	0.0585
Bucket link	moment of inertia around Gx axis	0.6156
	moment of inertia around Gy axis	1.1398
	moment of inertia around Gz axis	0.7967

Figure 4-8: Complete Amesim model framework

4.3 Dynamic model

For the development of a multi-domain simulation model, a CAD model of the test platform was developed to couple the dynamics when simulating control algorithms. The

42

developed CAD model in Siemens NX environment is shown in Fig. 4-9. The CAD model was developed to have inertia properties as given in Table 4-2.

Figure 4-9: CAD model

The dynamic equation of motion for a manipulator such as an excavator is well known and is presented in [37, 47, 48] and can be expressed in general as below in Eq. (4-13).

$$D(\theta)\ddot{\theta} + H(\theta,\dot{\theta}) = \tau(\theta) - \tau_e(\theta) \qquad (4\text{-}13)$$

where $D(\theta)$ is an $n \times n$ inertial matrix, $H(\theta,\dot{\theta})$ is an $n \times 1$ combined Coriolis, centrifugal and gravity vector. $\tau(\theta)$ is the $n \times 1$ joint torque vector generated by the manipulator, and $\tau_e(\theta)$ is the external joint torque applied to the manipulator by the environment.

Due to the complexity of manipulators such as the excavator, it is hard to obtain the information described in Eq. (4-13), to obtain a calculated control input. Researchers in robotics have addressed this issue to mitigate the dynamic uncertainties. The time-delayed control method (TDC) is one of the ways that this uncertainty can be minimized. Time-delayed control is recognized as an effective and practical method for controlling robot manipulators. For the TDC scheme, the following should be taken care of [49]

- The sampling time should be fast enough to satisfy the control action to be continuous.
- Estimation of acceleration signals
- Selection of inertia matrix

Eq. (4-13) can be rearranged as Eq. (4-14) to represent the required torque:

$$\tau(\theta) = D(\theta)\ddot{\theta} + H(\theta,\dot{\theta}) + \tau_e(\theta) \tag{4-14}$$

This can be again simplified as introducing a constant diagonal matrix $\tilde{D}(\theta)$ [50], which is an estimation of the matrix $D(\theta)$.

$$\tau(\theta) = \tilde{D}(\theta)\ddot{\theta} + N(\theta,\dot{\theta},\ddot{\theta}) \tag{4-15}$$

where $N(\theta,\dot{\theta},\ddot{\theta})$ is the summation of all the nonlinear dynamics representation of the manipulator given as;

$$N(\theta,\dot{\theta},\ddot{\theta}) = (D(\theta) - \tilde{D})\ddot{\theta} + H(\theta,\dot{\theta}) + \tau(\theta) \tag{4-16}$$

Considering Eq. (4-15) we can estimate $N(\theta,\dot{\theta},\ddot{\theta})$ in time domain if the sample time is sufficiently small as given below in Eq. (4-17). Generally, in the discrete-time control, the sufficiently small sampling time is selected [51].

$$N(\theta,\dot{\theta},\ddot{\theta})_t \approx \tau(\theta)_{t-\delta} - \tilde{D}\ddot{\theta}_{t-\delta} \tag{4-17}$$
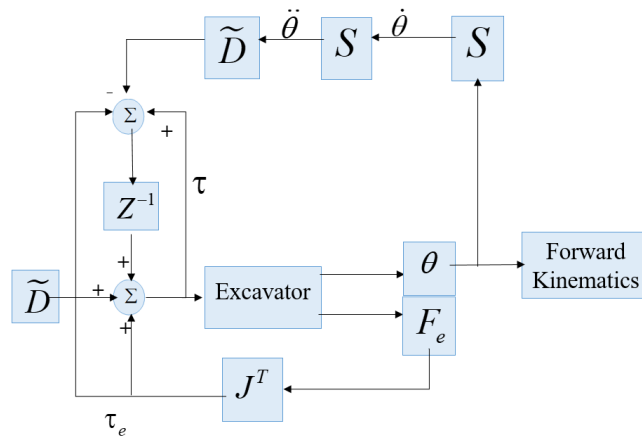

Figure 4-10: TDC block diagram

$\tilde{D}$ is an $n \times n$ diagonal estimated matrix of $D(\theta)$ and δ is the sample time. This method can be used to estimate the unmolded dynamic components given that the inertia of the excavator does not change suddenly. Since the movement of excavator links are much slower and steady compared to other robotic manipulators, this method can be adopted. The stability bound to estimate a dynamic matrix has been documented as [52–54] given in Eq. (4-18) below where D is the real inertia matrix and $\tilde{D}$ is the user-specified constant matrix.

$$\| I - D^{-1}\tilde{D} \| < 1 \tag{4-18}$$

To accommodate this method for the application of autonomous excavation Eq. (4-14) can be written as [55] in the actuator space where $l \in \mathbb{R}^3$ is the hydraulic actuator displacement.

$$F_e(l) = D(l)\ddot{l} + H(l,\dot{l}) + F(l) \tag{4-19}$$

The Force balance equation for the hydraulic actuator is well known and is given as:

$$F = A_h P_h - A_r P_r \tag{4-20}$$

where A_h, P_h, A_r, P_r represent the hydraulic actuator head side area, head side pressure, rod side area, and rod side pressure.

More generally, the joint torques to actuator force can be given as [56]:

$$\tau = J(\theta)^T F \tag{4-21}$$

where the Jacobian matrix of the excavator $J(\theta)$ relates the actuator forces to the joint torques. By substituting Eq. (4-20) to Eq. (4-21) we obtain

$$\tau = J(\theta)^T (A_h P_h - A_r P_r) \tag{4-22}$$

4.4 Integrated simulation model for co-simulation

The separate simulation analysis of a coupled system such as an excavator which is composed of hydraulic, mechanical and control systems can be inaccurate [57]. Due to this reason co-simulation is the better choice for the simulation study. The co-simulation

45

was run between MATLAB Simulink and Simcenter Amesim. Figure 4-11 shows the configuration for co-simulation between these two platforms. Amesim which is a specialized software package for multi-physics simulation focusing on hydraulics [58], consisted of both hydraulic and imported dynamic properties of the simulation model. The dynamic properties of the excavator were imported into the Amesim model from the developed CAD model. The dynamic model was developed in NX by Siemens. It is an advanced high-end commercial software for CAD/CAM/CAE applications. Sufficient dynamic properties were extracted from the developed CAD model such as inertia which is vital for simulation model development. The imported CAD model is then defined by kinematic pairs and constraints. The most significant component focused on this study, which is the control model was developed in Simulink. Since the main contribution is to develop control algorithms, Simulink was selected as the master platform whereas Amesim was the slave platform. A sample time of 0.01 was used with ode15s (Stiff/NDF) type solver which is suitable for stiff hydraulic systems.
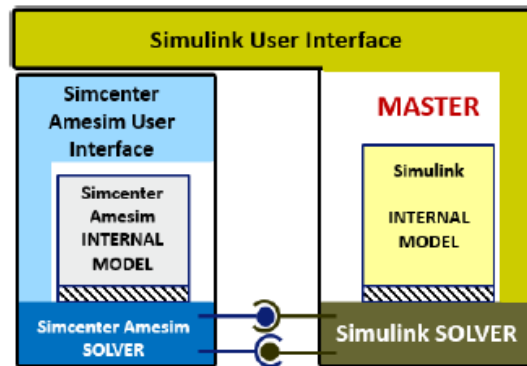
Figure 4-11: Co-simulation interface of the simulation model

By developing this setup, the following advantages were explored in the process of developing the complete simulation model for the excavator.

(1) Was able to fully utilize the two software simulation packages where Amesim focuses on the hydraulic, dynamic component simulation and Simulink focuses on the control component simulation.

(2) Unique features of modelling, simulation, and analysis capabilities of both software packages could be used simultaneously.

(3) Both the software packages can run in their solver type suitable for each domain.

(4) Finally, realistic simulation results could be obtained compared to those of mathematical model simulation.

The co-simulation methodology is expressed in Fig. 4-12. Interface blocks are constructed in the Amesim environment for variable exchange. The constructed Amesim model is converted into a Simulink S-function. This constructed S-function can then be imported and used within the Simulink environment. The advantage of this interface is that many of the Amesim facilities can still be used while the model is running in Simulink.
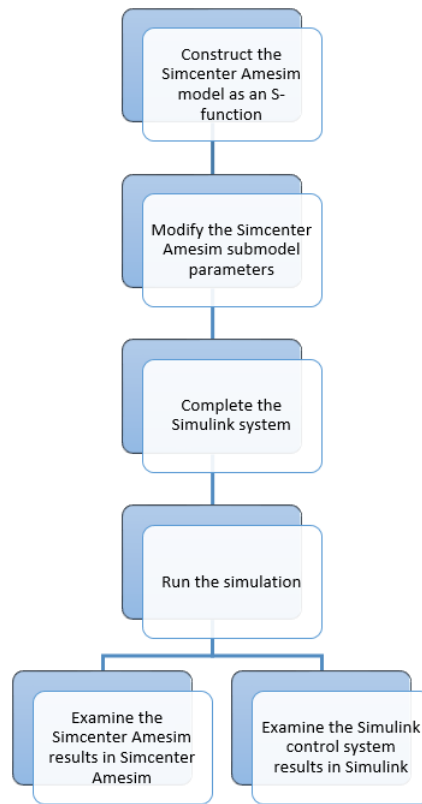
Figure 4-12: Co-simulation methodology

4.5 Summary

In summary, this chapter describes the development of the simulation model required for the controller design. A multi-domain simulation model was developed to test the designed control algorithms described in Chapter 5 and provided a foundation that can be extended for experimental validations using a real-world system. As a core component of the developed simulation model, kinematic, hydraulic, and dynamic models were

introduced. Finally, the integration of the sub-models for co-simulation was presented. The structure of the developed overall simulation model can be seen in Fig. 4-10.

Figure 4-13: Co-simulation model framework

Chapter 5. Control strategy

This chapter describes the control algorithms adopted to control the excavator manipulator.

5.1 Position control

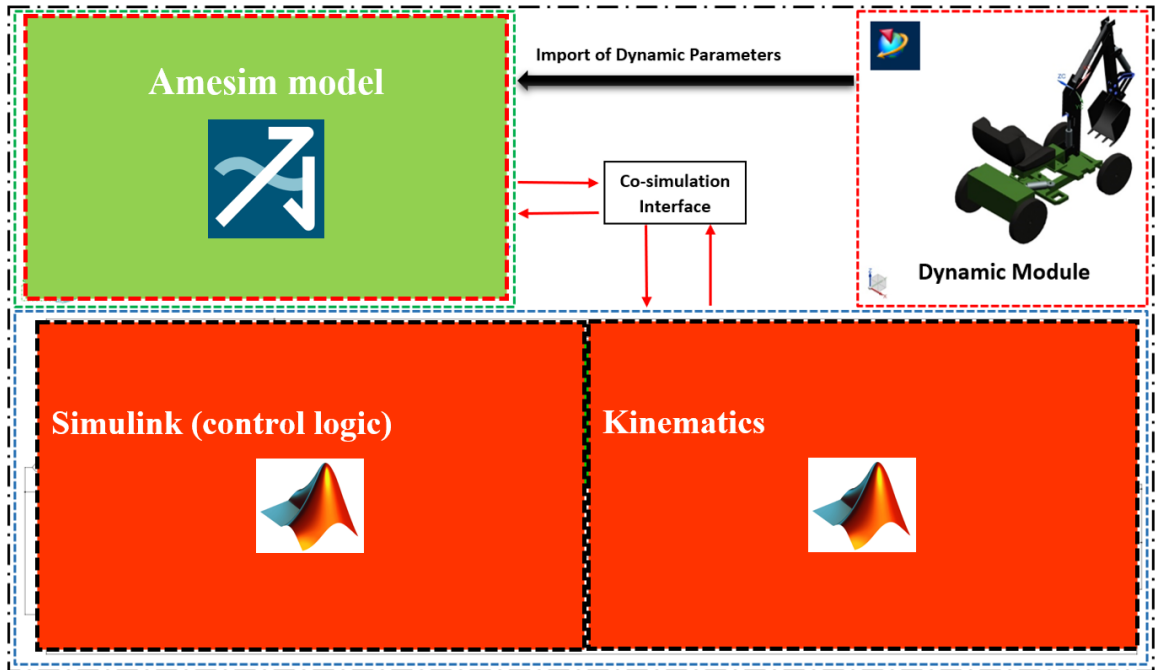Precise Position control of the hydraulic actuators can be challenging due to various reasons as discussed. The inherent dynamic uncertainties such as friction, valve dead zone, fluid leakages, and other uncertainties make this task difficult. Considering this, the position controller of a hydraulic cylinder should demonstrate the following characteristics [59]:

- It should exhibit both tracking and regulating abilities.
- Should be able to react to quick changes in reference point despite the said nonlinear characteristics.
- When the actuator is in the need to change direction, it should be able to do so quickly while minimizing the overshoot.

A nonlinear PI controller was applied to achieve the above properties for non-linear hydraulic actuator control [29, 59]. This is because the PI control scheme enables more robust stability compared to the PD control that rapidly changes outputs, and thus results in noisy outputs [59]. Therefore, the PI controller is more suited for the earthmoving tasks using an excavator that require not speedy but stable motions against mechanical vibrations and resistive ground forces. The integral term of the adopted NPI controller is different from the normal PI controller because it changes with the sampling time. Equation (5-1) below shows the integral component of this adopted NPI controller.

$$I_t = (I_{t-\delta t} + e\delta t + K_a \ddot{\theta}_d \delta t) \frac{a}{a + \dot{e}^2} \qquad (5\text{-}1)$$

where δt is the sampling time, e is the error, $\ddot{\theta}_d$ is the target angular acceleration, and K_a and a are constants. The rate varying factor $\frac{a}{a + \dot{e}^2} = 1$ when $\dot{e} \rightarrow 0$ and, $\frac{a}{a + \dot{e}^2} < 1$ when $\dot{e} \neq 0$. The value a determines the converging behavior of I_t. This tries to minimize the

issues associated with the integration of windup and saturation of actuators. Also, $\ddot{\theta}_d$ is used to further minimize the overshoot as the integral term is slow to change when velocity is changing. In other words, the integral is slow to approach zero when the desired velocity setpoint is approached to zero. $\ddot{\theta}_d = 0$ if $\ddot{\theta}_d \cdot \dot{\theta}_d \geq 0$ and, $\ddot{\theta}_d = \ddot{\theta}_d$ if $\ddot{\theta}_d \cdot \dot{\theta}_d < 0$. Table 5-1 provides the controller gains used for position control.

Figure 5-1 shows the closed-loop system for the NPI controller where feedback is taken by the LVDT sensor.
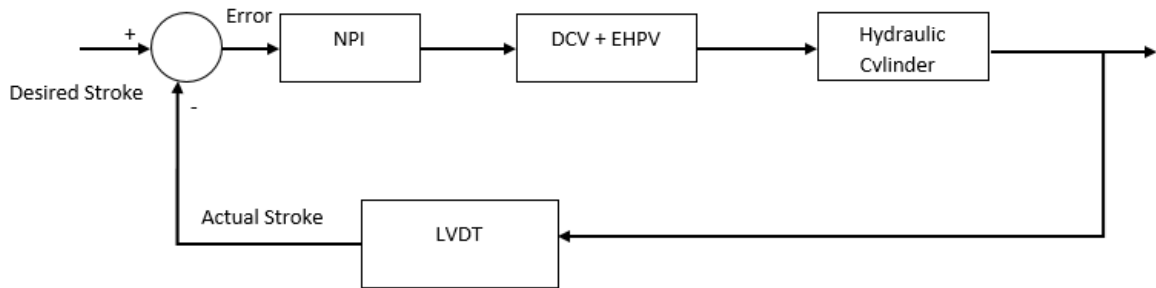

Figure 5-1: Closed-loop NPI controller

Table 5-1 provides the controller gain parameters used for the experimental work carried out in Chapter 7. Here, K_P and K_I are the proportional and integral terms, respectively.

Table 5-1: Control parameters for position controller

Parameters	Boom	Arm	Bucket
K_P	15.4375	11.4125	11.4125
K_I	0.5	0.3	0.3
K_a	1	1	1

5.2 Contour control

The goal of contour control is to reduce the contour error of the bucket tip's position that is defined as the shortest distance between the current actual position and desired trajectory path of the bucket tip. As given in Fig. 2-2, the decomposed contour errors in x and y-axis directions can be calculated as given in

$$e_c = \begin{bmatrix} e_{cx} \\ e_{cy} \end{bmatrix} = \begin{bmatrix} C_x \varepsilon \\ C_y \varepsilon \end{bmatrix} \qquad (5\text{-}2)$$

C_x and C_y can be calculated as $C_x = \sin\theta = \dfrac{l_y}{L}, C_y = \cos\theta = \dfrac{l_x}{L}$ and ε gives the contour error. The ultimate goal of using the contour error compensation along with the position control is to reduce the contour error along with the tracking error. The contour error e_c is defined in the Cartesian space. This can be converted into joint space given that $\dot{J}$ and $\ddot{J}$ are small for slow contouring motion [60] given that the errors are sufficiently small.

$$\theta_e = J^{-1} e_c \qquad (5\text{-}3)$$

Considering the link lengths of the boom, arm, and bucket, a major portion for the contour error is caused by the boom and arm links as the bucket link is much smaller than that of the boom or the arm link. To reduce the contour error as given in Fig. 2-3, the x-axis contour error compensation should be subtracted from the current x position and simultaneously, the y-axis contour error compensation should be added to the current y position. Hence, the contour compensation control signal to the boom and arm actuators can be given as in

$$U_c = \begin{bmatrix} -U_{cx} \\ U_{cy} \end{bmatrix} = J^{-1}\theta_e \begin{bmatrix} -w_1 C_x \varepsilon \\ w_2 C_y \varepsilon \end{bmatrix} \qquad (5\text{-}4)$$

where w_1 and w_2 can be used to adjust and optimize the sensitivity of the contour compensation. The following steps describe the workflow in applying for the contour error compensation in detail:

- From the desired trajectory planning obtain the current expected reference bucket tip coordinates as $(x_R(t), z_R(t))$. By using forward kinematics, obtain the current actual bucket tip coordinates as $(x_A(t), z_A(t))$.

- Calculate the contouring angle, $\theta(t) = \arctan\left(\dfrac{(z_R(t) - z_R(t - \lambda))}{(x_R(t) - x_R(t - \lambda))} \right)$ where $(x_R(t - \lambda), z_R(t - \lambda))$ is the last expected bucket tip coordinates.

51

- The tracking errors in *x*-axis and *y*-axis, respectively can be calculated as $\left(x_R(t) - x_A(t)\ ,\ z_R(t) - z_A(t)\right)$.

- Using trigonometric relationships, the contour error ε can be calculated as $\varepsilon = e_y \cos\theta - e_x \sin\theta$ using the tracking errors.

- Using Eq. (5-3) e_c can be converted into the joint space and added for compensating the contour error as given in Eq. (5-4).

5.3 Force control

For the implementation of force control, the dynamic relationship between the bucket tip and the environment can be modelled as [37] Eq. (5-5). This is also known as the impedance function.

$$M\ddot{E} + B\dot{E} + KE = F_E \qquad\qquad\qquad (5\text{-}5)$$

where $E\,(E \in \mathfrak{R}^3)$ is the error between the desired reference location X_r $(X_r \in \mathfrak{R}^3)$ and actual current location X_c $(X \in \mathfrak{R}^3)$, F_E $(F_E \in \mathfrak{R}^3)$ is the external force from the environment; *M, B*, and *K* are the impedance gains that can be used to tune for the desired dynamic response. These parameters can be selected accordingly to their physical significance. *K* represents the desired interaction stiffness. When *K* is chosen as a large value, the resulting contact force becomes large. *B* represents the desired damping of the system. A larger value of B means that the motion of the manipulators tends to be slow. In other words, the value of B can help in reducing oscillations. M represents the desired inertial properties. When this is chosen a larger value may force the manipulator to produce low frequency and high amplitude oscillations [32].

Since the initial work of impedance control which was spearheaded by Hogan [34], [61] there have been potential research improvements identified by researchers in the area of impedance control [62].

- Impedance controller should obtain force tracking control ability
- Position tracking errors due to unknown dynamics should be minimized
- The controller should be able to deal with unknown environments and stiffness

Using the desired force F_d ($F_d \in \Re^3$), and environment position X_e ($X_e \in \Re^3$), the force tracking capability to the impedance function in Eq. (5-5) can be formulated for a respective one dimension and can be obtained as [63].

$$m\ddot{\varepsilon} + b(\dot{\varepsilon} + w) = f_e - f_d \tag{5-6}$$

where $\varepsilon = x_e - x_c$ and w is the adaptive law given as $w(t) = w(t-\delta) + \eta \dfrac{f_d(t-\delta) - f_e(t-\delta)}{b}$; δ is the sample time, η is the adaptive gain to tune, and b is an impedance gain. $w(t)$, the adaptive variable impedance is introduced [64] to achieve adaptive force tracking. Figure 5-2 shows the formulated impedance control strategy. The controller component V consists of the force and position components as seen in Eq. (5-7) and Eq. (5-8) respectively.

$$V = \frac{1}{m}\left[b(\dot{\varepsilon} + w) + f_d - f_e\right] \tag{5-7}$$

$$V = \ddot{x}_r + b\dot{e} + ke \tag{5-8}$$

where b, k are controller gains. The control input u is then given as in Eq. (5-9)

$$u = \ddot{q} = J^{-1}(\ddot{V} - \dot{J}\dot{q}) \tag{5-9}$$

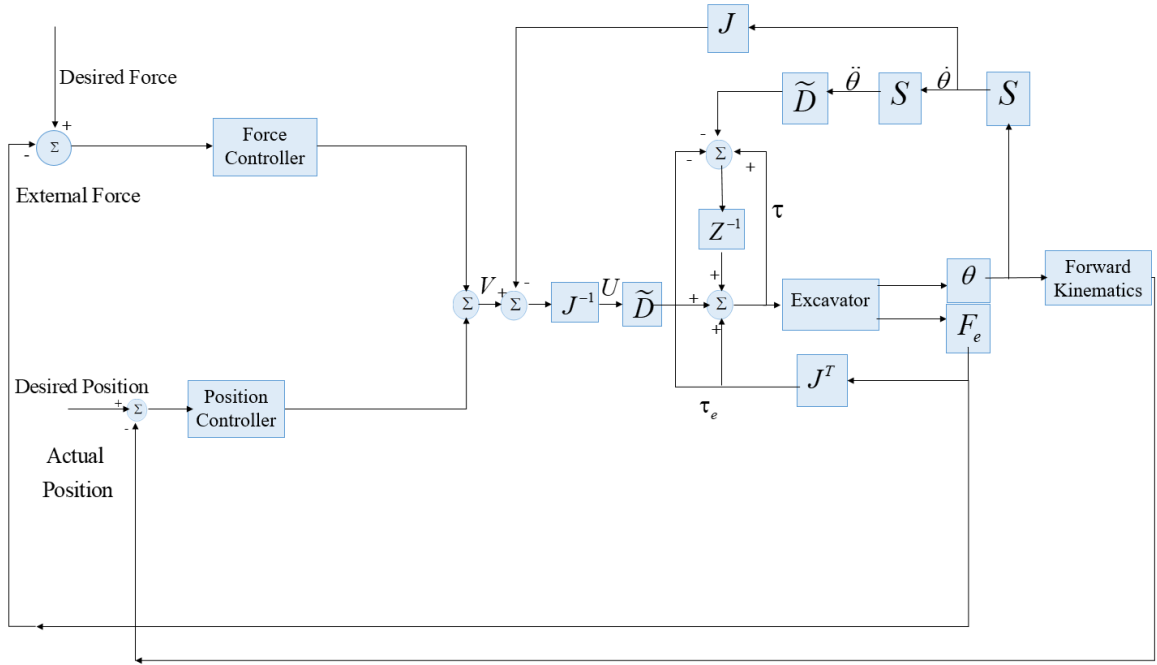The input signal u is then fed to the time-delayed controller to estimate the unknown dynamics.

Figure 5-2: Impedance controller framework

The stability criteria for the impedance function is important in choosing the impedance parameters as well as the adaptive gain for the variable impedance. Equation (5-6) can be written as Eqs. (5-10) and (5-11) by replacing ε with $\hat{\varepsilon} = \varepsilon + \delta x_e$ where δx_e is the uncertainty of ε [65].

$$m\ddot{\hat{\varepsilon}} + b(\dot{\hat{\varepsilon}} + w) = f_e - f_d \tag{5-10}$$

$$m\ddot{\varepsilon} + m\ddot{\delta}x_e + b\dot{\varepsilon} + b\dot{x}_e + bw(t-\delta) + \eta\big(f_d(t-\delta) - f_e(t-\delta)\big) = f_e - f_d \tag{5-11}$$

Approximating the environment to $f_e = -k_e\varepsilon$, Eq. (5-11) can be written as

$$
\begin{aligned}
&-m\ddot{f}_e - b\dot{f}_e + bk_e w(t-\delta) + \eta k_e\big(f_d(t-\delta) - f_e(t-\delta)\big) \\
&= -mk_e\ddot{\delta}x_e - bk_e\dot{\delta}x_e + k_e(f_e - f_d)
\end{aligned}
\tag{5-12}
$$

Additionally, $\hat{f}_e = k_e\delta x_e$. Substituting it to Eq. (5-12) and adding the component $m\ddot{f}_d + b\dot{f}_d$ to both sides of the equation Eq. (5-13) is obtained.

$$
\begin{aligned}
&m\ddot{f}_d - m\ddot{f}_e + b\dot{f}_d - b\dot{f}_e + bk_e w(t-\delta) + \eta k_e\big(f_d(t-\delta) - f_e(t-\delta)\big) - k_e(f_e - f_d) \\
&= m\ddot{f}_d - m\ddot{\hat{f}}_e + b\dot{f}_d - b\dot{\hat{f}}_e
\end{aligned}
\tag{5-13}
$$

54

By substituting, $o(t) = f_d(t) - f_e(t)$ and $p(t) = f_d(t) - \hat{f}_e(t)$ Eq. (5-13) can be expressed as below

$$m\ddot{o} + b\dot{o} + bk_e w(t-\delta) + \eta k_e o(t-\delta) + k_e o = m\ddot{p} + b\dot{p} \tag{5-14}$$

According to [62] for $\underline{n}$ elements of the series, $bw(t-\delta)$ can be written as

$$bw(t-\delta) = bw(t-(n+1)\delta) + \eta o(t-(n+1)\delta) + ... + \eta o(t-2\delta) \tag{5-15}$$

Since $w(0) = 0$ initially $bw(t-(n+1)\delta) = 0$, then Eq. (5-15) can be written as

$$m\ddot{o} + b\dot{o} + k_e o + \eta k_e \left(o(t-(n+1)\delta) + ... + o(t-\delta) \right) + k_e o = m\ddot{p} + b\dot{p} \tag{5-16}$$

Converting Eq. (5-16) to Laplace domain using the delay property Eq. (5-17) is obtained. From this, the component $p(s)$ becomes the characteristic equation.

$$\frac{o(s)}{p(s)} = \frac{ms^2 + bs}{ms^2 + bs + k_e + \eta k_e \left(e^{-(n+1)\delta s} + ... + e^{-\delta s} \right)} \tag{5-17}$$

Using the relationship $e^{-\delta s} \approx 1 - \delta s$ from the Taylor series expansion, the characteristic equation $p(s)$ becomes

$$\delta m s^3 + \delta b s^2 + k_e \delta(1-\eta)s + \eta k_e = 0 \tag{5-18}$$

By using Routh-Hurwitz stability criteria the range for η is given as

$$0 < \eta < \frac{b\delta}{b\delta + m} \tag{5-19}$$

5.4 Summary

In summary, this chapter described the control components of the used integrative control strategy. Three main sub-topics as given below were discussed.

1. Position control

    A non-linear PI controller was implemented and considered for this study. The mathematical model of the used PI controller was explained. In addition, the

benefits of the NPI controller were explained considering the position control requirements for a hydraulic system.

2. Contour control

   The steps required for the application of contour control for a robotic excavator system were described along with the mathematical model of the contour controller.

3. Force control

   The mathematical model of the used impedance controller was provided. The impedance function included force tracking ability to track the desired force for excavation. Also, the stability range for the variable impedance function was given.

Chapter 6. Simulation Results

In this chapter verification of the developed simulation model as well as the simulation results on the performance of designed controllers will be discussed. A sampling time of 0.01 was used for all the simulations. Manual ground moving tasks were carried out by the excavator and the current signals (input control signals) to EHPV's were recorded. The non-contact moving task was also considered to validate the developed simulation model.

6.1 Simulation model verification

6.1.1 Simulation model verification for non-contact region

Figure 6-1 shows the recorded input current data for EHPV's of each boom, arm, and bucket actuators, respectively. The same recorded current profiles were inputted into the simulation model to compare the actuator displacement responses. Figs. 6-2, 6-3 and 6-4 show the displacement of the hydraulic actuators in comparison with the simulation model for the same current inputs. The results show that the developed multi-domain simulation model can represent the dynamics of the actual prototype excavator platform.
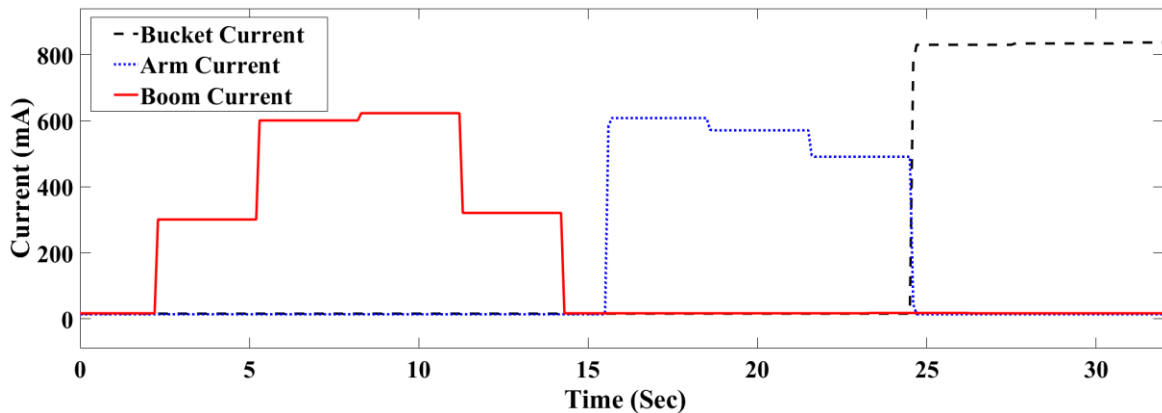

Figure 6-1: Current input data to actuators non-contact space
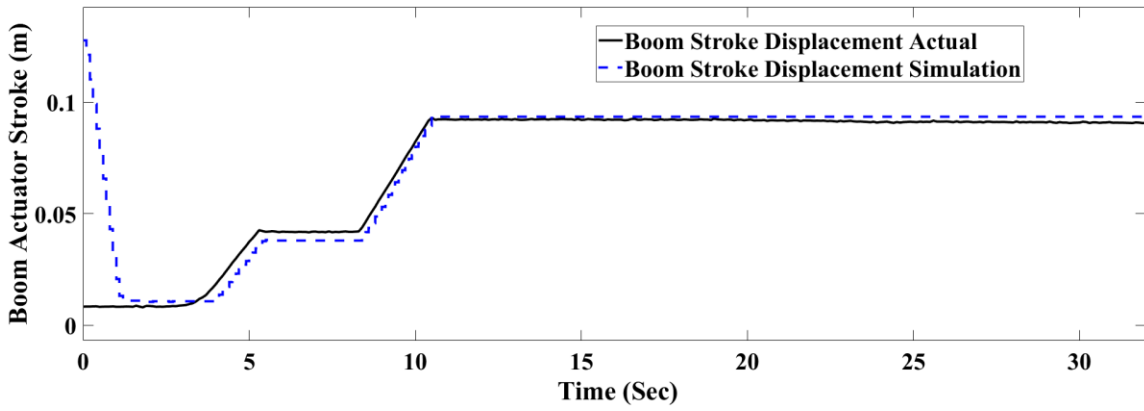
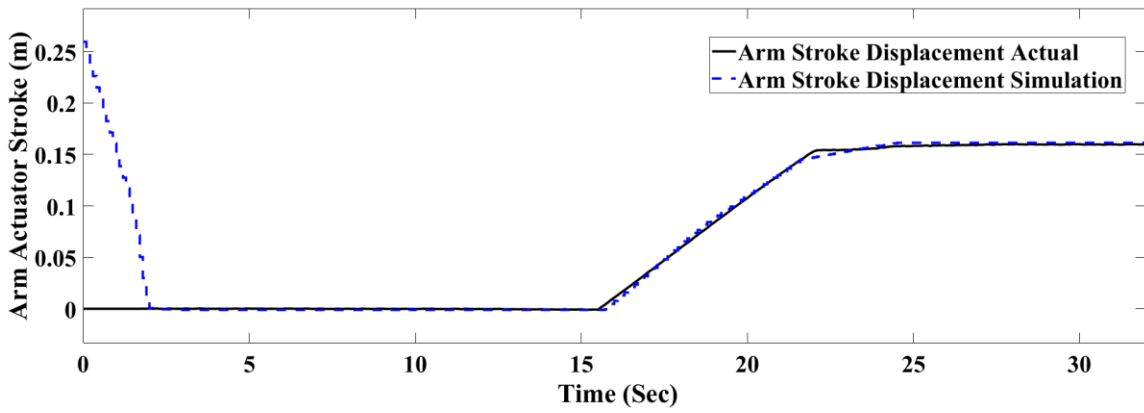Figure 6-2: Boom stroke displacement non-contact space

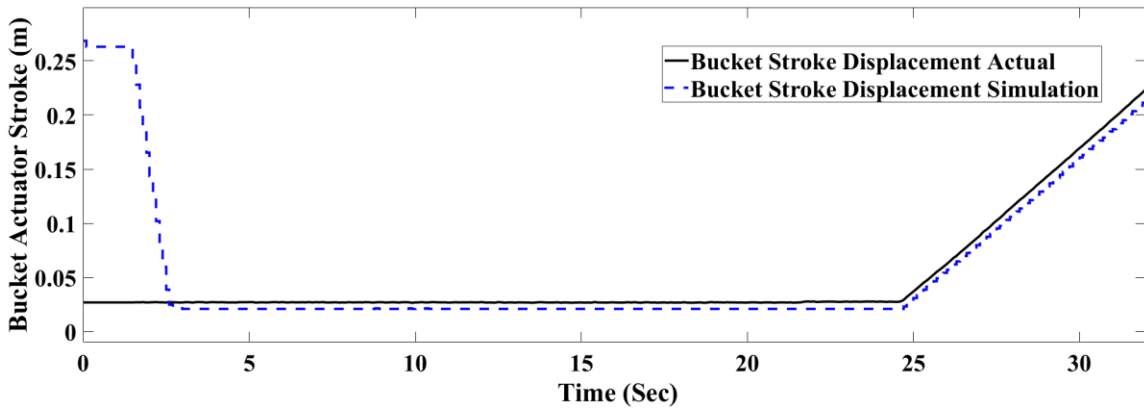Figure 6-3: Arm stroke displacement non-contact space

Figure 6-4: Bucket stroke displacement non-contact space

6.1.2 Simulation model verification for contact region

Similar to the experiment conducted in the above section, the current profile was recorded for a ground digging task that requires the motion with the arm and bucket manipulators to remove soil while the boom position is maintained.
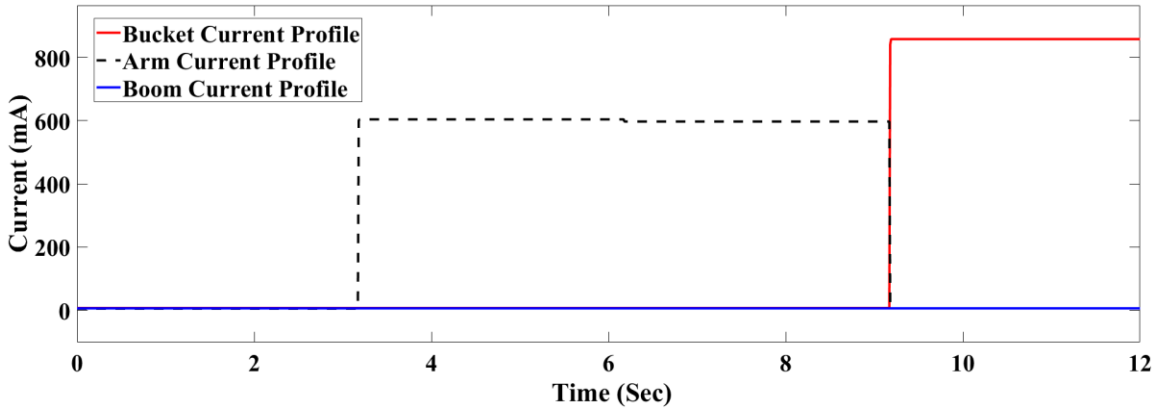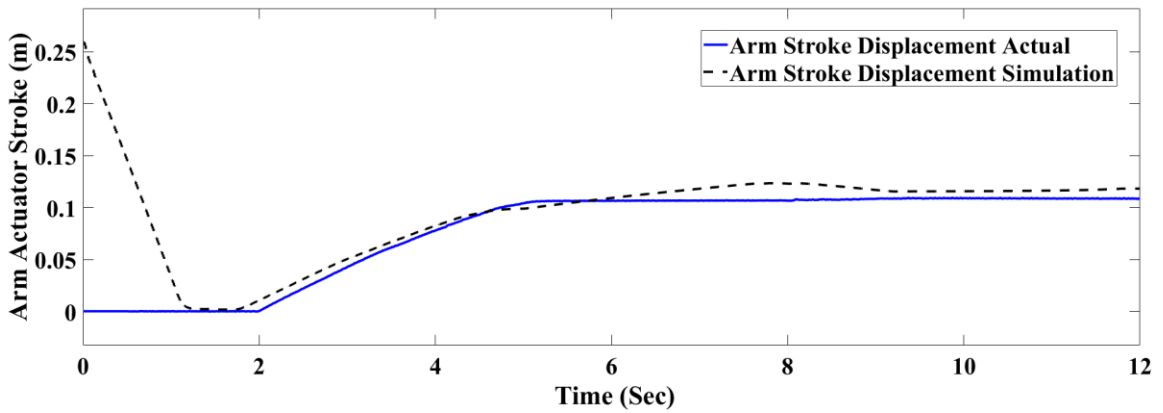

Figure 6-5: Current input to actuators contact space

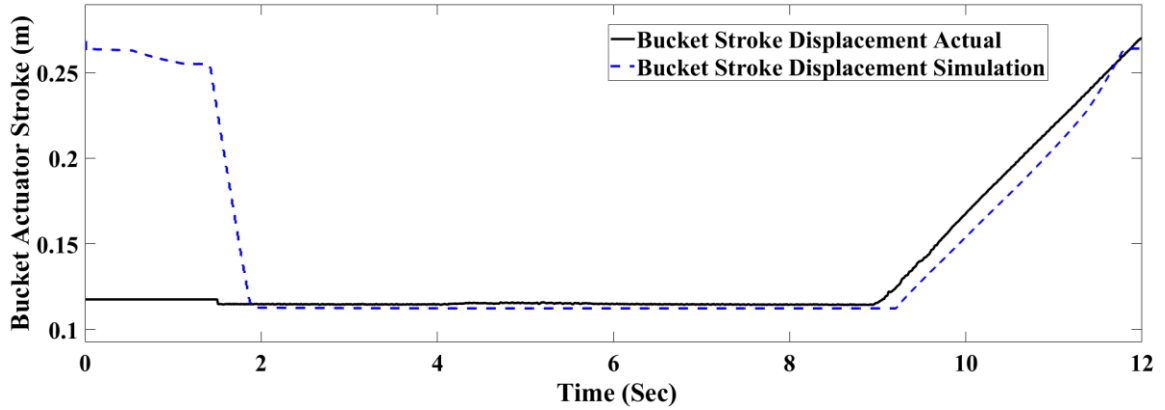Figure 6-6: Arm stroke displacement contact space

59

Figure 6-7: Bucket stroke displacement contact space

6.2 Simulation results for ground levelling

For ground levelling simulation, a ground levelling profile was considered as shown in Fig. 6-8. Ground levelling simulation was carried out to focus on contour compensation since a desired flat ground was targeted for this task. Figs. 6-9, 6-10 and, 6-11 respectively show the position tracking performance between the NPI and PI controllers. From the figures, it is found that the NPI controller provides good tracking performance compared to the PI controller in terms of transient and steady-state response.
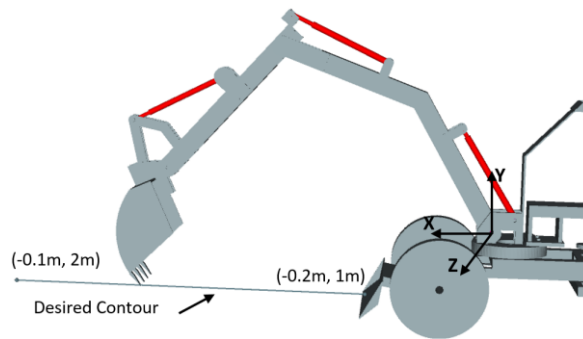

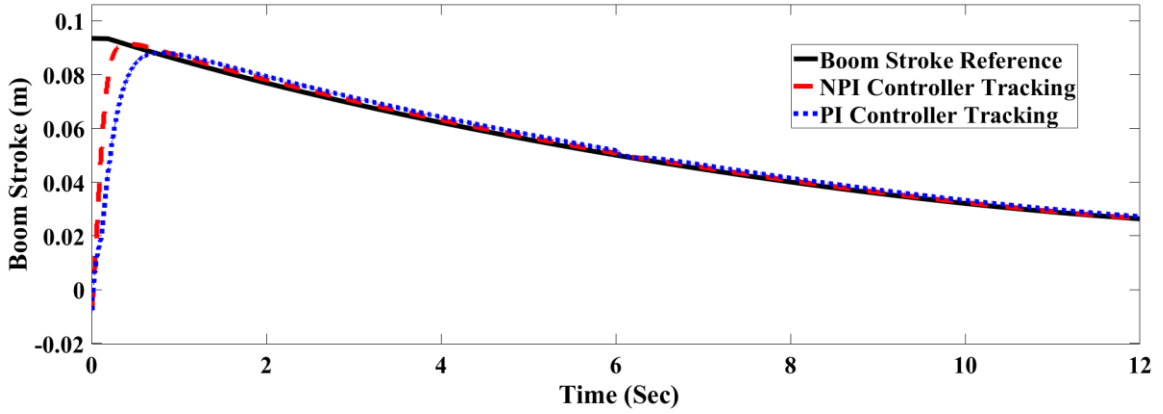Figure 6-8: Ground levelling scenario

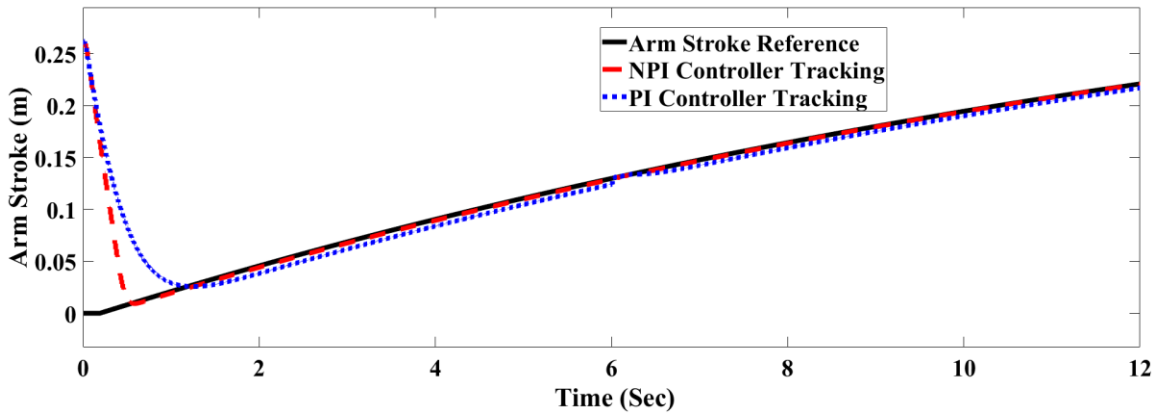Figure 6-9: Boom stroke tracking position controller

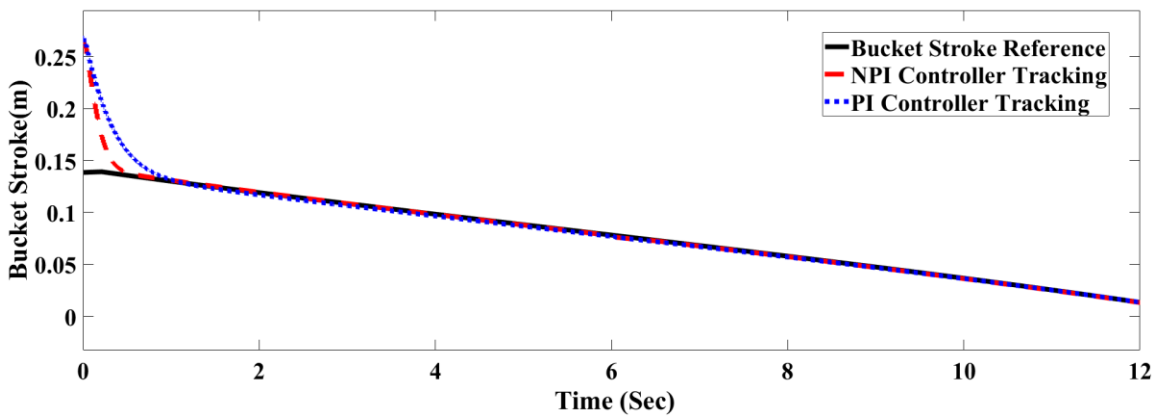Figure 6-10: Arm stroke tracking position controller

Figure 6-11: Bucket stroke tracking position controller

Figure 6-12 shows the desired contour tracking with respect to a reference profile. As shown in the simulation, the contour compensation control enables accurate tracking by reducing the contour and tracking errors.
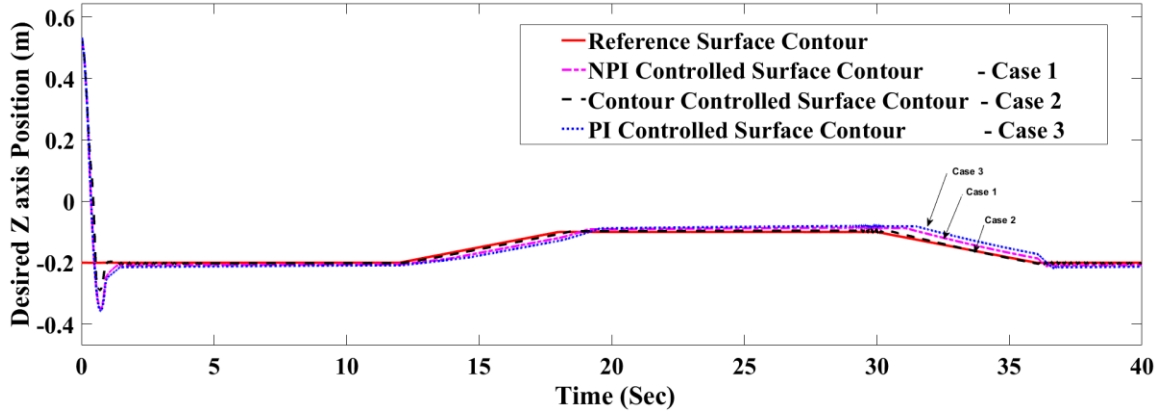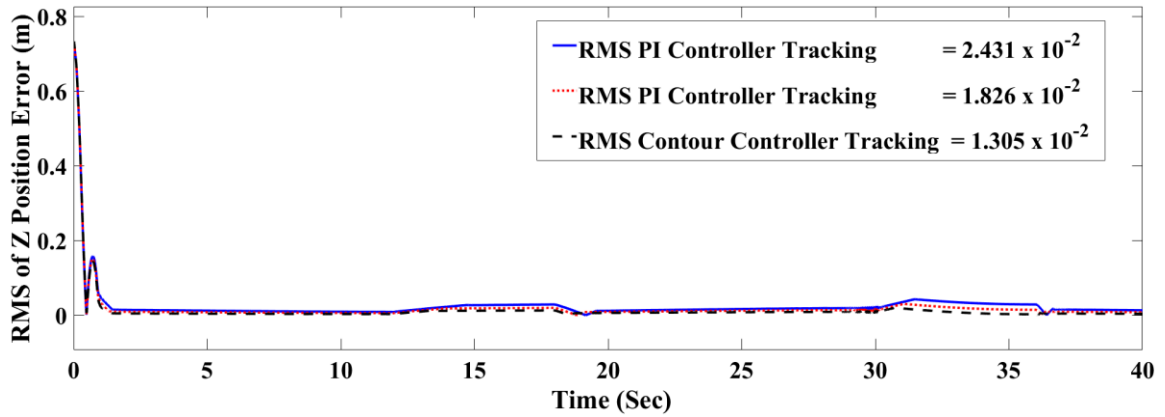
Figure 6-12: Z axis contour tracking

Figure 6-13: Z axis contour tracking RMS

Chapter 7. Experimental Results and Discussion

7.1 Introduction

In this chapter, experimental results using the developed test platform are provided to validate the proposed control algorithms. The tracking performance of the bucket tip is compared among the following types of controllers for ground levelling and digging tasks.

1. PI controller only
2. NPI controller only
3. NPI position controller with Contour Control compensation
4. NPI position controller with Contour Control compensation and Force control.

The digging experiments were carried out using sand and soil to consider different reactive forces from the ground. Finally, a ZED camera was used to check and calculate the difference between the excavated ground profile and the desired ground profile. As shown in Fig. 7-1, the average error was calculated at user-defined points using the data (point cloud) obtained by the camera. As given in Eq. (7-1) the average error along y-axis can be calculated. Here $e_1..e_n$ present average errors for each column along xy axes of the error matrix given in Eq. (7-2), where e_{ij} gives the error at the ith location of x-axis and j^{th} location of y-axis. e_n, gives the average error of the nth column of the error matrix.
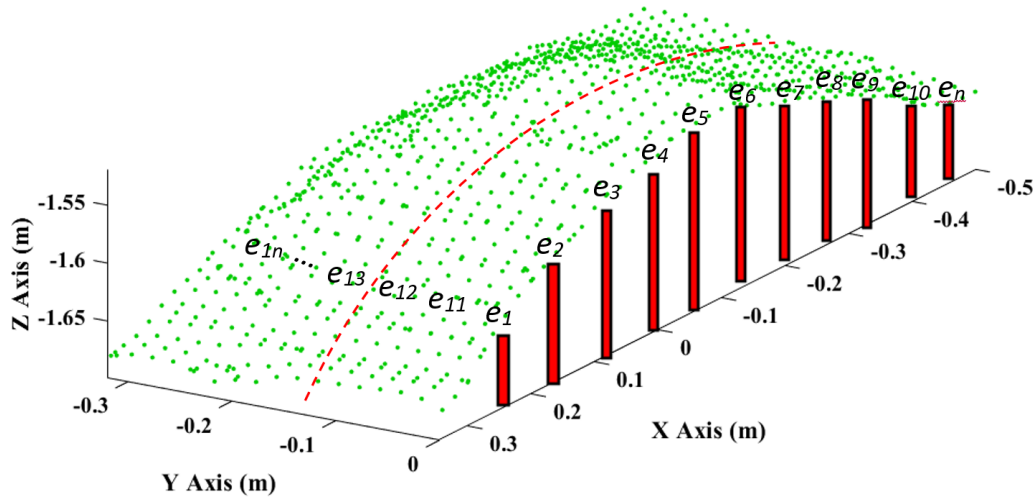

Figure 7-1: Error calculation for excavation progress

$$e_1 = \frac{e_{11} + e_{12} + e_{13} + \ldots + e_{1n}}{n} \tag{7-1}$$

$$e_{ij} = \begin{bmatrix} e_{11} & \cdots & e_{n1} \\ \vdots & \ddots & \vdots \\ e_{1n} & \cdots & e_{nn} \end{bmatrix} \tag{7-2}$$

An error matrix with a dimension of 20×20 was considered and used in these experiments.

7.2 Ground levelling experimental results

As shown in Fig. 7-2 ground levelling experiments were carried out using the prototype mini excavator. The excavator manipulator tries to grade the ground by removing soil in x- and y- directions compared to the excavator origin coordinate system. Five repetitive runs of leveling motion of the excavator were performed by the excavator for each control method.

Figure 7-2: Ground levelling experiment with prototype excavator

Figure 7-3 shows the ground profile in z-x plane captured using the ZED camera before the levelling task was carried out. This captured ground profile was then used to compare and calculate the error after the completion of levelling operation. Figure 7-4 presents the tracking profiles with different controllers that were recorded through the LVDT sensor data. From this figure, it is evident that the tracking control performance of

the contour controller combined with the NPI controller outperforms other types of control methods used for the experiment.
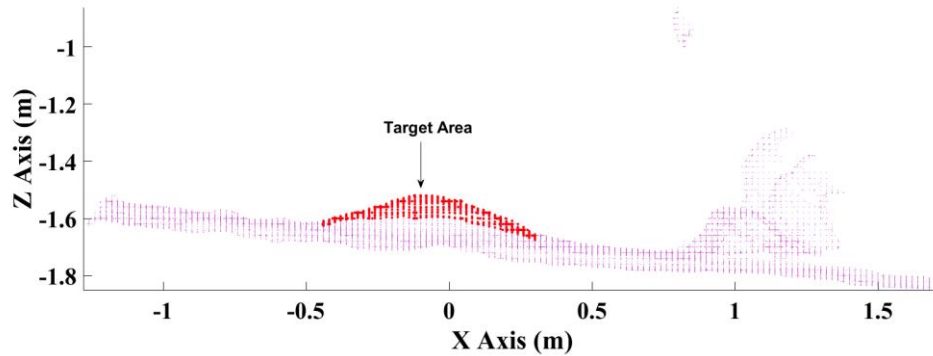

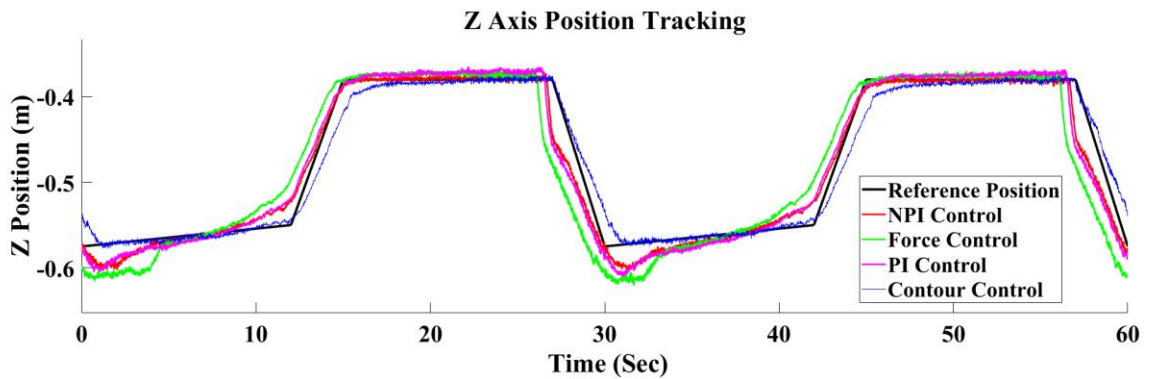Figure 7-3: Ground profile before levelling

Figure 7-4: Bucket tip position tracking in z axis of ground levelling

Although the controller tries to reduce the position error of the bucket tip, a control function is required to terminate the excavation cycle when the desired deviation tolerance between the desired ground profile and excavated ground profile is achieved. This can be achieved by an appropriate sensing methodology to measure the errors e_{ij} in Eq. (7-2). To measure e_{ij}, the ZED camera was used. Utilizing these error values, standard deviation (STD) of the variation of errors can be obtained. STD can be used as a criterion to stop the machine once the desired tolerance is achieved [66]. In the following section, experimental results are provided along with the calculation of the average excavation error and standard deviation. When calculating the average profile after an excavation task, the ground profile surrounding the middle of the bucket area is considered.

7.2.1 Ground levelling with PI control

Figure 7-5: Average error and standard deviation for before and after ground levelling using PI

Figure 7-6: Average ground profile for before and after ground levelling using PI

7.2.2 Ground levelling with NPI control

Figure 7-7: Average error and standard deviation for before and after ground levelling using NPI
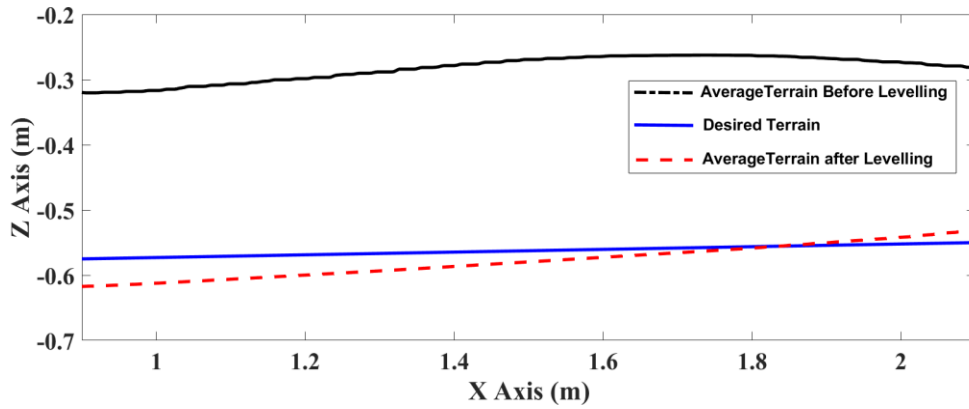
Figure 7-8: Average ground profile for before and after ground levelling using NPI

7.2.3 Ground levelling with NPI and CCP control
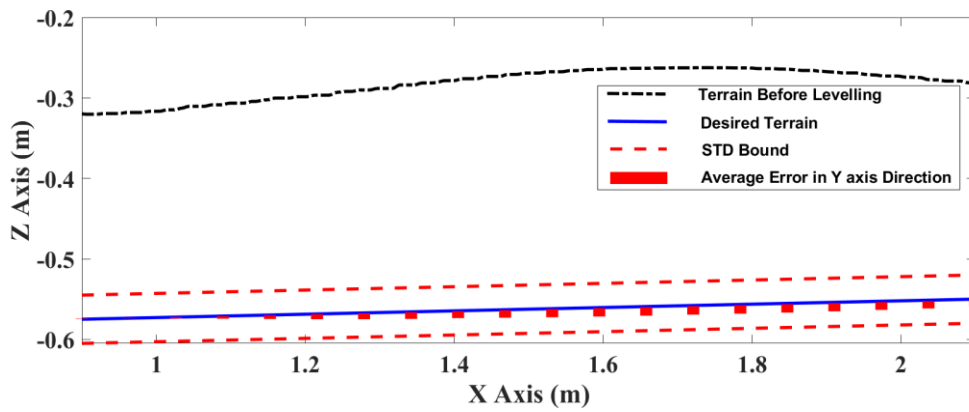
Figure 7-9: Average error and standard deviation for before and after ground levelling using NPI and CCP
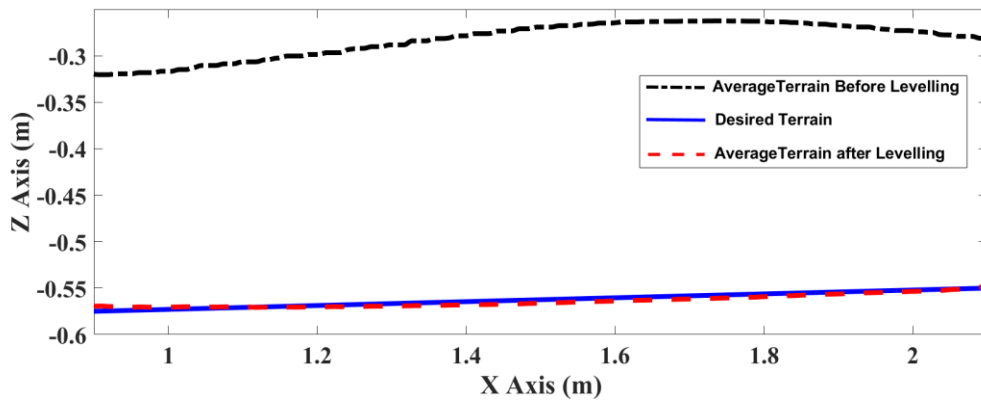
Figure 7-10: Average ground profile for before and after ground levelling using NPI and CCP

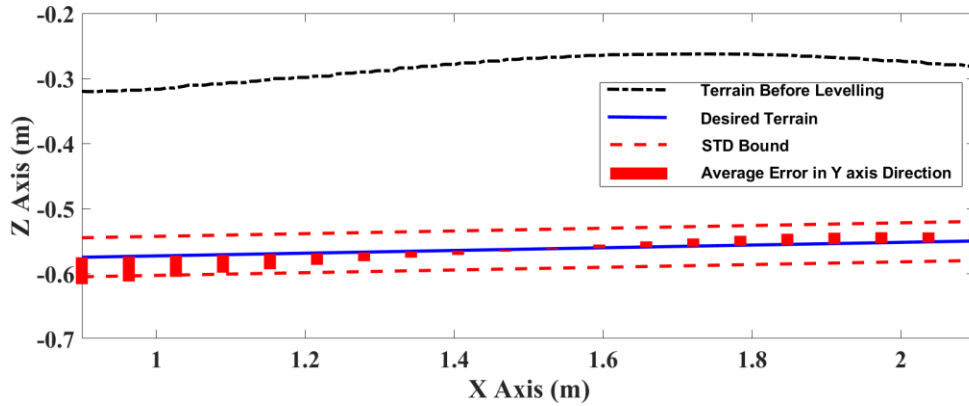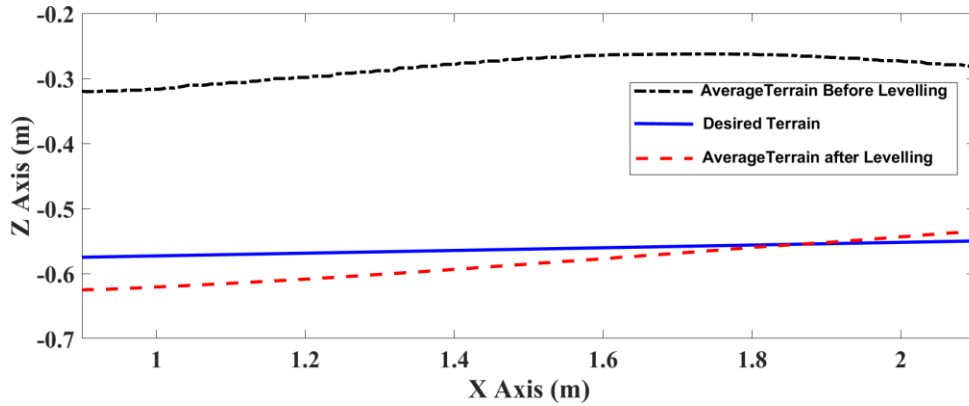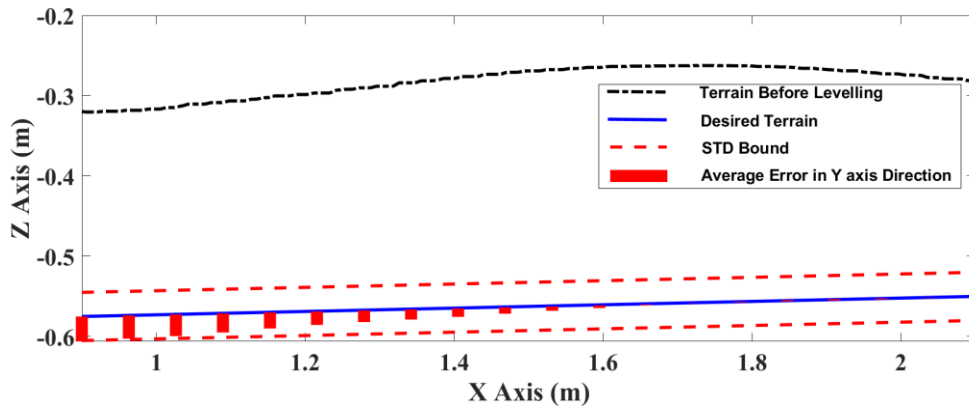7.2.4 Ground levelling with NPI, CCP and Force control
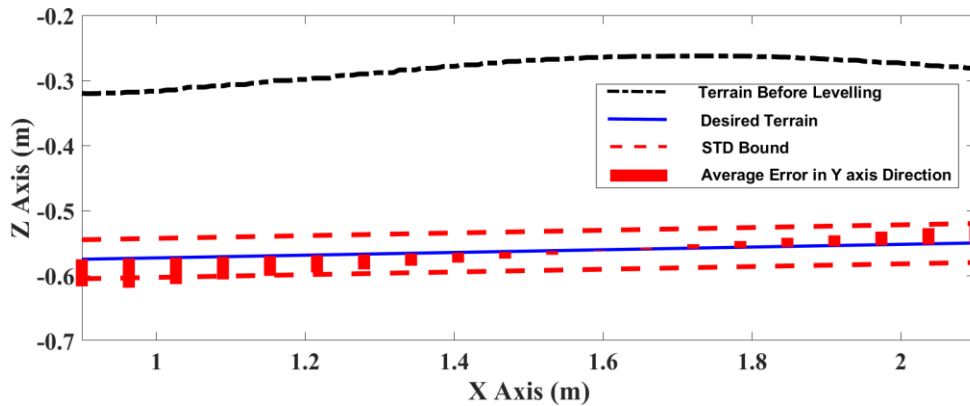
Figure 7-11: Average error and standard deviation for before and after ground levelling using NPI, CCP and FC
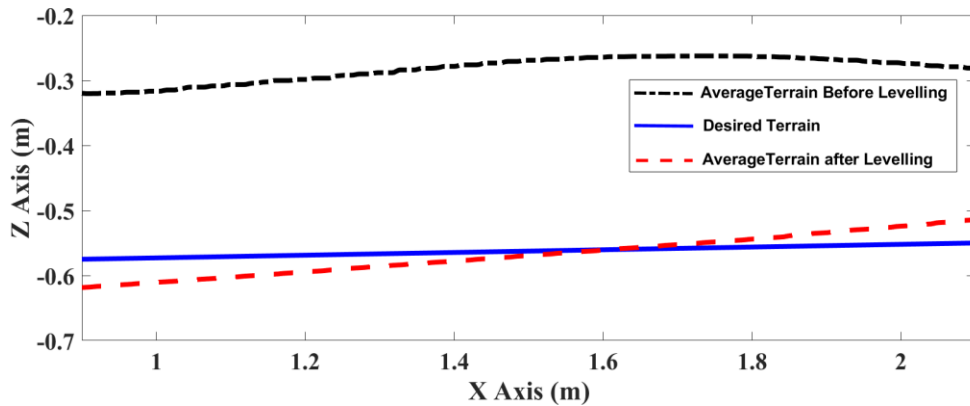
Figure 7-12: Average ground profile for before and after ground levelling using NPI, CCP, and FC

7.3 Ground levelling experimental results discussion

The error matrix below shows the average error calculated according to each control method where row 1, 2, 3, and 4 correspond to average errors occurring from PI, NPI, NPI + CCP, NPI + CCP + FC, respectively.

Table 7-1: Average error values along *y*-axis for ground levelling experiments

Average error in y axis for ground levelling (mm)				
Data point	PI	NPI	CCP	FC
1	-41.4	-31	0.6	-41.7
2	-38.5	-28.9	0.3	-45.1
3	-32.7	-27	1.6	-40.7
4	-27.5	-23.7	3.1	-34.8
5	-23.5	-20	4.7	-30.6
6	-18	-16.8	6.2	-26.7
7	-13.6	-14.5	7.5	-23.1
8	-9.5	-12.6	8.4	-18.9
9	-6.6	-10.5	8.6	-15.2
10	-2.9	-7.9	9.4	-10.3
11	1.6	-5.4	10	-5.6
12	5.8	-3.3	10.4	-1.3
13	9.4	-1.1	10.6	0.3
14	12.7	0.3	10.6	6.9
15	15.5	0.9	10.6	10.4
16	17.4	1.6	10.5	14.2
17	17.7	1.7	10.2	16.8
18	17.2	1.4	9.7	21.2
19	15.7	0.4	9.1	25.3
20	13	0.9	8.2	29.7
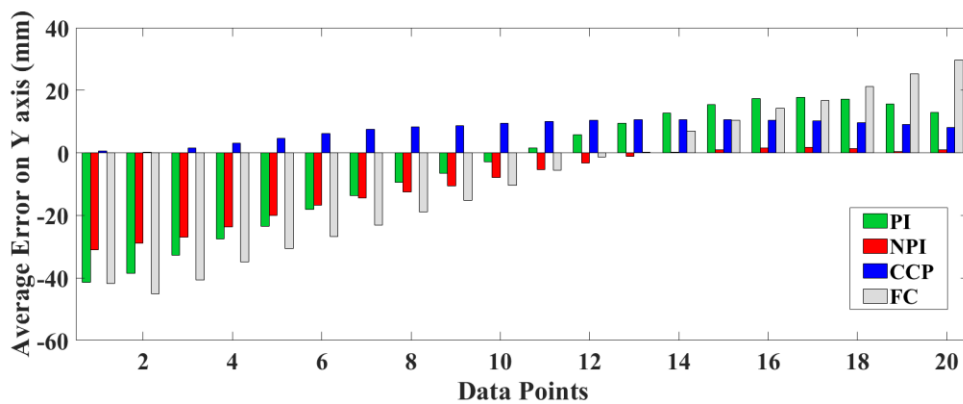
Figure 7-13: Average error variation ground levelling

Table 7-1 depicts the standard deviation of average errors in *y*-axis for each control method.

Table 7-2: Standard deviation for ground levelling

Controller Type	Standard Deviation (mm)
PI	20.0981
NPI	14.7671
NPI + CCP	8.2642
FC	24.6597

From the ground leveling experimental results, NPI position control with contour control compensation provided the best tracking results for the ground levelling task compared to other controllers. It is also apparent that NPI with contour control minimizes the STD ($< 1cm$) by simultaneously reducing the contour error (i.e., the smallest deviation from the ground profile) and tracking error.

7.4 Digging experiments

Digging experiments were conducted using two forms of media sand and soil respectively to test the controller. Figure 7-14 shows the experimental ground setup. The excavation error tolerance was calculated in a similar manner in which it was calculated for ground levelling operations. The cycle of a typical digging task consists of penetration, drag and rotate (curl) [67]. Using this tactic, the digging trajectories were set.

Figure 7-14: Digging setup for experiments

7.4.1 Sand digging experiments

Figure 7-15 shows the bucket tip tracking for sand digging. Figure 7-24 shows the digging profile considering the media as soil. As it can be seen, the control method which included force control is the closest to the desired trajectory. Sand digging experiments were carried out to achieve a STD of 5 cm from the desired ground profile. As displayed in Table 7-2 the control method combining position, contour and force achieved an excavation profile within the bound of 5cm.
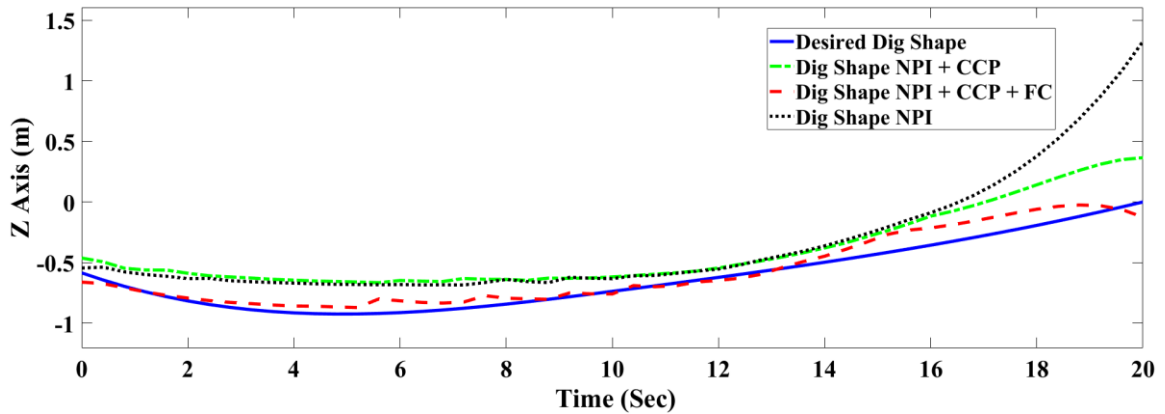
Figure 7-15: Sand digging bucket tip tracking

Figs. 7-15 and 7-16 show force tracking in z-axis and x-axis, respectively. The desired tracking forces in X and Z axes were chosen as -1500N each. This was estimated experimentally. The desired force in the z-axis profile is positive towards the end since it must produce force opposite to the direction of the ground at the end to lift up the dug soil. The controller provided sufficient force tracking results in the presence of the dynamic uncertainties to achieve the preliminary excavation task.
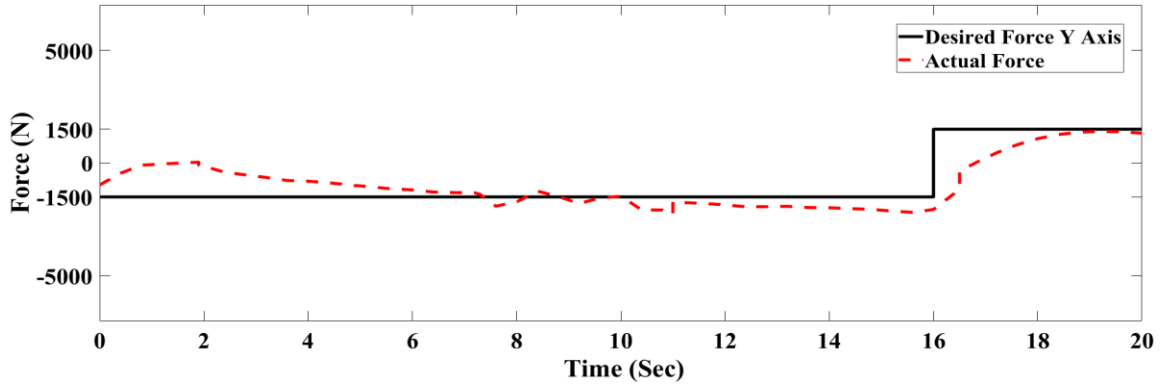
Figure 7-16: *Z*-axis force tracking for sand
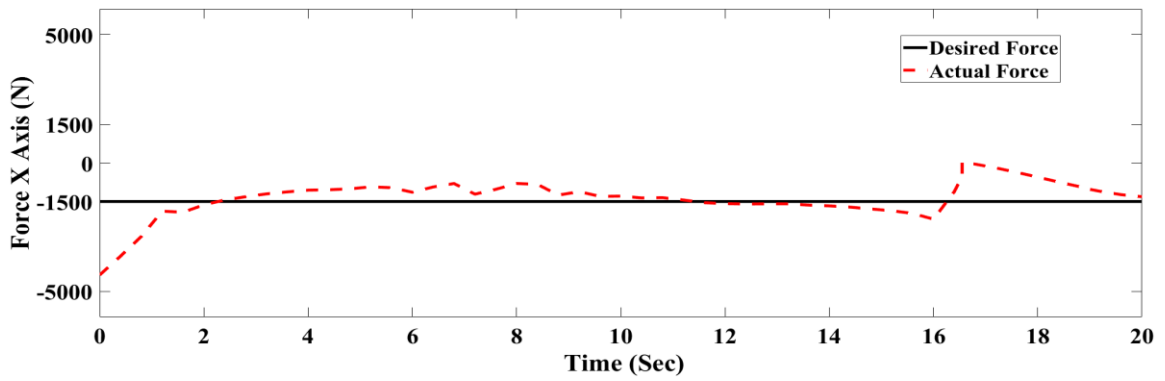
Figure 7-17: *X*-axis force tracking for sand

The amount of sand excavated is analyzed in each of the following subtopics.

7.4.1.1 Sand digging with position control only

Figure 7-18 shows a digging experiment conducted in sand media using position control only. Figure 7-19 shows the deviation of average error along the *y*-axis.
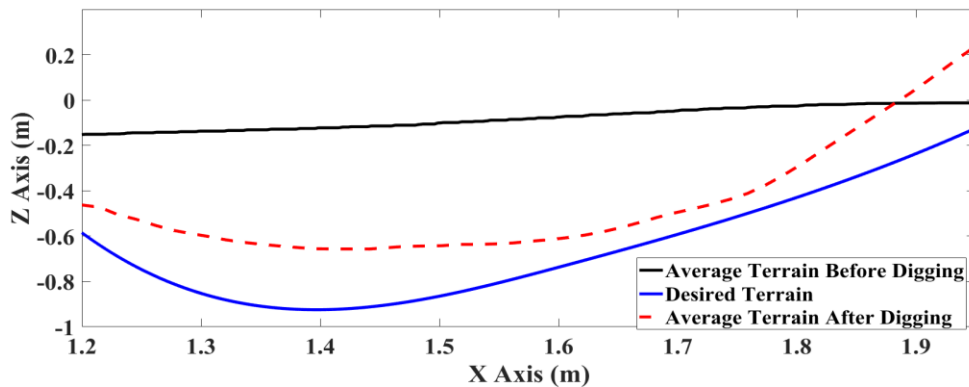
Figure 7-18: Average ground profile for before and after digging using NPI control

Figure 7-19: Average error and STD for soil digging using NPI and CCP control

7.4.1.2 Sand Digging with position control and contour control

Figure 7-20 shows a digging experiment conducted in sand media using position control and contour control. Figure 7-21 shows the deviation of average error along the *y*-axis.
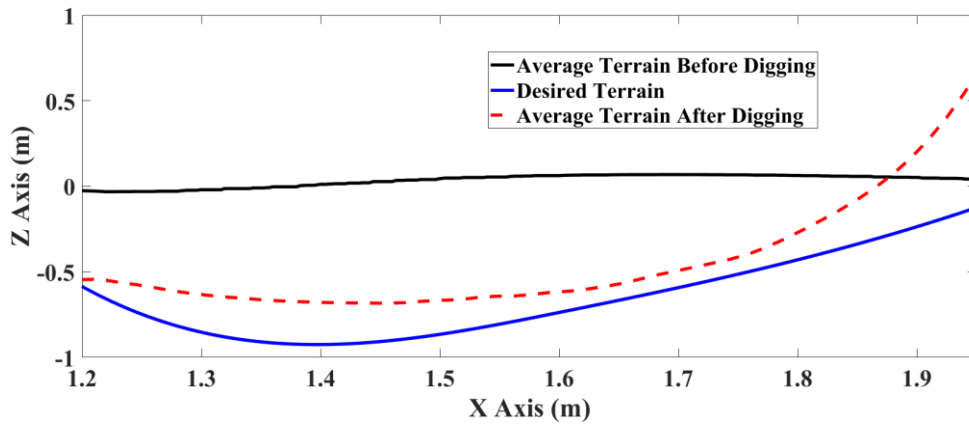
Figure 7-20: Average ground profile for before and after digging using NPI and CCP control
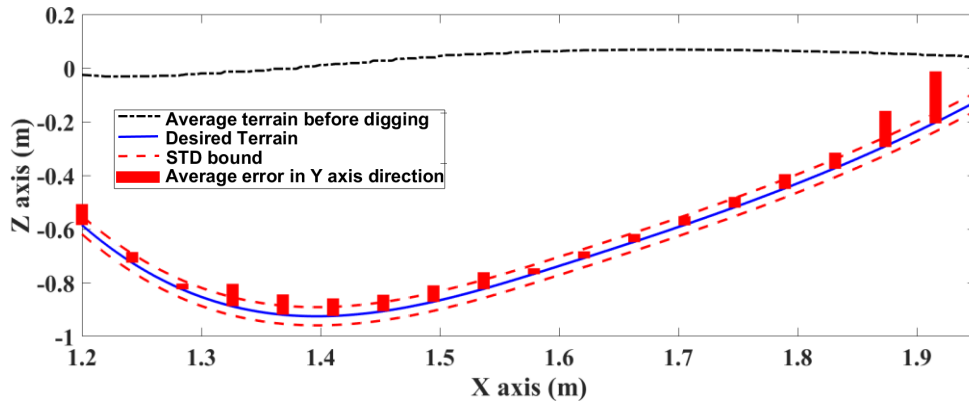
Figure 7-21: Average error and standard deviation for before and after digging using NPI, CCP, and FC control

7.4.1.3 Sand Digging with position control, contour control and force control

Figure 7-22 shows a digging experiment conducted in sand media using position control, contour control and force control combined. Figure 7-23 shows the deviation of average error along the *y*-axis.
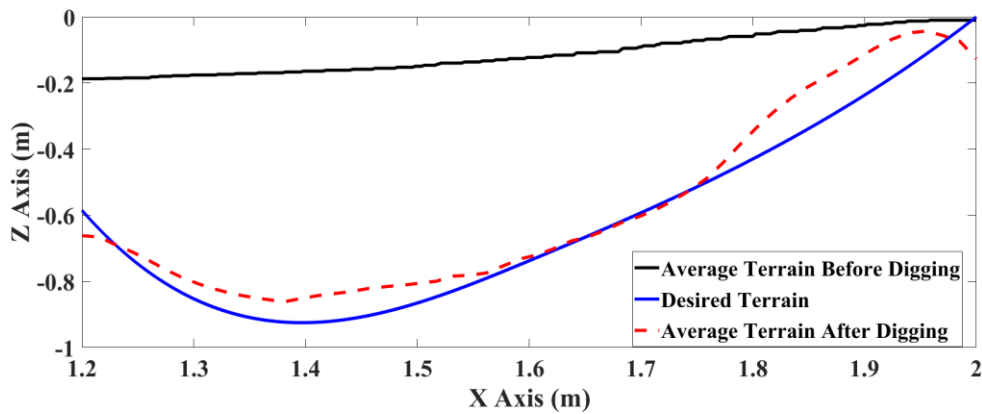
Figure 7-22: Average ground profile for sand digging using NPI, CCP, and FC control
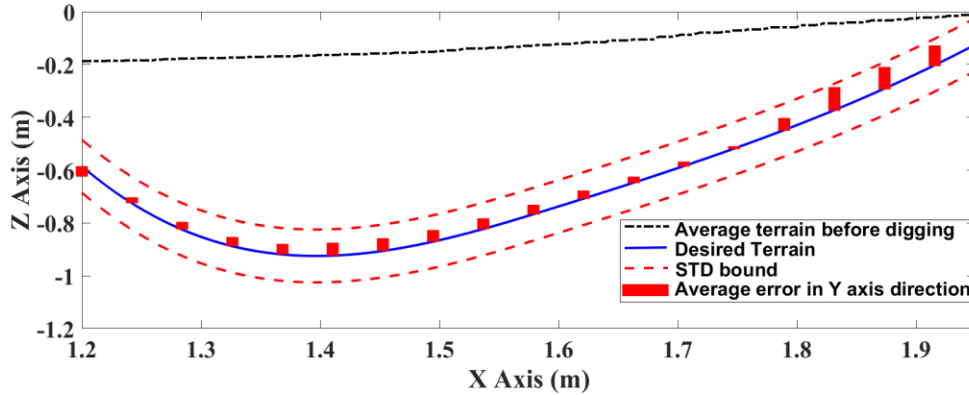
Figure 7-23: Average error and standard deviation for before and after digging using
NPI, CCP, and FC control

7.4.2 Soil digging experiments

Figure 7-15 shows the bucket tip tracking for soil digging experiments. As it can be seen the deviation of the bucket tip from the desired trajectory is much high compared to sand digging experiments. This is due to the higher density of soil compared to sand and hence higher resistive ground forces [68]. Furthermore, the deviation of control methods without force control is much higher compared to sand digging experiments. This confirms the necessity of force control for autonomous excavation. The soil digging experiments were conducted to achieve a STD of 10 cm. As displayed in Table 7-2, the control method combining position, contour and force achieved an excavation profile within the bound of 5cm. The estimated digging forces were approximated as given in Fig. 7-24 and Fig. 7-25. For comparison, the NPI control, NPI+CCP control, and NPI+CCP+FC combined control methods were investigated separately for the average error and standard deviation of the excavated profile.
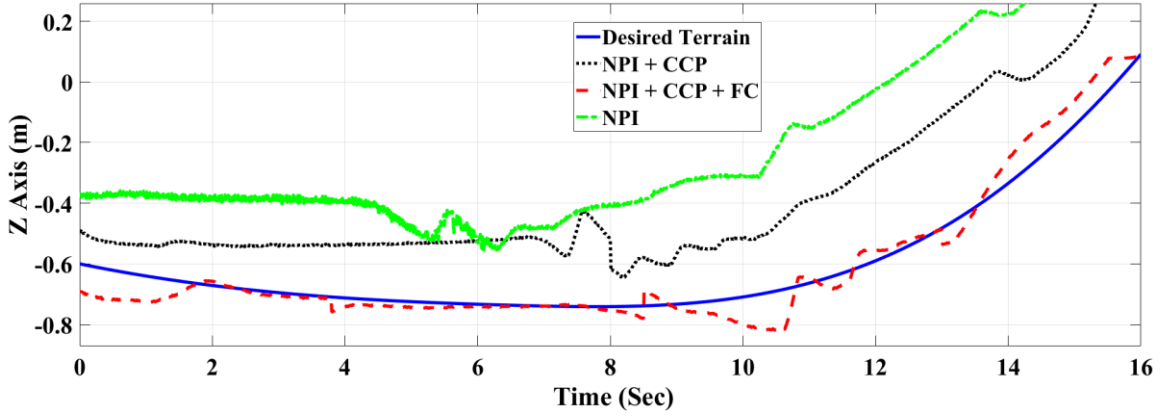
Figure 7-24: Soil digging bucket tip tracking
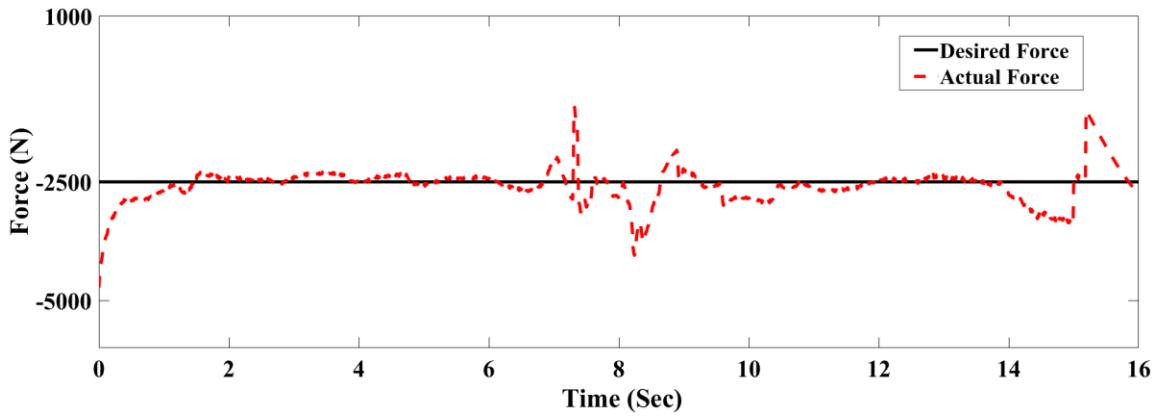
Figure 7-25: *X*-axis force tracking for soil
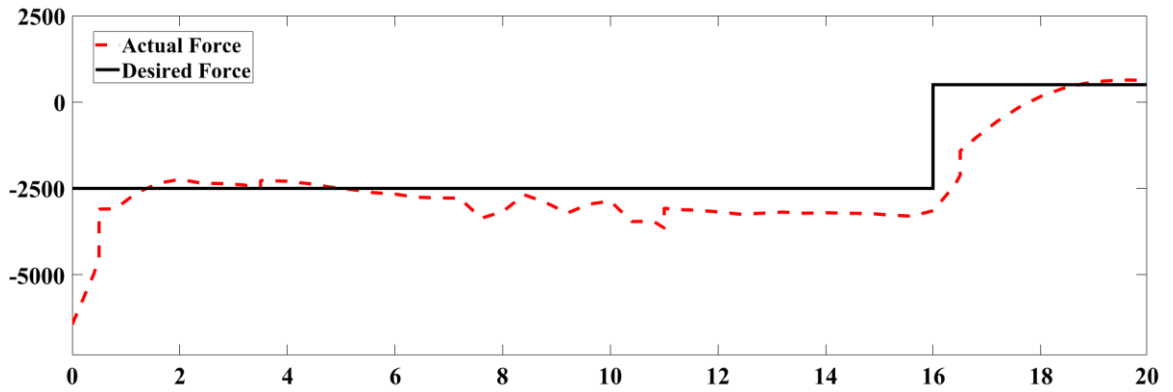
Figure 7-26: *Y*-axis force tracking for soil

7.4.2.1 Soil digging with position control only
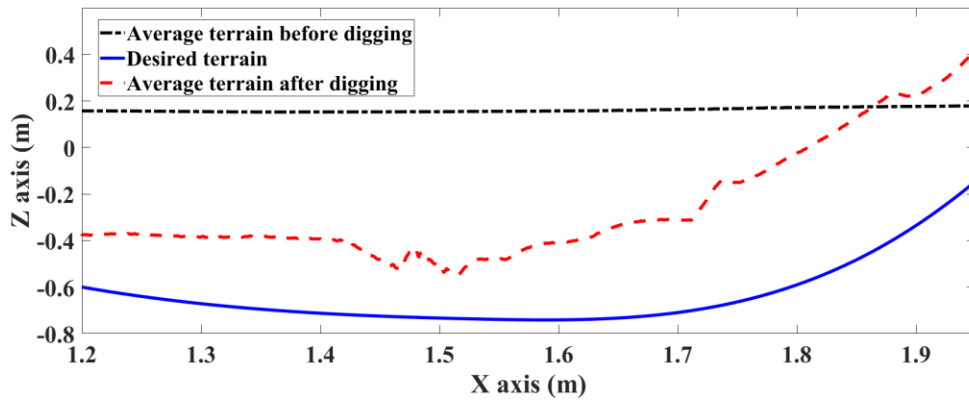
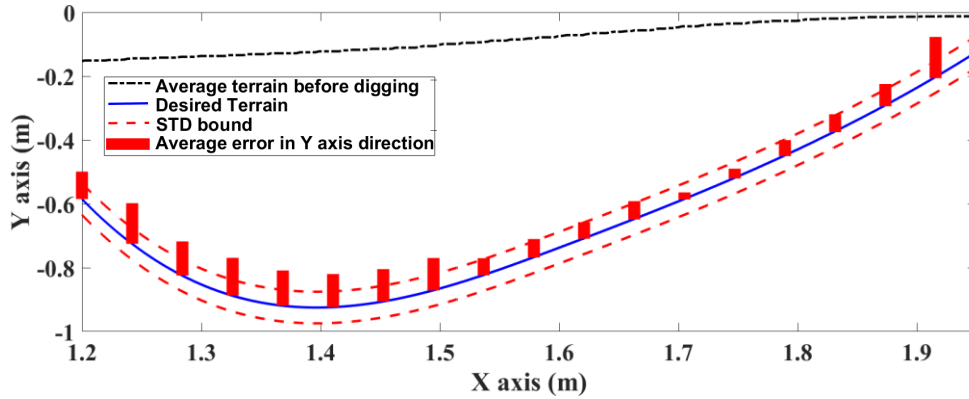Figure 7-27: Average ground profile for soil digging with NPI control
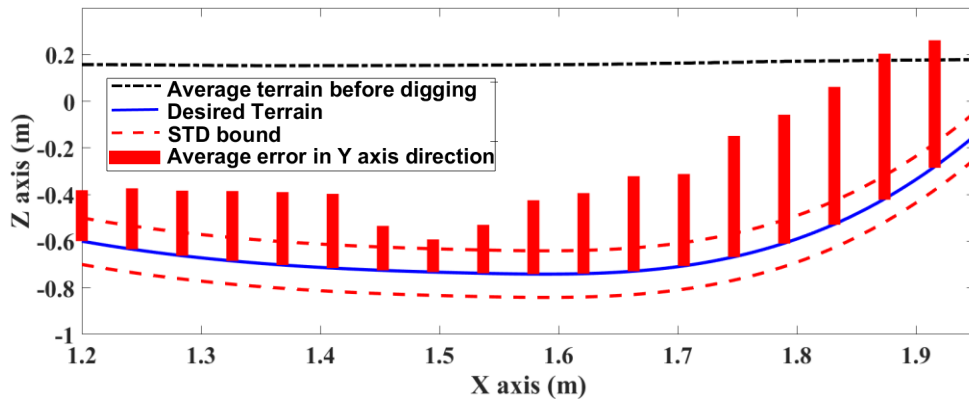
Figure 7-28: Average error and STD for soil digging with NPI control

7.4.2.2 Soil digging with position control and contour control
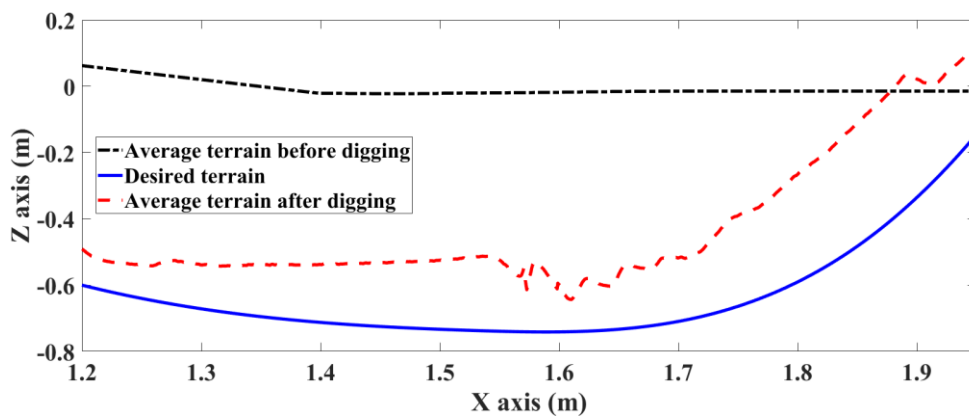
Figure 7-29: Average ground profile for soil digging with NPI and CCP control
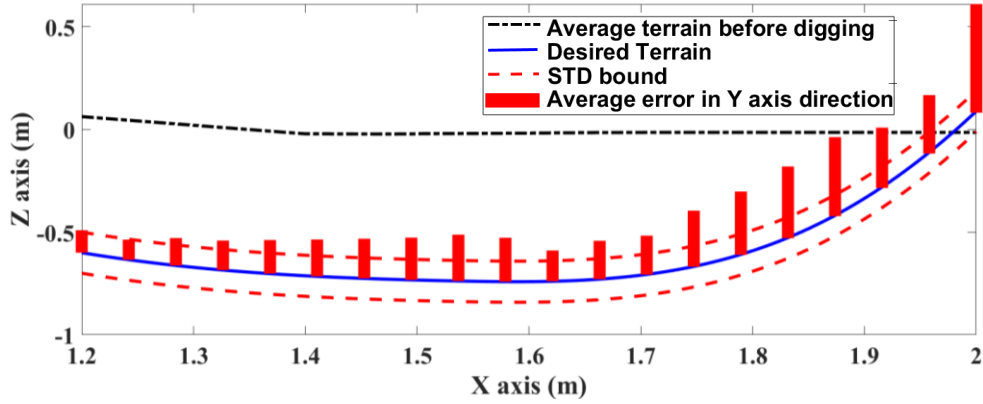
Figure 7-30: Average error and STD for soil digging with NPI and CCP control

7.4.2.3 Soil digging with position control, contour control and force control
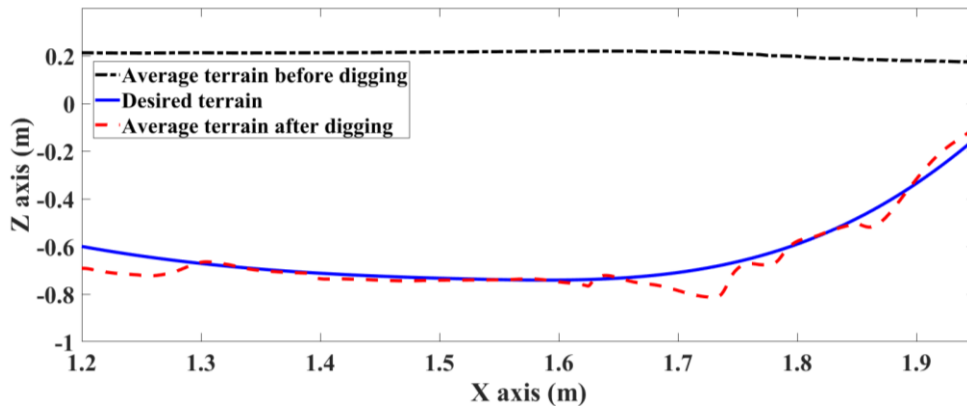
Figure 7-31: Average ground profile for soil digging with NPI, CCP and FC
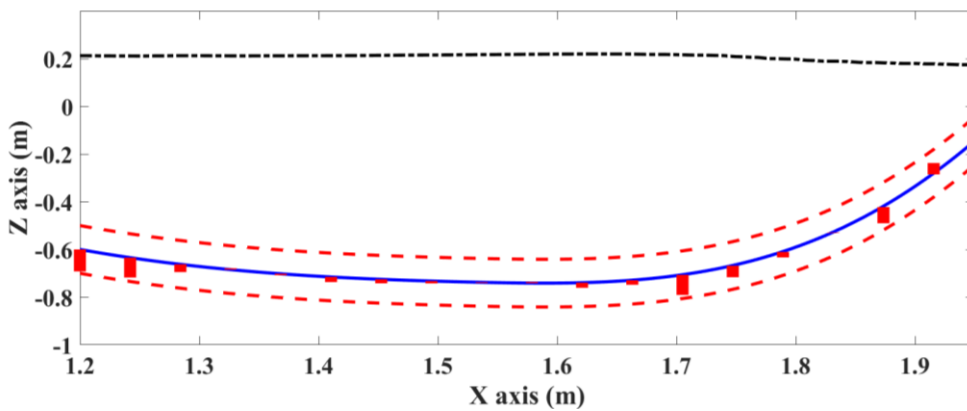
Figure 7-32: Average error and STD for soil digging with NPI, CCP, and FC

Table 7-2 provides the average error values along the *y*-axis for the sand digging and soil digging experiments. From the average errors, it can be seen that the controller

comprising of position, contour, and force provides the least average error achieving the STD bounds. Also, through the error variation between the sand and soil experiments, it can be concluded that the soil induced higher resistive forces compared to sand. In addition, Fig. 7-33 and Fig. 7-34 shows the deviation between the desired ground terrain and the actual excavated ground terrain. As given in Table 7-3, a STD of 3.23 cm was achieved during the sand digging experiment and was within the user-defined STD bound of 5 cm. A STD of 5.5718 cm was achieved for the soil digging experiment and was within the defined STD bound of 10 cm.

Table 7-3: Average error along the *y*-axis for digging experiments

| Average error in *y*-axis of excavation profile						
Data point	Sand digging (cm)			Soil Digging (cm)		
	NPI	CCP	FC	NPI	CCP	FC
1	8.59	7.82	-1.03	21.86	10.91	-9.2
2	12.73	3.97	2.24	26.10	9.79	-8.3
3	10.67	2.17	2.87	27.88	13.32	-3.2
4	11.84	8.35	3.46	29.95	14.36	0.55
5	11.03	7.57	4.01	31.24	16.36	-0.57
6	10.38	6.55	4.9	31.81	17.94	-2.1
7	10.17	6.19	4.86	24.07	19.32	-16
8	10.02	6.19	4.47	24.01	20.57	-0.99
9	6.31	5.34	4.17	25.78	22.52	-0.31
10	2.24	5.81	3.73	31.66	30.37	0.46
11	2.63	5.19	3.2	34.55	15.01	-2.12
12	3.09	5.74	2.44	40.77	18.68	-1.89
13	3.46	2.21	1.88	39..46	18.93	-8.41
14	4.03	3.06	1.1	51.95	27.27	-4.83
15	5.53	5.03	-0.19	55.26	30.82	-2.3
16	6.05	5.62	0.98	59.14	34.92	-0.19
17	13.5	7.00	1.49	62.63	38.47	-6.78
18	19.39	12.91	2.16	54.69	29.37	4.77
19	26.51	15.64	3.91	56.67	28.46	4.26
20	27.09	17.23	4.87	52.35	52.89	-0.7

Table 7-4: Standard deviation for digging experiments

Controller Type	Standard Deviation Sand Digging (cm)	Standard Deviation Soil Digging (cm)
PI	12.3989	41.3355
NPI	7.9957	25.6995
NPI + CCP	3.2335	5.5718
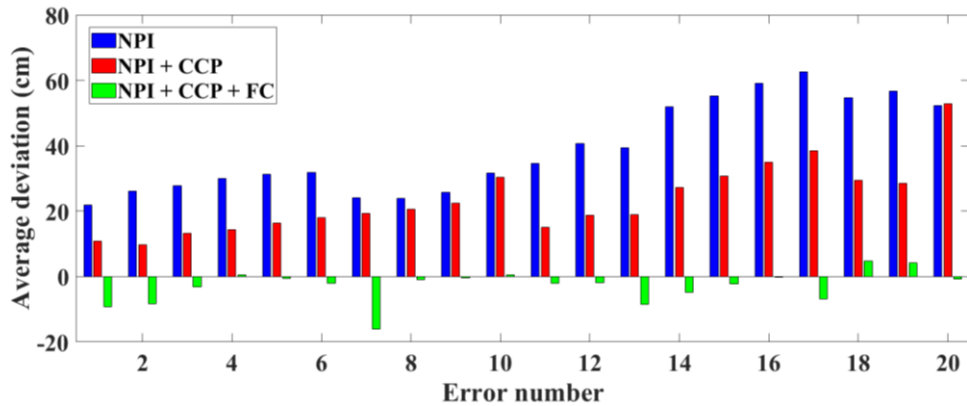
Figure 7-33: Average variation of deviation along *y*-axis for soil digging experiment
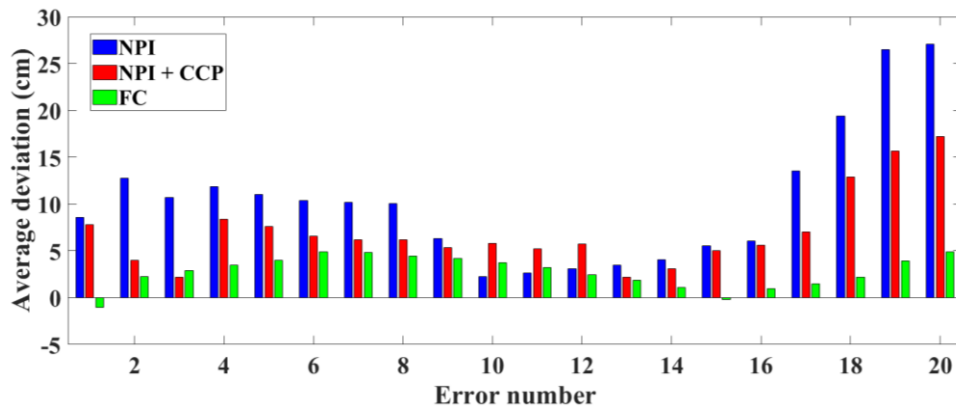
Figure 7-34: Average variation of deviation along *y*-axis for sand digging experiment

Chapter 8. Conclusion and Future Improvements

The goal of this study is to provide an effective control strategy for autonomous excavation that can integrate different control aspects of the position, contour, and force tracking. The design of controllers was carried out based on the understanding of the unique behaviors and characteristics of the excavator's system and earthmoving operations as below.

First of all, traditional control methods have a limitation in achieving high precision tracking control of the bucket tip due to the nonlinear characteristics arising from the hydraulic and dynamic systems of the excavator. As a critical factor that influences tracking control, the ground resistive force can be transmitted to the bucket tip in contact with the ground and therefore makes tracking control significantly challenging. Thus, compliant control techniques that cater to both force and position tracking are required. Furthermore, the coordinated control of the boom, arm and bucket link is required since position control of the hydraulic actuator only focuses on reducing the tracking error of the individual hydraulic actuator. Due to this reason, apart from the force/position control requirement, a coordinated compensation technique of the contour error (i.e. the shortest distance from the desired trajectory to the current trajectory) was applied to the developed control strategy and combined with the force and position control components. Finally, the estimation of nonlinear dynamics was also incorporated into the designed control strategy by applying time-delayed control.

For system modeling and simulation, a multi-domain simulation model was developed using Amesim and MATLAB/Simulink by considering various aspects from kinematics, mechanical, hydraulics, and control systems of the excavator. Based on this simulation model, the designed control algorithms were evaluated through the co-simulation environment that allows to couple the plant model and controllers defined in different physical domains and provides a solid foundation for system/control validation before an experimental test. To conduct an experimental study, a prototype autonomous excavator was developed as a test platform by modifying the existent excavator and implementing an HW controller (dSPACE), EHPVs with drivers and a relay box, a battery system, and diverse sensors such as pressure sensor, LVDT, encoder, and stereo vision sensor. To

validate the tracking performance of the designed control algorithms with the test platform, ground leveling and digging tasks were considered as a test scenario. Tracking accuracy was analyzed by verifying the tracking error of the bucket tip using the LVDT sensors as well as the deviation of the excavated ground surface from the target profile using a stereo vision sensor. Experimental results show that accurate ground leveling could be achieved by the designed contour control algorithms along with the NPI control. For the digging task, two different excavation media, i.e., sand and soil were applied to validate and compare the tracking performance of the designed controllers. From the experimental tests, it is concluded that a comprehensive approach of position, contour, and force control can clearly improve the tracking precision for the digging operation against the ground resistive forces.

Furthermore, the below is a list of challenges faced during the work and some suggestions on how to improve the tracking accuracy of position, contour, and force.

- Parameter Tuning

  Some form of adaptive parameter tuning is required as it is a tedious process to tune the various parameters including the impedance parameters as it is not very user friendly. Also, it is impossible that a digging site would contain homogeneous material. Therefore researchers have identified research directions where there is a need to adjust the impedance gains online according to some form of feedback information such as the measured tracking errors of force in the view of compliant control [32].

- Ground resistive force determination

  Ground resistive forces determination is vital moving forward for autonomous excavation. Techniques such as machine learning can be used for accurate estimation of ground resistive forces. The recent simulation environment development in optimization of earthmoving operations using reinforcement learning looks promising [69].

- Dynamic uncertainties

  Although an efficient time-delayed control method was introduced in this work, the control performance could be improved by introducing intelligent compensators (intelligent disturbance observer-based control methods) to compensate for

components such as Coulomb friction and other nonlinearities existing in the hydraulic circuit.

- Control Strategies for different phases of digging

  Digging accuracy can be improved by controlling the digging trajectory according to its various stages. The digging cycle cannot be modelled as a single phase. It can be characterized as an integration of the penetration, dragging, and curling phase where the final filling of the bucket is done by rotation of the bucket. Throughout these phases, soil keeps accumulating in the bucket, which increases the force required by the controller to track the desired trajectory in a nonlinear manner. This adds uncertainty to the designed controllers that causes increased tracking errors. Hence, an intelligent algorithm to estimate or identify the filling of the bucket is required to compensate for the uncertainty. Also, this algorithm can be used to determine the timing to stop the digging cycle when the bucket has reached its full capacity. In other words, merely following the digging trajectory after filling the bucket completely cannot achieve perfect autonomy in the excavation. Thereby, consideration of this factor for future experiments can greatly increase the level of autonomy of the excavator.

- Test platform improvements

  The physical improvement of the test platform can also be made to increase the accuracy of the control system. As an example, hydraulic servo valves can be introduced in place of EHPV's used in the current platform, which provide precise control of the position for hydraulic actuators through a feedback (or closed-loop) control [70].

REFERENCES

[1]   P. K. N. Narasimha and M. A. Vinay, "Automation and Robotics in the Construction Industry - a Review," *i-manager's J. Futur. Eng. Technol.*, vol. 14, no. 3, p. 49, 2019.

[2]   Q. Chen, B. García de Soto, and B. T. Adey, "Construction automation: Research areas, industry concerns and suggestions for advancement," *Autom. Constr.*, vol. 94, no. December 2017, pp. 22–38, 2018.

[3]   F. Mrad, M. Asem Abdul-Malak, S. Sadek, and Z. Khudr, "Automated excavation in construction using robotics trajectory and envelop generation," *Eng. Constr. Archit. Manag.*, vol. 9, no. 4, pp. 325–335, 2002.

[4]   B. W. Jo, Y. S. Lee, J. H. Kim, D. K. Kim, and P. H. Choi, "Proximity warning and excavator control system for prevention of collision accidents," *Sustain.*, vol. 9, no. 8, 2017.

[5]   J. Lee, S. J. Lorenc, and L. E. Bernold, "Saving Lives and Money with Robotic Trenching and Pipe Installation," *J. Aerosp. Eng.*, vol. 12, no. 2, pp. 43–49, Apr. 1999.

[6]   P. Palensky, A. A. Van Der Meer, C. D. López, A. Joseph, and K. Pan, "Cosimulation of Intelligent Power Systems: Fundamentals, Software Architecture, Numerics, and Coupling," *IEEE Ind. Electron. Mag.*, vol. 11, no. 1, pp. 34–50, 2017.

[7]   Q. Chang and T. Maruyama, "Real-Time Stereo Vision System: A Multi-Block Matching on GPU," *IEEE Access*, vol. 6, pp. 42030–42046, 2018.

[8]   M. Di Natale, H. Zeng, P. Giusto, and A. Ghosal, *Understanding and Using the Controller Area Network Communication Protocol*. New York, NY: Springer New York, 2012.

[9]   J. K. Woodacre, R. J. Bauer, and R. Irani, "Hydraulic valve-based active-heave compensation using a model-predictive controller with non-linear valve compensations," *Ocean Eng.*, vol. 152, no. January, pp. 47–56, 2018.

[10]   B. Xu, Q. Su, J. Zhang, and Z. Lu, "A dead-band model and its online detection for the pilot stage of a two-stage directional flow control valve," *Proc. Inst. Mech. Eng. Part C J. Mech. Eng. Sci.*, vol. 230, no. 4, pp. 639–654, 2016.

[11]   S. Dadhich, U. Bodin, and U. Andersson, "Key challenges in automation of earthmoving machines," *Autom. Constr.*, vol. 68, pp. 212–222, 2016.

[12]   William Richardson-Little and C. J. Damaren, "Position accommodation and compliance control for robotic excavation," *Proc. 2005 IEEE Conf. Control Appl. 2005. CCA 2005.*, pp. 1194–1199, 2005.

[13]   S. Blouin, A. Hemami, and M. Lipsett, "Review of Resistive Force Models for Earthmoving Processes," *J. Aerosp. Eng.*, vol. 14, no. 3, pp. 102–111, Jul. 2001.

[14]   J. Kim, M. Jin, W. Choi, and J. Lee, "Discrete time delay control for hydraulic excavator motion control with terminal sliding mode control," *Mechatronics*, vol. 60, no. August 2018, pp. 15–25, 2019.

[15]   A. Hemami, "Fundamental Analysis of Automatic Excavation," *J. Aerosp. Eng.*, vol. 8, no. 4, pp. 175–179, Oct. 1995.

[16]   J. A. Marshall, P. F. Murphy, and L. K. Daneshmend, "Toward autonomous excavation of fragmented rock: Full-scale experiments," *IEEE Trans. Autom. Sci. Eng.*, vol. 5, no. 3, pp. 562–566, 2008.

[17]   D. Le Hanh, K. K. Ahn, N. B. Kha, and W. K. Jo, "Trajectory control of electro-hydraulic excavator using fuzzy self tuning algorithm with neural network," *J. Mech. Sci. Technol.*, vol. 23, no. 1, pp. 149–160, 2009.

[18]   B. Li, J. Yan, G. Guo, Y. Zeng, and W. Luo, "High performance control of hydraulic excavator based on Fuzzy-PI soft-switch controller," *Proc. - 2011 IEEE Int. Conf. Comput. Sci. Autom. Eng. CSAE 2011*, vol. 2, pp. 676–679, 2011.

[19]   D. Zhenmian, Y. Zhengmao, Z. Hui, B. Hua, X. Yuanli, and J. Xianguo, "The study of trajectory automatic control based on RBF neural network PID control," in *2015 International Conference on Fluid Power and Mechatronics (FPM)*, 2015, pp. 1234–1238.

[20] C. S. Lee, J. Bae, and D. Hong, "Contour control for leveling work with robotic excavator," *Int. J. Precis. Eng. Manuf.*, vol. 14, no. 12, pp. 2055–2060, 2013.

[21] K. Y. Kim, D. S. Jang, Y. L. Cho, and J. H. Jang, "Development of electro-hydraulic control valve for intelligent excavator," *ICCAS-SICE 2009 - ICROS-SICE Int. Jt. Conf. 2009, Proc.*, pp. 2212–2216, 2009.

[22] S. Kang *et al.*, "Path tracking for a hydraulic excavator utilizing proportional-derivative and linear quadratic control," *2014 IEEE Conf. Control Appl. CCA 2014*, pp. 808–813, 2014.

[23] H. Feng *et al.*, "Robotic excavator trajectory control using an improved GA based PID controller," *Mech. Syst. Signal Process.*, vol. 105, pp. 153–168, 2018.

[24] Y. Ye, C. B. Yin, Y. Gong, and J. jing Zhou, "Position control of nonlinear hydraulic system using an improved PSO based PID controller," *Mech. Syst. Signal Process.*, vol. 83, pp. 241–259, 2017.

[25] T. Tomatsu, K. Nonaka, K. Sekiguchi, and K. Suzuki, "Model predictive trajectory tracking control for hydraulic excavator on digging operation," in *2015 IEEE Conference on Control Applications (CCA)*, 2015, pp. 1136–1141.

[26] F. A. Bender, S. Goltz, T. Braunl, and O. Sawodny, "Modeling and Offset-Free Model Predictive Control of a Hydraulic Mini Excavator," *IEEE Trans. Autom. Sci. Eng.*, vol. 14, no. 4, pp. 1682–1694, 2017.

[27] Y. Altintas and M. R. Khoshdarregi, "Contour error control of CNC machine tools with vibration avoidance," *CIRP Ann. - Manuf. Technol.*, vol. 61, no. 1, pp. 335–338, 2012.

[28] J. Ling, Z. Feng, D. Yao, and X. Xiao, "Non-linear contour tracking using feedback PID and feedforward position domain cross-coupled iterative learning control," *Trans. Inst. Meas. Control*, vol. 40, no. 6, pp. 1970–1982, 2018.

[29] D. Wang, L. Zheng, H. Yu, W. Zhou, and L. Shao, "Robotic excavator motion control using a nonlinear proportional-integral controller and cross-coupled pre-compensation," *Autom. Constr.*, vol. 64, pp. 1–6, 2016.

[30] J. Mattila, J. Koivumaki, D. G. Caldwell, and C. Semini, "A survey on control of hydraulic robotic manipulators with projection to future trends," *IEEE/ASME Trans. Mechatronics*, vol. 22, no. 2, pp. 669–680, 2017.

[31] D. Jud, G. Hottiger, P. Leemann, and M. Hutter, "Planning and Control for Autonomous Excavation," *IEEE Robot. Autom. Lett.*, vol. 2, no. 4, pp. 2151–2158, 2017.

[32] P. Song, Y. Yu, and X. Zhang, "A Tutorial Survey and Comparison of Impedance Control on Robotic Manipulation," *Robotica*, vol. 37, no. 5, pp. 801–836, 2019.

[33] S. Chiaverini, B. Siciliano, and L. Villani, "A survey of robot interaction control schemes with experimental comparison," *IEEE/ASME Trans. Mechatronics*, vol. 4, no. 3, pp. 273–285, 1999.

[34] N. Hogan, "Impedance Control: An Approach to Manipulation," in *1984 American Control Conference*, 1984, vol. 107, no. March 1985, pp. 304–313.

[35] S. Tafazoli, S. E. Salcudean, K. Hashtrudi-Zaad, and P. D. Lawrence, "Impedance control of a teleoperated excavator," *IEEE Trans. Control Syst. Technol.*, vol. 10, no. 3, pp. 355–367, 2002.

[36] S. E. Salcudean, S. Tafazoli, P. D. Lawrence, and I. Chau, "Impedance control of a teleoperated mini excavator," *1997 8th Int. Conf. Adv. Robot. Proceedings. ICAR'97*, vol. 10, no. 3, pp. 355–367, 1997.

[37] Q. P. Ha, Q. H. Nguyen, D. C. Rye, and H. F. Durrant-Whyte, "Impedance control of a hydraulically actuated robotic excavator," *Autom. Constr.*, vol. 9, no. 5, pp. 421–435, 2000.

[38] W. Acuña-Bravo, E. Canuto, M. Agostani, and M. Bonadei, "Proportional electro-hydraulic valves: An Embedded Model Control solution," *Control Eng. Pract.*, vol. 62, no. March, pp. 22–35, 2017.

[39] R. Amirante, L. A. Catalano, C. Poloni, and P. Tamburrano, "Fluid-dynamic design optimization of hydraulic proportional directional valves," *Eng. Optim.*, vol. 46, no. 10, pp. 1295–1314, 2014.

[40] X. Liu, X. Liu, L. Wang, and J. Chen, "The dynamic analysis and experimental research of counter balance valve used in truck crane," *Proc. - Int. Conf. Electr. Control Eng. ICECE 2010*, pp. 2332–2335, 2010.

[41] B. Zhang, S. Wang, Y. Liu, and H. Yang, "Research on Trajectory Planning and Autodig of Hydraulic Excavator," *Math. Probl. Eng.*, vol. 2017, pp. 1–10, 2017.

[42] Jaho Seo; Niraj Reginald, "Force/Position Control for an Excavator with Contour Control Compensation," pp. 176–187, 2019.

[43] J. Huang, P. Hu, K. Wu, and M. Zeng, "Optimal time-jerk trajectory planning for industrial robots," *Mech. Mach. Theory*, vol. 121, pp. 530–544, 2018.

[44] T. Knohl and H. Unbehauen, "Adaptive position control of electrohydraulic servo systems using ANN," *Mechatronics*, vol. 10, no. 1–2, pp. 127–143, Feb. 2000.

[45] H. Han, Y. Liu, L. Ma, and Z. Liu, "Analyze the characteristics of electro-hydraulic servo system's position-pressure master-slave control Advances," *Adv. Mech. Eng.*, vol. 10, no. 6, pp. 1–9, 2018.

[46] N. Vasiliu, D. Vasiliu, C. Călinoiu, and R. Puhalschi, *Simulation of Fluid Power Systems with Simcenter Amesim*. Boca Raton : Taylor & Francis, CRC Press, 2018.: CRC Press, 2018.

[47] A. J. Koivo, "Kinematics of Excavators (Backhoes) for Transferring Surface Material," *J. Aerosp. Eng.*, vol. 7, no. 1, pp. 17–32, 1994.

[48] P. K. Vähä and M. J. Skibniewski, "Dynamic Model of Excavator," *J. Aerosp. Eng.*, vol. 6, no. 2, pp. 148–158, Apr. 1993.

[49] S. Jung, *A Neural Network Compensation Technique for an Inertia Estimation Error of a Time-Delayed Controller for a Robot Manipulator*, vol. 11307 LNCS. Springer International Publishing, 2018.

[50] T. C. Hsia and L. S. Gao, "Robot manipulator control using decentralized linear time-invariant time-delayed joint controllers," in *Proceedings., IEEE International Conference on Robotics and Automation*, 1990, pp. 2070–2075.

[51]   M. Jin, S. H. Kang, P. H. Chang, and J. Lee, "Robust Control of Robot Manipulators Using Inclusive and Enhanced Time Delay Control," *IEEE/ASME Trans. Mechatronics*, vol. 22, no. 5, pp. 2141–2152, 2017.

[52]   M. Jin, S. H. Kang, and P. H. Chang, "Robust compliant motion control of robot with nonlinear friction using time-delay estimation," *IEEE Trans. Ind. Electron.*, vol. 55, no. 1, pp. 258–269, 2008.

[53]   M. Jin, J. Lee, P. H. Chang, and C. Choi, "Practical nonsingular terminal sliding-mode control of robot manipulators for high-accuracy tracking control," *IEEE Trans. Ind. Electron.*, vol. 56, no. 9, pp. 3593–3601, 2009.

[54]   S. Jung, "Analysis of inertial effect on control performance of a time-delayed controller for a robot manipulator," *Int. Conf. Control. Autom. Syst.*, vol. 2018-Octob, no. Iccas, pp. 1096–1099, 2018.

[55]   S. U. Lee and P. H. Chang, "Control of a heavy-duty robotic excavator using time delay control with integral sliding surface," *Control Eng. Pract.*, vol. 10, no. 7, pp. 697–711, 2002.

[56]   J. Park, "The relationship between controlled joint torque and end-effector force in underactuated robotic systems," *Robotica*, vol. 29, no. 4, pp. 581–584, 2011.

[57]   F. Xu, X. Liu, W. Chen, C. Zhou, and B. Cao, "Modeling and co-simulation based on Adams and AMESim of pivot steering system," *J. Eng.*, vol. 2019, no. 13, pp. 392–396, 2019.

[58]   D. Pan, S. Gu, G. Guo, H. Kuang, H. Zhong, and F. Gao, "Co-simulation design and experimental study on the hydraulic-pneumatic-powered driving system of main steam and feed water isolation valves for CAP1400," *Adv. Mech. Eng.*, vol. 9, no. 8, pp. 1–11, 2017.

[59]   N. Sepehri, a. a. Khayyat, and B. Heinrichs, "Development of a nonlinear PI controller for accurate positioning of an industrial hydraulic manipulator," *Mechatronics*, vol. 7, no. 8, pp. 683–700, 1997.

[60]   H. Hanafusa, "on Contouring Control of Articulated Robot Arms.," *IFAC Proc.*

Vol., vol. 15, no. 9, pp. 23–31, 1983.

[61]   N. Hogan, "Impedance control: An approach to manipulation: Part III-applications," *J. Dyn. Syst. Meas. Control. Trans. ASME*, vol. 107, no. 1, pp. 17–24, 1985.

[62]   S. Jung, T. C. Hsia, and R. G. Bonitz, "Force Tracking Impedance Control of Robot Manipulators Under Unknown Environment," *IEEE Trans. Control Syst. Technol.*, vol. 12, no. 3, pp. 474–483, May 2004.

[63]   S. Jung and T. C. Hsia, "Force Tracking Impedance Control of Robot Manipulators for Environment with Damping," in *IECON 2007 - 33rd Annual Conference of the IEEE Industrial Electronics Society*, 2007, no. 1, pp. 2742–2747.

[64]   J. Duan, Y. Gan, M. Chen, and X. Dai, "Adaptive variable impedance control for dynamic contact force tracking in uncertain environment," *Rob. Auton. Syst.*, vol. 102, pp. 54–65, 2018.

[65]   S. Jung, T. C. Hsia, and R. G. Bonitz, "Force Tracking Impedance Control for Robot Manipulators with an Unknown Environment: Theory, Simulation, and Experiment," *Int. J. Rob. Res.*, vol. 20, no. 9, pp. 765–774, Sep. 2001.

[66]   C. Hu, Y. H. Zhou, C. J. Zhao, and Z. G. Pan, "Slope excavation quality assessment and excavated volume calculation in hydraulic projects based on laser scanning technology," *Water Sci. Eng.*, vol. 8, no. 2, pp. 164–173, 2015.

[67]   D. A. Bradley and D. W. Seward, "The Development, Control and Operation of an Autonomous Robotic Excavator," *J. Intell. Robot. Syst. Theory Appl.*, vol. 21, no. 1, pp. 73–97, 1998.

[68]   C. W. W. Ng, *Advanced Unsaturated Soil Mechanics and Engineering*. CRC Press, 2014.

[69]   V. Shitole, J. Louis, and P. Tadepalli, "Optimizing Earthmoving Operations Via Reinforcement Learning," in *2019 Winter Simulation Conference (WSC)*, 2019, pp. 2954–2965.

[70]   Q. Ha, M. Santos, Q. Nguyen, D. Rye, and H. Durrant-Whyte, "Robotic excavation

in construction automation," *IEEE Robot. Autom. Mag.*, vol. 9, no. 1, pp. 20–28, 2002.

APPENDICES

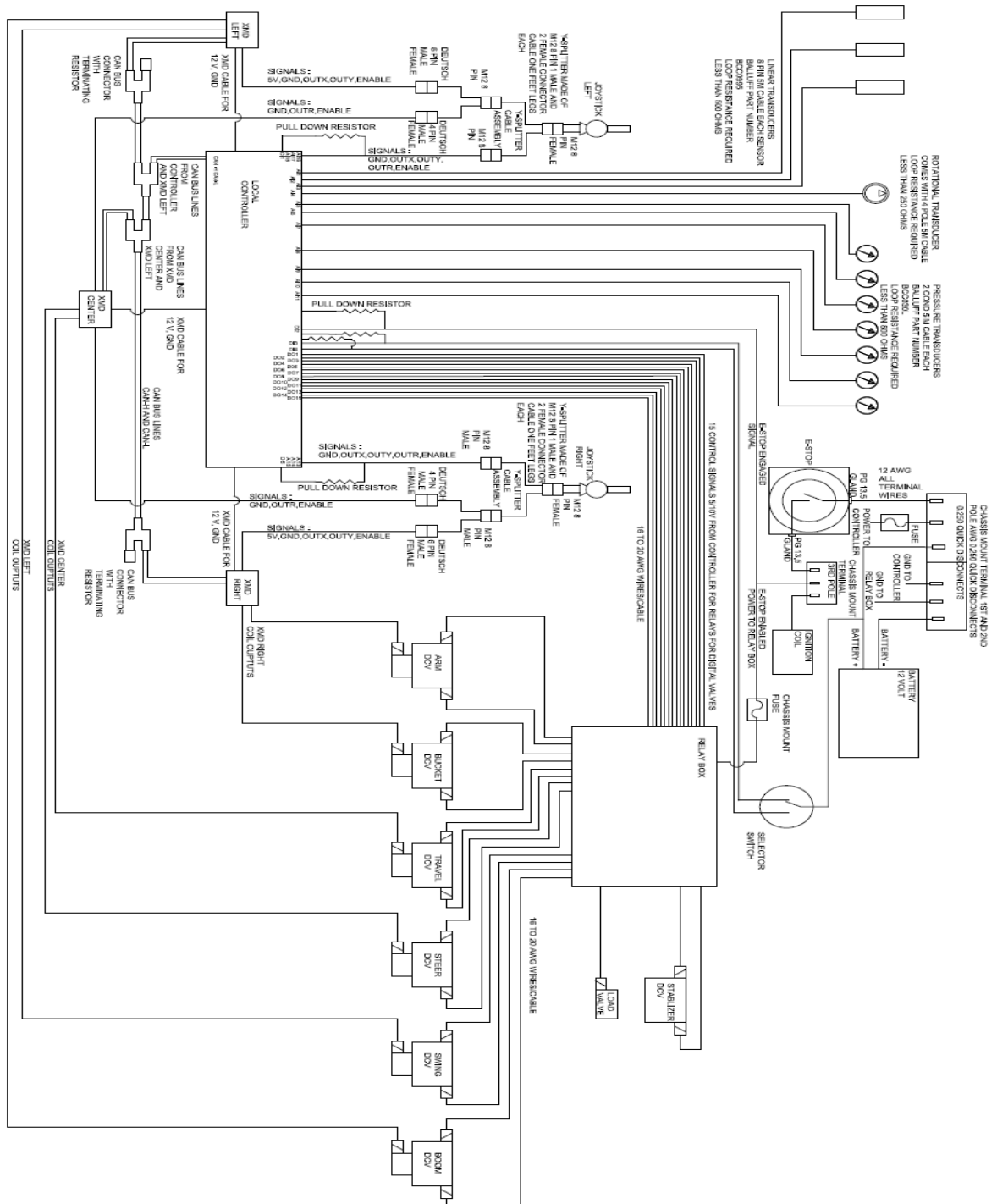## Appendix A.   Designed electronic diagram

Figure A-1: Electrical and Electronic Diagram

Appendix B.   Kinematic transformations

B1.   Cylinder stroke to joint angle mapping

A simplified version of the boom, arm and bucket links are provided in Fig. B-1 and Fig. B-2, respectively. Table B-1 provide the measured physical data needed for the actuator stroke to joint angle conversion.
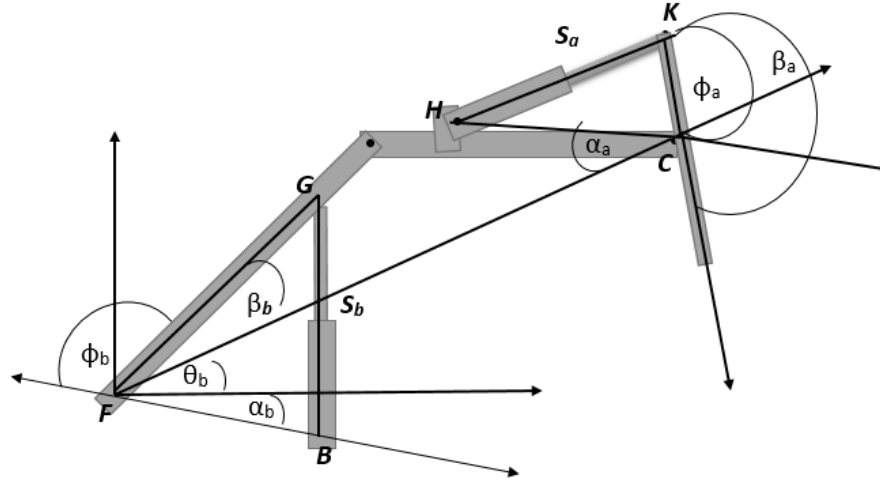

Figure B-1: Boom, arm actuator and their links

The boom angle θ_b can be calculated given the boom actuator stroke S_b. The angles β_b, α_b are constants which are measured.

$$\phi_b = a\cos(\frac{FB^2 + FG^2 - S_b^2}{2 \cdot FG \cdot FB}) \qquad \text{(B-1)}$$

$$\theta_b = \pi - \beta_b - \alpha_b - \phi_b \qquad \text{(B-2)}$$

The arm angle θ_a can be calculated given the boom actuator stroke S_a as given in Eq. (B-3). The angles β_a, α_a are constants which are measured.

$$\phi_a = a\cos\left(\frac{S_a^2 - HC^2 - CK^2}{2 \cdot HC \cdot CK}\right) \qquad \text{(B-3)}$$

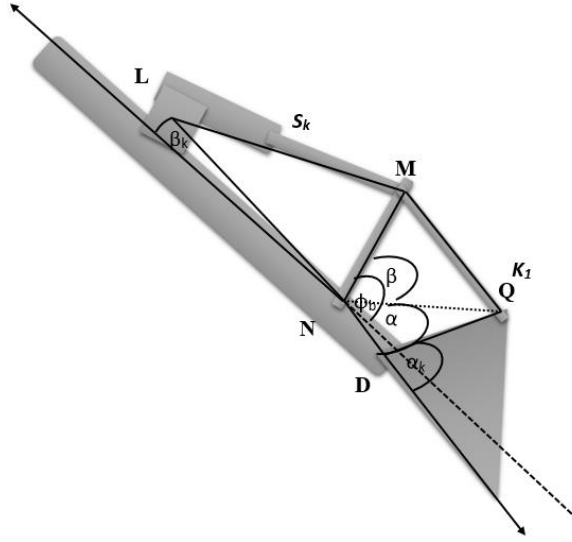$$\theta_a = 2\pi - \beta_a - \alpha_a + \phi_a \qquad \text{(B-4)}$$

Figure B-2: Bucket actuator and links

The bucket angle θ_k can be calculated given the boom actuator stroke S_k as given in Eq. (B-3). The bucket motion is driven by the four-bar mechanism NMQD. The kinematics of this four-bar mechanism can be analysed by finding the angle $M\hat{N}D$ which is the driving angle of this four-bar mechanism. The angles β_k, α_k are constants which are measured.

$$\phi_k = a\cos\left(\frac{LN^2 + NM^2 - S_k^2}{2 \cdot LN \cdot NM}\right) \tag{B-5}$$

$$M\hat{N}D = \pi - \varphi_k - \beta_4 \tag{B-6}$$

$$k_1 = \sqrt{NP^2 + ND^2 - 2 \cdot ND \cdot NP.\cos(M\hat{N}D)} \tag{B-7}$$

$$\alpha = a\cos\left(\frac{ND^2 + k_1^2 - NP^2}{2 \cdot ND \cdot k_1}\right) \tag{B-8}$$

$$\beta = a\cos\left(\frac{k_1^2 + DQ^2 - PQ^2}{2 \cdot DQ \cdot k_1}\right) \tag{B-9}$$

$$\mu = \alpha + \beta \tag{B-10}$$

$$\theta_k = 3\pi - \mu - \alpha_k \tag{B-11}$$

Table B-1: Physical measurements of excavator

Measurement	Value	Measurement	Value
FB	0.175 m	β_b	31°
FG	0.576 m	α_b	45°
HC	0.549 m	β_a	157.5°
CK	0.187 m	α_a	34°
LN	0.450 m	β_k	15°
NM	0.298 m	α_k	87°
PQ	0.249 m		
DQ	0.120 m		
ND	0.111 m		

B2. Cylinder force to joint torque mapping

A simplified form of drawing of the excavator boom and arm links can be drawn as shown in Fig. B-1. From the excavator X_i and Y_i values are constants which can be measured from the test platform. The angles φ and α are varying with hydraulic actuator length L_i.
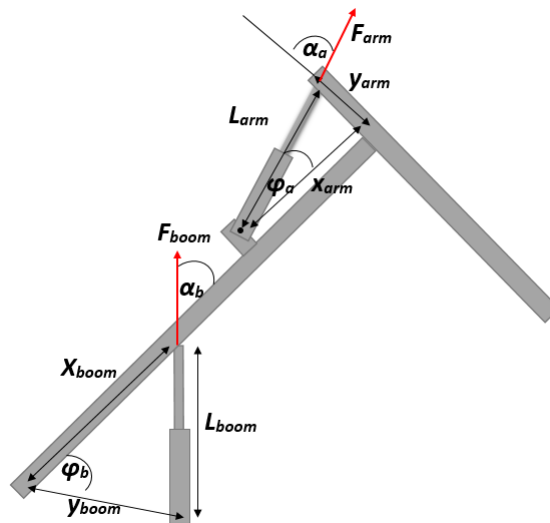

Figure B-3: Simplified drawing of boom and arm links

By applying cosine law to the two triangles we can obtain the relationship between the angle varying γ_i and stroke length L_i.

$$L_i = \sqrt{(a_i^2 + b_i^2 - 2a_i b_i \cos \varphi_i}$$ (B-12)

Again, applying cosine law to the triangles along with trigonometric identity we have

$$\sin \alpha_i = \sqrt{\left(1 - \left(\frac{b_i^2 - L_i^2 - a_i^2}{2L_i a_i}\right)^2\right)}$$ (B-13)

Now the lever arms to both arm and boom joints can be found and cylinder force required can be expressed with the torque as:

$$F_i = \frac{\tau_i}{a_i \sin \alpha_i} = \frac{\tau_i}{a_i \sqrt{\left(1 - \left(\frac{b_i^2 - L_i^2 - a_i^2}{2L_i a_i}\right)^2\right)}}$$ (B-14)
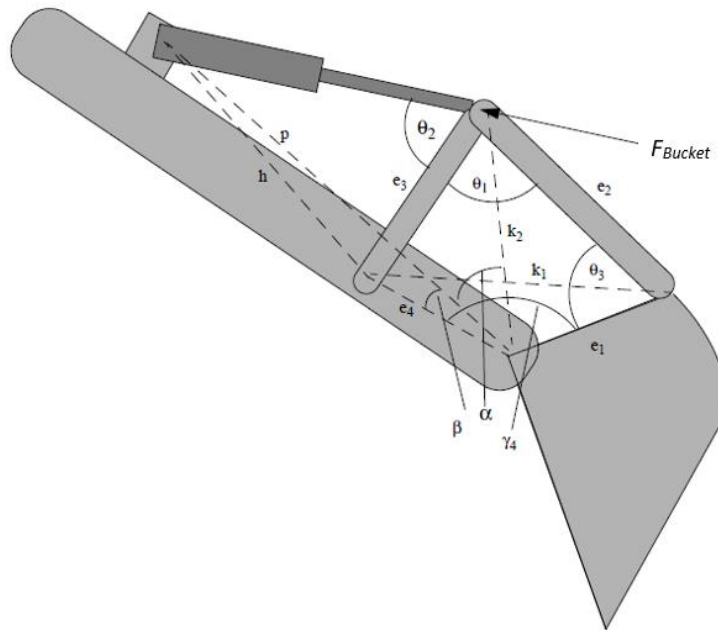

Figure B-4: Simplified drawing of bucket link

Using cosine laws to the four-bar mechanism, the following Equations are obtained.

$$k_1 = \sqrt{\left(e_4^2 + e_1^2 - 2e_4 e_1 \cos\gamma_4\right)}$$ (B-15)

$$\theta_1 = \cos^{-1}\sqrt{\left(\frac{e_3^2 + e_2^2 - k_1^2}{2e_3 e_2}\right)}$$ (B-16)

$$\theta_3 = \cos^{-1}\sqrt{\left(\frac{e_2^2 + k_1^2 - e_3^2}{2e_2 k_1}\right)} + \cos^{-1}\sqrt{\left(\frac{e_1^2 + k_1^2 - e_4^2}{2e_1 k_1}\right)}$$ (B-17)

$$k_1 = \sqrt{\left(e_1^2 + e_2^2 - 2e_1 e_2 \cos\theta_3\right)}$$ (B-18)

$$\alpha = \cos^{-1}\sqrt{\left(\frac{e_4^2 + k_2^2 - e_3^2}{2e_4 k_2}\right)} - \beta$$ (B-19)

$$L_4 = \sqrt{\left(k_2^2 + p^2 - 2k_2 p \cos\alpha\right)}$$ (B-20)

$$\theta_2 = \cos^{-1}\sqrt{\left(\frac{L_4^2 + e_3^2 - h^2}{2e_3 L_4}\right)}$$ (B-21)

As depicted in the above Fig. B-4, there are two members transmitting the force towards the bucket. By summation of force in the direction of F_4 and perpendicular to it we have Eq.'s (B-22) & (B-23)

$$F_{Bucket} - F_{e_3}\cos\theta_2 - F_{e_3}\cos(\theta_1 + \theta_2) = 0$$ (B-22)

$$F_{e_3}\sin\theta_2 - F_{e_3}\sin(\theta_1 + \theta_2) = 0$$ (B-23)

Solving these two equations we have

$$F_{bucket} = F_{e_2}\left(\cos(\theta_1 + \theta_2) - \sin(\theta_1 + \theta_2)\cot(\theta_2)\right)$$ (B-24)

$$F_{e_2} = \frac{\tau}{e_1 \sin\theta_3}$$ (B-25)

Therefore, force of bucket cylinder to torque relationship is given as:

$$F_{bucket} = \tau_4 \left(\frac{\left(\cos(\theta_1 + \theta_2) - \sin(\theta_1 + \theta_2)\cot(\theta_2) \right)}{e_1 \sin\theta_3} \right) \qquad \text{(B-26)}$$